

Coaxial Resonator Filters

by
Susan Maas

*Thesis presented in partial fulfilment of the requirements for the degree
Master of Science in Engineering at
Stellenbosch University*



Supervisor: Prof. Petrie Meyer
Co-supervisor: Prof. Pieter Willem van der Walt
Department of Electrical & Electronic Engineering

December 2011

Declaration

By submitting this thesis electronically, I declare that the entirety of the work contained therein is my own, original work, that I am the sole author thereof (save to the extent explicitly otherwise stated), that reproduction and publication thereof by Stellenbosch University will not infringe any third party rights and that I have not previously in its entirety or in part submitted it for obtaining any qualification.

Date: June 2011

Copyright © 2011 Stellenbosch University

All rights reserved

Abstract

The purpose of this project is to develop a number of coaxial resonator filters.

Firstly, the theoretical model of the filter is discussed, with a Tchebyscheff LC-ladder prototype filter used to derive a generalised bandpass filter. From this, generalised Compline- and Interdigital filters are derived. Following this, various options and limitations in the mechanics of microwave filters are discussed. Results are shown for an in-depth study considering the unloaded quality factor for thirteen different resonators. Each resonator is unique in the method of manufacturing, polishing, as well as plating.

Utilizing the information obtained from the unloaded quality factor measurements, three coupled coaxial resonator filters, are designed for use in a radar system, namely a sixth order 2125 MHz Compline filter, a sixth order 9250 MHz Interdigital filter and a third order 9250 MHz Interdigital filter.

Optimal results were obtained when both resonators and coupled transmission line filters were constructed from aluminium that was wire-cut and then silver electroplated.

Opsomming

Die omvang van hierdie projek behels die ontwerp en bou van ko-aksiale resoneerder filters.

Eerstens word die teoretiese modellering van die filters bespreek. 'n Tchebyscheff LC-leer prototipe filter word gebruik as basis vir 'n generiese banddeurlaat filter. Die banddeurlaat filter word gebruik om die afgeleide Kamlyn- en Interdigitale filter te definieer. Hierna volg 'n bespreking aangaande die verskillende moontlikhede in die meganiese vervaardiging van mikrogolf filters. 'n Gedetailleerde studie word gedoen om die onbelaste kwaliteitsfaktore van 13 verskillende resoneerders te bepaal. Elkeen van hierdie resoneerders is uniek in die metode van vervaardiging, polering, asook die platering daarvan.

Deur gebruik te maak van die resultate van die onbelaste kwaliteitsfaktore, word drie gekoppelde ko-aksiale resoneerder filters ontwikkel vir die gebruik in 'n radarstelsel, naamlik 'n sesde-orde 2125 MHz Kamlyn filter, 'n sesde orde 9250 MHz Interdigitale filter, asook 'n derde orde 9250 MHz Interdigitale filter.

Die beste resultate was gevind toe beide resoneerders en gekoppelde ko-aksiale resoneerder filters vervaardig is uit aluminium wat gedraadsny en silwer geplateer is.

Acknowledgements

To say "thank you" cannot sufficiently express the thankfulness I experience in my heart. There are so many people that contributed to this thesis.

First and foremost, I would like to thank my Heavenly Father for the privilege to have been able to continue further in my academic career. He has given me talents, strength, and perseverance. My heart is filled with thankfulness.

Secondly, I would like to thank Prof. P. Meyer and Prof. P.W. van der Walt. They have taught me so much more than just knowledge about filters. Humbleness, appreciation, thankfulness and respect are some of the key aspects that I could learn from them both and I am very thankful for that. Thank you very much for the honour to have worked with both of you and the knowledge you imparted with regards to filter design.

Thirdly, I would like to thank Reutech Radar Systems for making it possible in terms of my project as well as the financial support I received. I am very thankful for it.

I would also like to thank my family and friends. Thank you for your love, prayers and support. From the bottom of my heart, I would like to thank my husband, Gualbert Maas for his support and time spent reading through my thesis. I would like to thank my mother Salomé Swart for her wisdom, love and always being there for me. I would also like to thank my mother in-law Hermien Maas, my mother and Charmaine Daffue for looking after our baby Altus during the last section of my thesis.

Hereby my uttermost thanks also to:

Madele van der Walt for the help with L^AT_EX. I am extremely thankful for that.

Executive Engineering for the machining of the filters and resonators. Thank you for all the knowledge I have gained from you guys.

Mtek for the silver plating.

Metalquip for the chemical polishing.

Contents

Declaration	i
Abstract	ii
Opsomming	iii
Acknowledgements	iv
Contents	v
List of Figures	viii
List of Tables	xi
List of Abbreviations	xii
List of Symbols	xiv
1 Introduction	1
1.1 Introduction to filtering radar signals [1]	1
1.2 Radar signal theory [1]	3
1.2.1 Rectangular and shaped pulses	3
1.2.2 Signal duration	5
1.2.3 Detection of radar pulses	8
1.3 Filter selection [1]	8
1.4 Filters in Radar systems	9
1.5 Layout of the Thesis	14
2 Coaxial Filters	16
2.1 Introduction	16
2.2 Tchebyscheff lowpass filter	16

<i>CONTENTS</i>	vi
2.3 Coupled Resonator Bandpass Prototypes	18
2.4 Parallel Coupled Transmission Lines	26
2.5 Narrowband Coaxial Resonator Filters	29
2.5.1 Compline Filter	30
2.5.2 Interdigital Filter	35
2.6 Conclusion	39
3 Filter Implementation Parameters	40
3.1 Introduction	40
3.2 Input Coupling	40
3.3 Inter-resonator Coupling	42
3.4 Resonator Q Factor	47
3.5 Conclusion	50
4 Filter Manufacturing	51
4.1 Introduction	51
4.2 Microwave Penetration	51
4.3 Materials used in Microwave filters	52
4.3.1 Copper	52
4.3.2 Invar	52
4.3.3 Aluminium Alloys	52
4.3.4 Brass	53
4.4 Properties of machining techniques	53
4.4.1 CNC Milling	54
4.4.2 CNC Electrical Discharge Machining (EDM)	54
4.4.3 CNC Laser Cutting	57
4.5 Surface finish	57
4.5.1 Silver plating	58
4.5.2 Chemical polishing	58
4.6 Connectors and Tuning elements	59
4.7 Resonator unloaded Q measurement	61
4.8 Conclusion	66
5 Prototypes	67
5.1 Introduction	67
5.2 Parallel Coupled Transmission Lines	68
5.2.1 Filter 1	68

<i>CONTENTS</i>	vii
5.2.2 Filter 2	76
5.2.3 Filter 3	82
5.3 Conclusion	86
6 Conclusion	87
Bibliography	89
A Filter 1 Dimensions	A-1
B Comblin Filter - MWO Simulation	B-1
C Interdigital Filter - Matlab Code	C-1
D Filter 2 Dimensions	D-1
E Filter 3 Dimensions	E-1

List of Figures

1.1	Generation of a transmit pulse in the time domain and the corresponding frequency domain spectra of the modulating and modulated signal.	3
1.2	Spectra of the rectangular pulse of duration $T = 1$	4
1.3	Cosine-squared pulse with duration $T_{eff} = 1$	5
1.4	Spectra of the cosine-squared pulse.	5
1.5	Differential group delay on a cosine-squared pulse.	7
1.6	Comparison of the time domain responses of different filter approximations with the same 50 dB attenuation frequency for a cosine-squared input pulse.	9
1.7	Pulse-Doppler Radar.	10
1.8	Compline filter.	11
1.9	Interdigital Filter.	12
1.10	Waffle-Iron Harmonic Filter.	12
1.11	Waveguide Band Pass and Harmonic Filter.	13
1.12	Third Order Interdigital Filter.	14
2.1	Tchebyscheff lowpass filter and its corresponding dual circuit shown in (b).	17
2.2	Lowpass prototype filter using admittance inverters [3].	19
2.3	A section of the lowpass prototype shown in (a), and its dual in (b). The analogous J -inverter form of these two circuits are shown in (c).	20
2.4	End section of the lowpass prototype circuit (a) and the corresponding end portion of Figure 2.2 is shown in (b).	21
2.5	Lowpass filter transformed to the bandpass equivalent.	22
2.6	Lumped element shunt resonator.	23
2.7	Generalised bandpass filter circuit, using admittance inverters and shunt resonators.	26
2.8	A three-wire coupled transmission line and its static capacitance network.	27
2.9	Compline Bandpass filter in strip-line form.	31

LIST OF FIGURES

ix

2.10	Electrical circuit of the Comblin filter, together with one of Kuroda's identities.	32
2.11	First section of a Comblin filter circuit up to the first resonator. . . .	33
2.12	Interdigital Bandpass filter.	36
2.13	Equivalent electrical circuit of a fifth-order Interdigital filter.	37
3.1	Magnetic coupling loop.	41
3.2	Coupling to the Magnetic Field.	41
3.3	Coupling to the Electric Field.	42
3.4	Magnetic Coupled LC Resonators.	43
3.5	Equivalent circuit with Even and Odd modes.	44
3.6	Inverters- (a) Impedance, (b) Admittance.	46
3.7	Two coupled resonators with external Q -factors of 50 and adjustable coupling factor [7].	47
3.8	LC parallel resonator with equivalent circuit.	48
4.1	Wire-cutting Procedure.	55
4.2	Wire-cutting surface finishes.	56
4.3	Surface Roughness.	58
4.4	Spark-plug SMA Connector.	59
4.5	Temex Tuning Element.	60
4.6	Manufacturing and assembly of a MW filter.	60
4.7	Solid Resonator.	61
4.8	Split Resonator.	61
4.9	2125 MHz Resonators.	62
4.10	Resonator unloaded Q measurements.	63
4.11	Resonator Surface Current.	64
4.12	Unloaded Q Percentage Error.	65
5.1	Three filters.	67
5.2	Filter 1.	69
5.3	Comblin Equations.	70
5.4	SMA connector with Shim Stock loop.	73
5.5	Input coupling of Filter 1.	74
5.6	Filter 1 Measurements.	74
5.7	Filter 1 - Group delay Response.	75
5.8	Filter 1, Wider Stopband Response.	76

LIST OF FIGURES

x

5.9	Sixth Order Interdigital Filter.	79
5.10	Filter 2 Measurements.	80
5.11	Filter 2 - Added shim stock.	81
5.12	Filter 2 - Group delay.	81
5.13	Third Order Interdigital Filter.	83
5.14	Filter 3 Measurements.	84
5.15	Filter 3, Added shim stock.	85
5.16	Filter 3 - Group delay.	86
A.1	Filter 1, Dimensions (a).	A-1
A.2	Filter 1, Dimensions (b).	A-2
A.3	Filter 1, Dimensions (c).	A-2
A.4	Filter 1, Dimensions (d).	A-3
A.5	Filter 1, Dimensions (e).	A-4
B.1	Filter 1 - MWO Simulation.	B-1
D.1	Filter 2 (Version1), Dimensions (a).	D-1
D.2	Filter 2 (Version 3), Dimensions (a).	D-2
D.3	Filter 2 (Version 3), Dimensions (b).	D-2
D.4	Filter 2 (Version 3), Dimensions (c).	D-3
E.1	Filter 3 (Version1), Dimensions (a).	E-1
E.2	Filter 3 (Version 3), Dimensions (a).	E-2
E.3	Filter 3 (Version 3), Dimensions (b).	E-3
E.4	Filter 3 (Version 3), Dimensions (c).	E-4

List of Tables

2.1	Equivalent open-wire line circuits for two TEM networks [3].	29
4.1	Calculated unloaded Q results.	62
5.1	The External Quality factors and Coupling coefficients.	69
5.2	Required input parameters for the Interdigital Filter 2 design.	78
5.3	Interdigital Filter 2 bar spacings.	78
5.4	Required input parameters for the Interdigital Filter 3 design.	82
5.5	Interdigital Filter 3 bar spacings.	83

List of Abbreviations

BW	Bandwidth
dBc	Decibel relative to carrier
dBm	Decibel relative to one milliwatt
CST	CST Microwave Studio (3D EM simulation software)
DFE	Digital Front End
IF	Intermediate Frequency
IFDF	Ideal Frequency Domain Filter
ITDF	Ideal Time Domain Filter
LNA	Low Noise Amplifier
LO	Local Oscillator
MW	Microwave
PCB	Printed Circuit Board
PRF	Pulse Repetition Frequency
Ra	Roughness of a surface
Radar	Radio Detection And Ranging
RF	Radio Frequency
RFE	RF Front End
RMS	Root Mean Square

LIST OF ABBREVIATIONS

xiii

SMA	Sub-Miniature Version A (connector)
SNR	Signal to Noise Ratio
TEM	Transverse Electromagnetic
TWT	Traveling-wave Tube (high power amplifier)
VHF	Very High Frequency
VME	Versa Module European
VNA	Vector Network Analyser
Q	Quality Factor

List of Symbols

Constants:

$$\pi = 3.1415926535897932384626433832795$$

$$\epsilon_0 = 8.854 \times 10^{-12} \text{ F/m}$$

$$\eta_0 = 376.7 \Omega$$

$$\mu_0 = 4\pi \times 10^{-7} \text{ H/m}$$

Chapter 1

Introduction

Coaxial Resonator Filters are the most commonly used filters in the low microwave range of frequencies and is of great importance in radar systems, a large number of which operate in this frequency band.

The thesis presents the design of various coaxial resonator filters for radar applications. A basic background to radar signals and discussion of typical filters in such a system are presented in this introduction, followed by a number of designs and measurements.

In the following chapters a very detailed analysis of the influence of machining and plating processes on the quality factor (Q) of coaxial resonators are presented, and it is shown that silver plating is a key aspect of Q improvement.

1.1 Introduction to filtering radar signals [1]

A radar system works on the principle of transmitting an electromagnetic wave towards an object. The wave is then reflected back from the target, to the radar's receiver where, through signal processing, various characteristics of the object can be derived. Continuous wave (CW) radars emit an unmodulated wave and rely on Doppler shift to measure the radial velocity of targets. Uses of such radars include the measuring of vehicle speed, and in sport activities where the speed of the ball is of importance, i.e. tennis and golf. These radars cannot measure the range to the target. To measure the range to a target, the illuminating waveform must be coded in some way, so that the time taken for the wave to propagate to the target and back can be measured. This time is given by

$$T_{return}(R) = \frac{2R}{c} \quad (1.1)$$

where R is the range to the target and c is the velocity of propagation of EM waves.

Typical coding schemes include amplitude modulation as in pulse radars, phase modulation as in frequency modulated CW radars, and combinations of amplitude and phase modulation as in pulse compression radars.

In what follows, pulsed radar signals will be analysed to arrive at the filtering requirements in modern radar systems. Similar considerations apply to phase-modulated signals. The discussion will be restricted to simple unchirped pulses, such as the pulse produced by the matched filter in a pulse compression radar.

The effective duration of a pulse $s(t)$ is defined as the duration of a rectangular pulse $p(t)$ with the same peak amplitude and with the same area as $s(t)$, namely

$$T_{eff} = \frac{\int_{-\infty}^{\infty} s(t) dt}{s(t)_{max}}. \quad (1.2)$$

The range resolution ΔR of a radar quantifies the ability to distinguish between two closely spaced targets of the same radar cross section and is directly dependent on the duration of the transmit pulse. Two targets can be distinguished if their return echoes arrive at the receiver with a greater time difference than the duration of the transmit pulse. It is calculated from $T_{eff} = T_{return}(R + \Delta R) - T_{return}(R)$ as

$$\Delta R = \frac{cT_{eff}}{2}. \quad (1.3)$$

It is clear that the ability of a radar to distinguish between echoes from targets with different radar cross sections will be impaired by ringing after the pulse, which is also known as range side-lobes.

A rectangular pulse is often used as an ideal waveform for a radar, since it has sharply defined edges and no ringing. It is however not a waveform that can be used in a real radar system because of its excessive bandwidth requirements and because of the difficulty to prevent ringing during filtering of the signal in the radar transceiver.

An concise review of radar signals will follow with the purpose of developing an understanding for the filtering requirements in the RF and IF stages of a modern radar transceiver.

1.2 Radar signal theory [1]

1.2.1 Rectangular and shaped pulses

In the time domain, a radar transmit pulse is obtained by modulating a RF carrier with a pulsed signal, as shown in Figure 1.1.

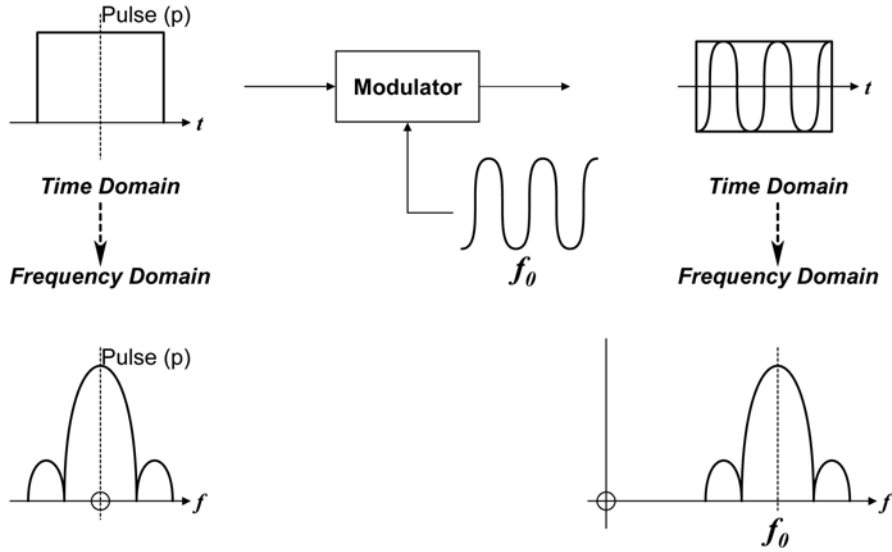


Figure 1.1: Generation of a transmit pulse in the time domain and the corresponding frequency domain spectra of the modulating and modulated signal.

In the frequency domain, the spectrum of the RF pulse can be found by translating the spectrum of the modulating signal, as shown in Figure 1.1. Clearly, all the information in the RF pulse is present in the modulating baseband signal. To arrive at the properties of radar signals, we restrict our analysis to baseband signals. These may, in general, include complex signals of the form

$$s(t) = \text{Re} \{s(t)\} + j \text{Im} \{s(t)\} = i(t) + jq(t). \quad (1.4)$$

The energy spectrum of a rectangular pulse $p(t)$ with unit amplitude and duration T seconds that is centred on the time origin is calculated with the Fourier transform and is given by

$$S(f) = \int_{-\frac{T}{2}}^{\frac{T}{2}} 1 \cdot e^{-j2\pi ft} dt = \frac{\sin(\pi f T)}{\pi f}. \quad (1.5)$$

The spectrum is shown in Figure 1.2(a) for a pulse with duration $T = T_{eff} = 1$ s. The magnitude of the spectrum in decibels is shown in Figure 1.2(b).

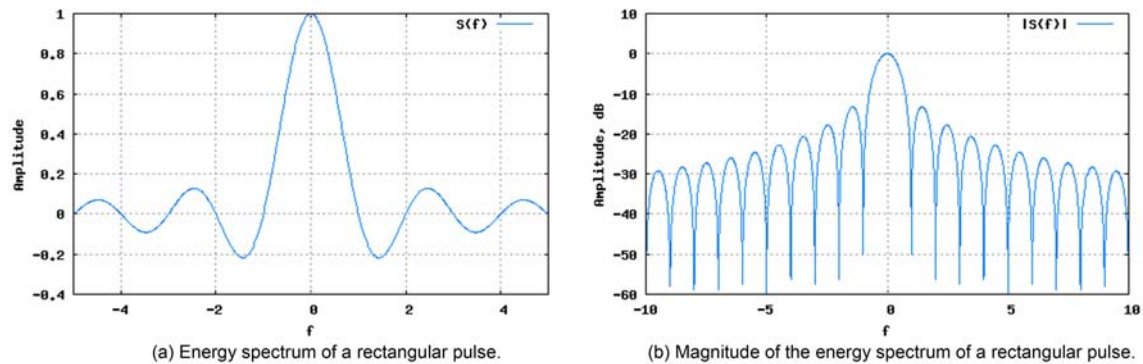


Figure 1.2: Spectra of the rectangular pulse of duration $T = 1$.

It can be noted that the signal has an unacceptably wide bandwidth and wastes both power and available radar spectrum.

One way to reduce the bandwidth is by using a suitable analogue filter, such as a Gaussian filter, which will produce an approximate Gaussian pulse. This approach severely limits the flexibility of the radar system, since different filters would be required for different waveforms.

The cosine-squared pulse is an example of a finite-duration shaped pulse. The effective duration of this pulse is the same as the -6 dB duration of the pulse. A cosine-squared pulse with a duration of $T_{eff} = 1$ s is defined by

$$s(t) = \cos^2(\pi t/2) \quad |t| < 1 \quad (1.6)$$

$$s(t) = 0 \quad |t| < 1 \quad (1.7)$$

and is shown in Figure 1.3.

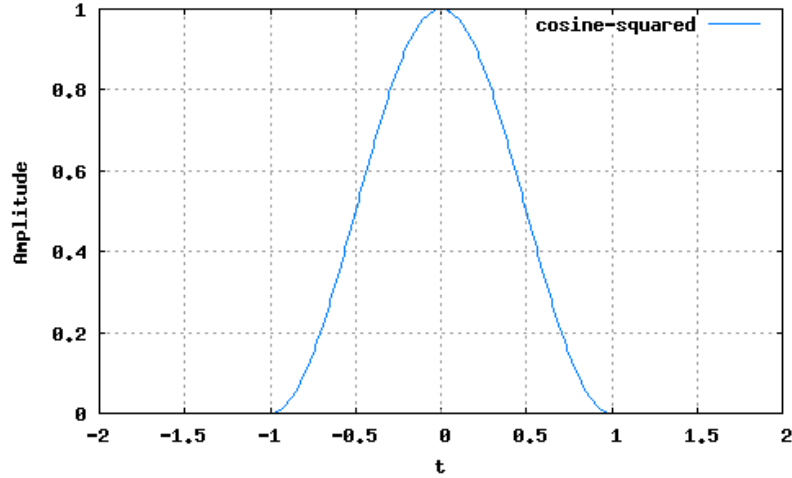


Figure 1.3: Cosine-squared pulse with duration $T_{eff} = 1$.

The energy spectrum of this pulse is shown in Figure 1.4.

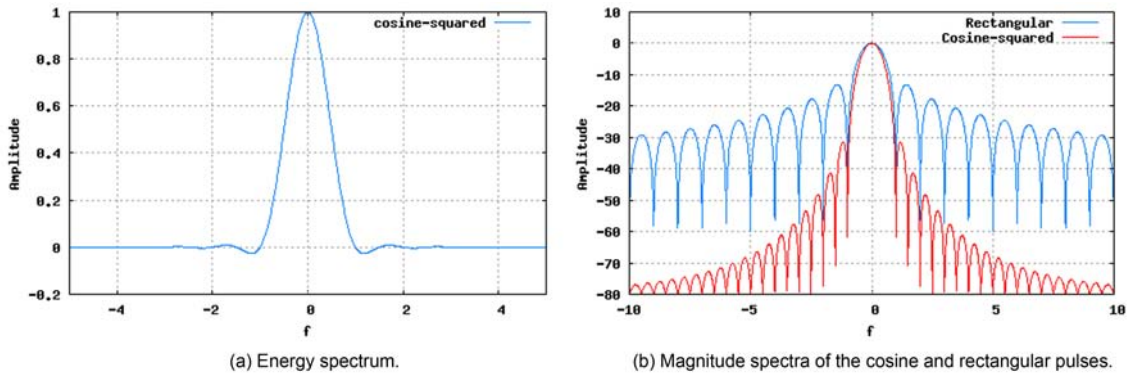


Figure 1.4: Spectra of the cosine-squared pulse.

The cosine-squared pulse utilizes far less of the available frequency spectrum, compared to the rectangular pulse in a practical radar system. Virtually all of the energy in the signal is contained in a bandwidth $\Delta f = \frac{2}{T_{eff}}$, between the first zeros of the spectrum adjacent to the origin.

1.2.2 Signal duration

The RMS duration of a signal $s(t)$ centred on the time origin is defined as

$$D_t = \sqrt{\frac{\int_{-\infty}^{\infty} t^2 |s(t)|^2 dt}{\int_{-\infty}^{\infty} |s(t)|^2 dt}}. \quad (1.8)$$

A 1 s long rectangular pulse has a RMS duration of 0.289 s, whereas a cosine-squared pulse with similar duration, has a RMS duration of only 0.245 s.

From the properties of the Fourier transform it is known that, if $F(\omega) = A(\omega)e^{j\phi(\omega)}$ is the Fourier transform of $F(t)$, then

$$\frac{dF}{d\omega} = \left(\frac{dA}{d\omega} + jA \frac{d\phi}{d\omega} \right) e^{j\phi} \leftrightarrow -jtf(t). \quad (1.9)$$

Parseval's formula states that

$$\int_{-\infty}^{\infty} |f(t)|^2 dt = \frac{1}{2\pi} \int_{-\infty}^{\infty} |F(\omega)|^2 d\omega. \quad (1.10)$$

Noting that

$$\left| \frac{dF}{d\omega} \right|^2 = \left(\frac{dA}{d\omega} \right)^2 + A^2 \left(\frac{d\phi}{d\omega} \right)^2 \quad (1.11)$$

it follows that

$$\int_{-\infty}^{\infty} t^2 |s(t)|^2 dt = \frac{1}{2\pi} \int_{-\infty}^{\infty} \left[\left(\frac{dA}{d\omega} \right)^2 + A^2 \left(\frac{d\phi}{d\omega} \right)^2 \right] d\omega \quad (1.12)$$

from which follows that

$$D_t^2 = \frac{\int_{-\infty}^{\infty} t^2 |s(t)|^2 dt}{\int_{-\infty}^{\infty} |s(t)|^2 dt} = \frac{1}{2\pi} \frac{\int_{-\infty}^{\infty} \left[\left(\frac{dA}{d\omega} \right)^2 + A^2 \left(\frac{d\phi}{d\omega} \right)^2 \right] d\omega}{\int_{-\infty}^{\infty} A^2 dt} \quad (1.13)$$

Clearly, the duration of a signal with a given amplitude spectrum is minimised if $\frac{d\phi}{d\omega} = 0$. For real pulsed signals with even symmetry around the origin, $\phi = 0$, therefore these signals are of minimum duration. If such a signal with RMS duration D_t is passed through a filter with transfer function

$$H(j\omega) = 1e^{-j\phi(\omega)}$$

and group delay

$$\tau_g = \frac{d\phi}{d\omega}, \quad (1.14)$$

the duration D_{tr} of the resultant signal will be related to the duration D_t of the original signal by

$$D_{tr}^2 = D_t^2 + \frac{1}{2\pi} \frac{\int_{-\infty}^{\infty} A^2 \tau_g^2 d\omega}{\int_{-\infty}^{\infty} A^2 dt}. \quad (1.15)$$

Equation 1.13 shows that ripples in the amplitude response of the filter will also increase the duration of the signal.

We conclude that in order to preserve the shape of the transmit pulse, the amplitude responses of the filters in the transceiver should remain constant while the differential group delay of the responses should be limited to typically less than 10% of the effective pulse duration within a (bandpass) bandwidth $\Delta f = \frac{2}{T_{eff}}$, where most of the energy of the pulse signal is concentrated.

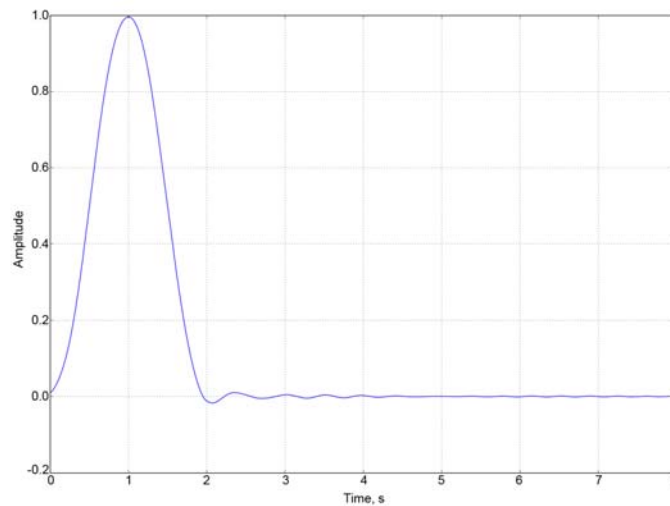


Figure 1.5: Differential group delay on a cosine-squared pulse.

Figure 1.5 shows the effect of differential group delay on a cosine-squared pulse. The pulse was passed through a filter with a phase response $\phi(\omega) = a\omega^5$, where a was chosen to produce a group delay of $T_{eff}/10$ at the frequency $f = \frac{1}{T_{eff}}$, corresponding to a band-pass bandwidth of $\frac{2}{T_{eff}}$. The first range side-lobe has an amplitude of -35 dB relative to the peak amplitude.

In early pulse-compression radars, zero-phase transmit pulses were passed through all-pass filters with parabolic phase to generate pulses of long duration, according to Equation 1.13. These pulses were then compressed by passing them through a filter with a complementary phase function that restored the phase of the pulse to a linear phase. In the time domain the output signal is a delayed version of the original pulse.

1.2.3 Detection of radar pulses

The power received by the radar in an echo is inversely proportional to the fourth power of the range to the target. To detect distant targets, the return signal must be processed to optimise the signal to noise ratio of the signal.

A matched filter is used to maximise the signal-to-noise ratio of a received pulse. The matched filter for a pulse $s(t)$ with spectrum $S(\omega)$ in a white noise background has a transfer function $G(j\omega) = S^*(\omega)$. The output $H(\omega) = S(\omega) \cdot G(j\omega)$ from the matched filter is the signal $|S(\omega)|^2$, which is a zero phase pulse and therefore a pulse of minimum duration. Matched filtering is equivalent to the correlation $h(t) = \int_{-\infty}^{\infty} s(t)s^*(t - \tau)d\tau$. In modern radars the matched filter is implemented digitally in the signal processor, usually as a correlator.

If the return from a point target is measured and used to define the matched filter, the matched filter will in principle compensate for the phase distortion of the transceiver, implying that the group delay specifications for filters in the transceiver may be relaxed. Even in this case, however, the designer of the transceiver must still keep a tight grip on group delay specifications, as ringing has further implications for the radar system. By way of example, ringing in the transmit pulse will force the designer to keep the receiver blocked by the transmit-receive switch for an unnecessary long time, limiting the minimum range of the radar.

1.3 Filter selection [1]

From the above discussion it is clear that the filters in the transceiver are not used to filter the radar signal, they should preferably leave the signal spectrum totally unscathed and leave this function to the matched filter. The important function of the filters in the transceiver is to reject unwanted signals.

Therefore, selecting the correct filter response is extremely important. Choosing the Tchebyscheff filter as approximation for the ideal “brick wall” filter response, is more efficient than, for example, the Gaussian filter approximation. To illustrate this further, consider Figure 1.6. If one compares the time domain responses of Gauss and Tchebyscheff filters with the same 50 dB attenuation frequency, it shows that a lossy Tchebyscheff filter is the best choice in this particular case.

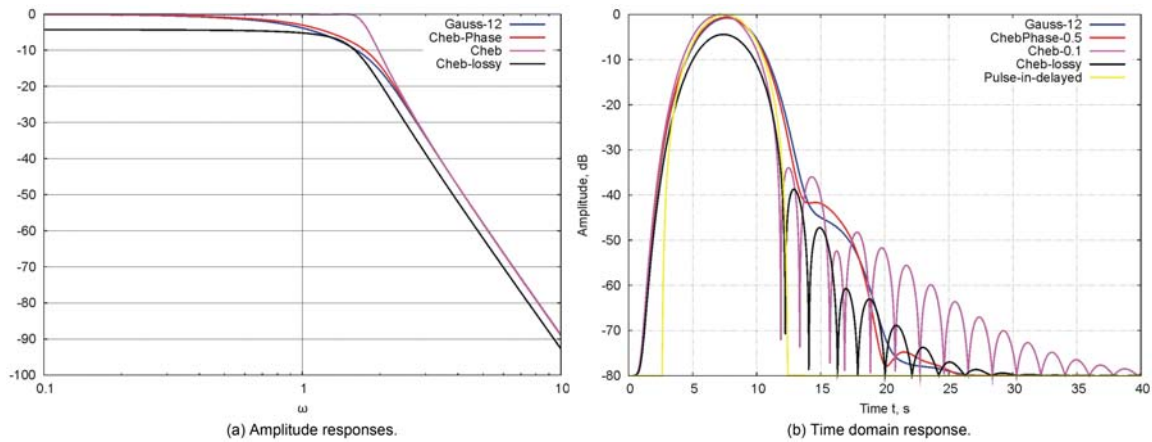


Figure 1.6: Comparison of the time domain responses of different filter approximations with the same 50 dB attenuation frequency for a cosine-squared input pulse.

The most critical filter in a radar receiver, using IF sampling, is the final IF filter, which usually has the narrowest bandwidth. The same filter is usually used in the transmitter path of a radar with digital signal generation at the IF frequency. The signal therefore traverses this filter twice.

1.4 Filters in Radar systems

In Figure 1.7 a broadband Pulse-Doppler Radar system will be used as an illustration to define the different building blocks and filters needed to block unwanted signals in a radar system. There are two main areas, namely the up-converter (exciter) and the down-converter (receiver).

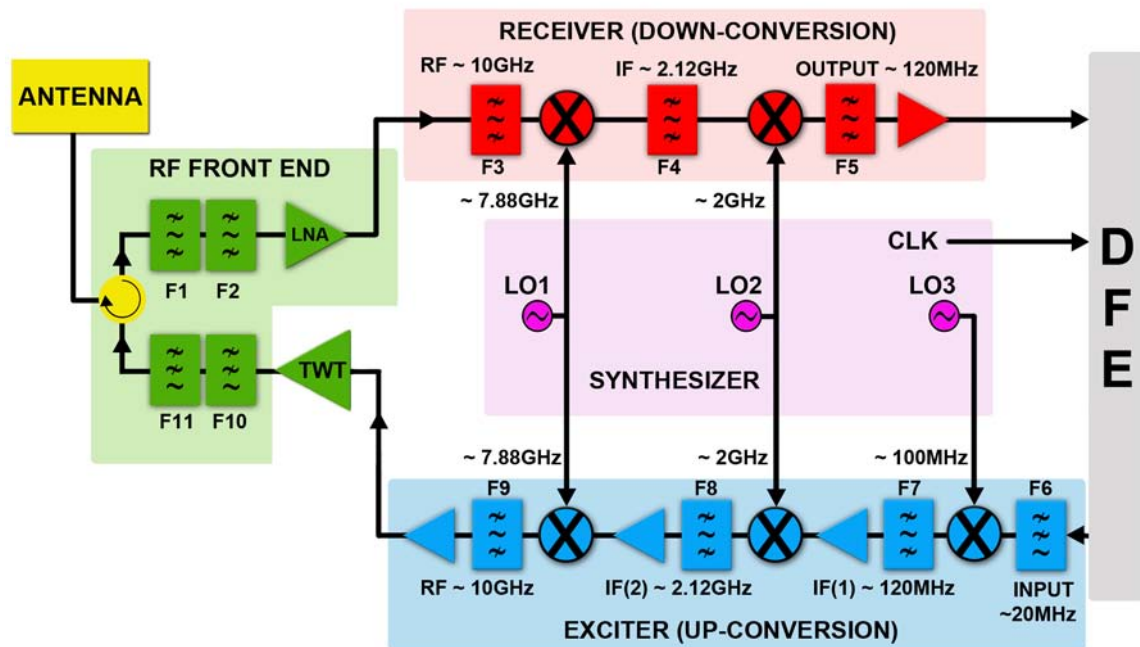


Figure 1.7: Pulse-Doppler Radar.

Up-conversion (Exciter) The Exciter generates a highly stable, low-power signal by converting the intermediate frequency (IF) to the radar band frequency (RF). The low-power signal is then amplified by the high power amplifier (TWT) in the transmitter and transmitted by the RF Front End (RFE) and antenna. Depending on the amount of power transmitted, the section from the transmitter to the antenna consists mostly of a waveguide run [2].

- **Filter F6 stage-** The input signal for the up-conversion chain is generated by the Digital Front End (DFE). This signal is generated around 20 MHz centre frequency by a digital to analogue converter which is clocked at 100 MHz. The low pass filter (F6) will remove the image at 80 MHz (100 MHz - 20 MHz) and the fifth harmonic around 120 MHz (because the first IF is 120 MHz). *This filter is usually constructed on PCB substrate (Lumped element filters).*
- **Filter F7 stage-** The signal is then up-converted to the first IF signal (120 MHz) by modulator LO3 and filtered by F7. This bandpass filter attenuates the 100 MHz LO3 signal as well as the modulator image located around 80 MHz

(100 MHz - 20 MHz). This filter is usually constructed on PCB substrate (Lumped element filters). The differential group delay for this filter must be less than 7.5 ns for a 20 MHz band around the centre frequency.

- **Filter F8 stage-** The 120 MHz signal is up-converted to the second IF signal (2120 MHz) by modulator LO2. This filter is a high order filter and must attenuate the leakage signal of the 2000 MHz LO2 modulator as well as to remove its generated image. This filter must not change the pulse shape significantly. Due to the high order and frequency, this filter cannot be constructed from Lumped elements, but rather from Microwave filter principles. *Figure 1.8 is an illustration of a sixth order Compline filter that can be used for F8. The differential group delay for this filter must be less than 1 ns for a 20 MHz band around the centre frequency.*

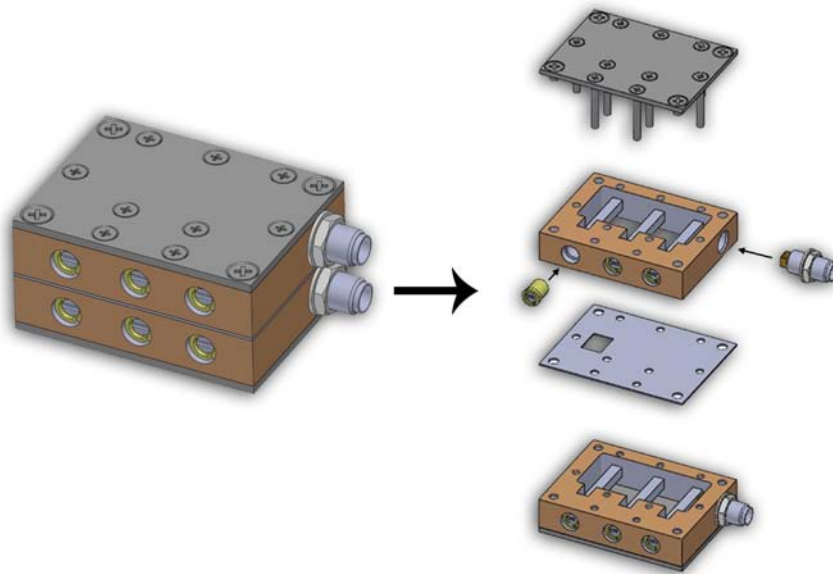


Figure 1.8: Compline filter.

- **Filter F9 stage-** The 2120 MHz signal is up-converted to the RF frequency (10 GHz band) by modulator LO1. This filter is a high order filter that must remove the LO1 signal leaking from the mixer, as well as its image. It must also pass the transmitted signal with no significant effect on the pulse shape. This filter is constructed from Microwave filter principles. *Figure 1.9 is an illustration*

of a sixth order Interdigital filter that can be used for F9. The differential group delay for this filter must be less than 1 ns for any 20 MHz band within the passband.

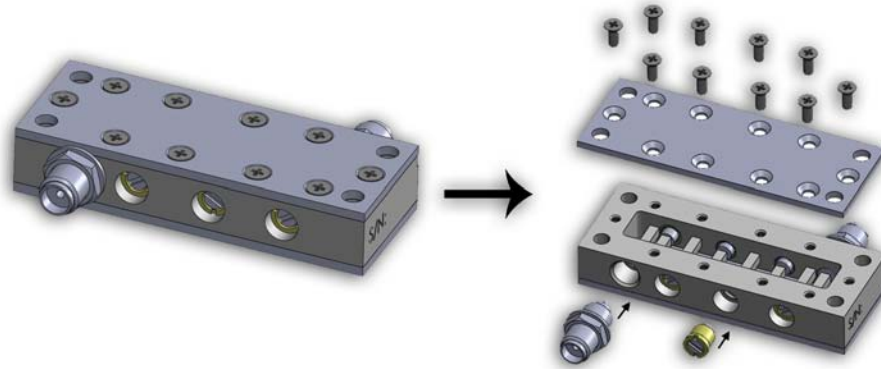


Figure 1.9: Interdigital Filter.

- **Filter F10 and Filter F11 stage-** The output RF signal is amplified by the high power amplifier (TWT) in the transmitter and sent through to the RF Front End (RFE). The high power signal is routed through F10 and F11, a waveguide absorptive filter and a waveguide harmonic filter. These filters must attenuate all harmonics from the high power amplifier (TWT). These filters are also constructed from Microwave filter principles. *Figure 1.10 is an illustration of a Waffle-Iron Harmonic (Lowpass) filter that can be used for F11.*

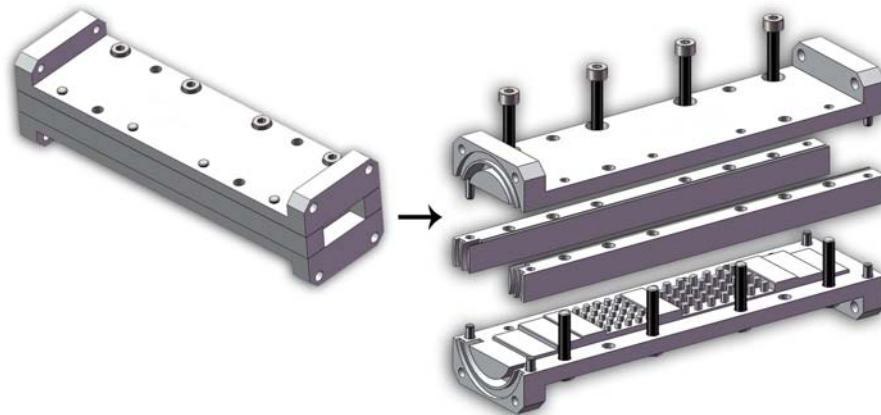


Figure 1.10: Waffle-Iron Harmonic Filter.

Down-conversion (Receiver) The first filter in the Receiver defines the acceptance bandwidth of the receiver. Thereafter, the Receiver amplifies and filters the received signal by converting the radar band (RF) frequency into an intermediate (IF) frequency. Multiple intermediate frequency translations are generally preformed to avoid problems with image frequencies [2].

- **Filter F1 and F2 stage-** This filter defines the receiver acceptance bandwidth of the radar and attenuates all out of band signals with >80 dB. The filter should pass signals within the radar bandwidth with the least possible reflections and must have very low loss. It also prevents radiation from LO1 leaking out of the receiver. Due to the low loss requirements (low noise figure) and sharp cut-off frequency, this filter is normally constructed in waveguide. *Figure 1.11 shows an example of a waveguide bandpass filter, cascaded with a waveguide harmonic filter, which can be used for filter F1. The differential group delay for this filter must be less than 1 ns for any 20 MHz band within the passband.*

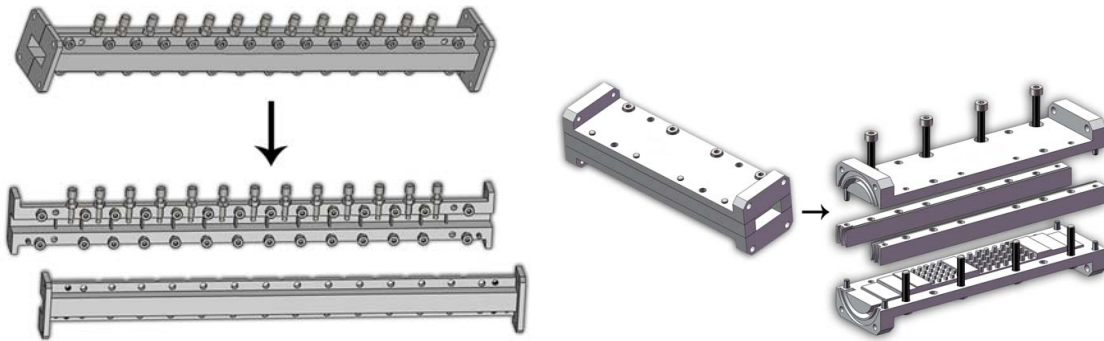


Figure 1.11: Waveguide Band Pass and Harmonic Filter.

- **Filter F3 stage-** The low noise amplifier (LNA) amplifies the respective receiver band. Next, the signal can be divided into more than one identical channel, depending on the radar topology. For this illustration, only one channel will be illustrated. Filter F3 prevents coupling of the IF (2120 MHz) signal between channels. It must pass signals in the radar bandwidth without distortion and attenuate all out of band signals. Due to the frequency, this filter is constructed from Microwave filter principles. *Figure 1.12 is an illustration of a third order Interdigital filter that can be used for F9. The differential group delay for this filter must be less than 1 ns for any 20 MHz band within the passband.*

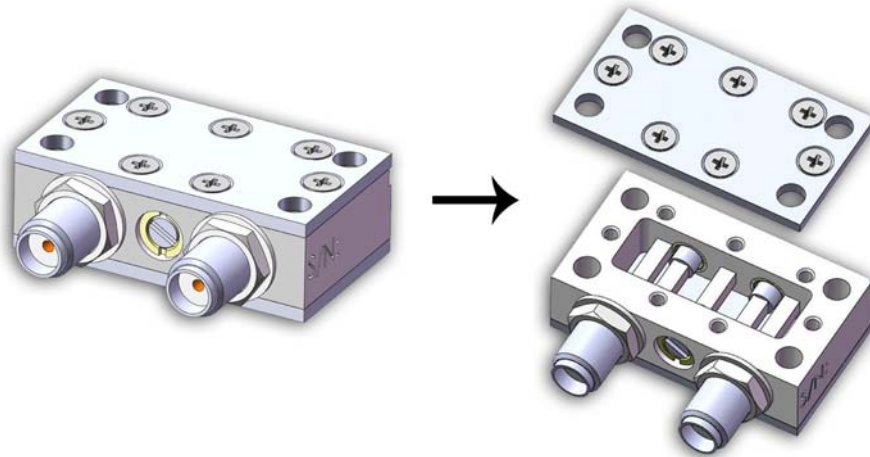


Figure 1.12: Third Order Interdigital Filter.

- **Filter F4 stage-** The received signal is down-converted to the first IF (2120 MHz) signal by modulator LO1, where it is filtered by the F4 filter. A high order filter is selected to filter out the image from the second mixer, which can pass through F1. Additionally, also attenuates the LO1 signal from the first mixer. This filter must not change the pulse shape significantly. *This filter is identical to filter F8 in the exciter. The differential group delay for this filter must be less than 1 ns for a 20 MHz band around the centre frequency.*
- **Filter F5 stage-** The first IF (2120 MHz) signal is down-converted to the second IF (120 MHz) by modulator LO2. This filter must filter out the image from the third mixer, which can pass through F1. The output signal from Filter F5 is converted to digital format by an analog to digital converter. The system uses IF sampling. *This filter is usually constructed on PCB substrate (Lumped element filters). The differential group delay for this filter must be less than 7.5 ns for a 20 MHz band around the centre frequency.*

1.5 Layout of the Thesis

Chapter 2 will discuss the well-known Tchebyscheff LC-ladder prototype filter which will be used to derive a generalised bandpass filter. From this, a generalised Combline- and Interdigital filter will be obtained.

In Chapter 3, three basic implementation parameters will be considered. These parameters play a critical role in the realisation and improvement of a microwave filter.

Chapter 4 discusses the various methods and limitations in the mechanics of a microwave filter. Thirteen different resonators will be analyzed in terms of their unloaded quality factor and the in-depth results will be discussed. Each resonator will be unique in method of manufacturing, polishing, as well as plating.

The design, modelling, optimisation and measured response of a Compline- and two Interdigital filters will be examined in Chapter 5.

The thesis will be concluded in Chapter 6.

Chapter 2

Coaxial Filters

2.1 Introduction

In this chapter the well-known Tchebyscheff LC-ladder prototype filter will be used to derive a generalised bandpass filter. This will then be used to obtain a generalised Compline- and Interdigital filter.

2.2 Tchebyscheff lowpass filter

The filter responses in this thesis are derived from the well known lumped Tchebyscheff lowpass filter prototype circuit, as shown in Figure 2.1(a). Its dual is shown in Figure 2.1(b). Both prototype topologies, give identical responses. The Tchebyscheff filter response was chosen, because of the sharper cut-off rate compared to Butterworth filters of similar order [3].

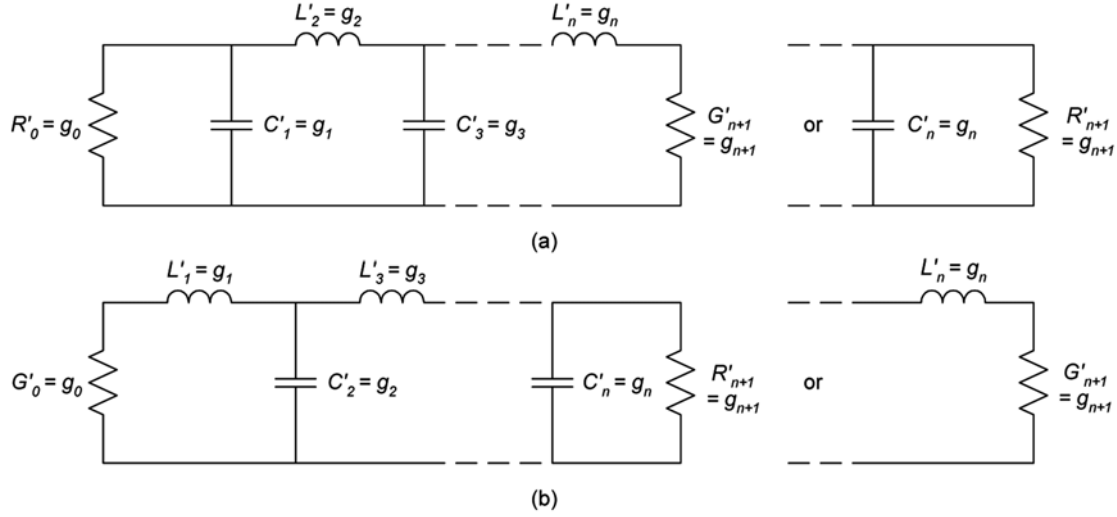


Figure 2.1: Techebyscheff lowpass filter and its corresponding dual circuit shown in (b).

The normalised lowpass prototype filter element values, for a Techebyscheff response with L_{Ar} dB passband ripple, $g_0 = 1$, and a ripple bandwidth of $\omega'_1 = 1$, are as follows [4],

$$C'_k = \frac{g_k}{2\pi f} \quad (2.1)$$

$$L'_k = \frac{g_k}{2\pi f} \quad (2.2)$$

$$g_1 = \frac{2a_1}{\sinh \left\{ \frac{\ln \left[\coth \left(\frac{L_{Ar}}{17.37} \right) \right]}{2n} \right\}} \quad (2.3)$$

$$g_k = \frac{4a_{k-1}a_k}{b_{k-1}g_{k-1}}, \quad k = 2, 3, \dots, n \quad (2.4)$$

$$g_{n+1} = \coth^2 \left\{ \frac{\ln \left[\coth \left(\frac{L_{Ar}}{17.37} \right) \right]}{4} \right\} \quad \text{for } n \text{ even}, \quad (2.5)$$

$$g_{n+1} = 1 \quad \text{for } n \text{ odd} \quad (2.6)$$

$$a_k = \sin \left(\frac{(2k-1)\pi}{2n} \right), \quad k = 1, 2, \dots, n \quad (2.7)$$

$$b_k = \sinh^2 \left\{ \frac{\ln \left[\coth \left(\frac{L_{Ar}}{17.37} \right) \right]}{2n} \right\} + \sin^2 \left(\frac{k\pi}{n} \right), \quad k = 1, 2, \dots, n \quad (2.8)$$

where

f = ripple (not 3 dB) corner frequency (Hz)

$R'_0 = g_0$ = source resistance (Ω)

$R'_{n+1} = g_{n+1}$ = required load resistance (Ω)

L_{Ar} = passband ripple (dB)

n = number of components in filter

k = component number

According to [4], 3 dB bandwidth and ripple bandwidth are related by

$$\frac{f_{3dB}}{f_{ripple}} = \cosh \left[\frac{1}{n} \cosh^{-1} \left(\frac{1}{\sqrt{10^{L_{Ar}/10} - 1}} \right) \right]. \quad (2.9)$$

2.3 Coupled Resonator Bandpass Prototypes

The design of bandpass filters, using the lowpass to bandpass network transformation, usually result in component values that are difficult to realise in a microwave structure, but by using coupled resonators, this problem can be alleviated. The coupled resonators consist of identical shunt or series resonators which couple to each other, through admittance or impedance inverters. For this reason, almost any type of resonator can be used. The main reason for using coupled resonator filters, is the high component quality factor (Q -factor) that can be achieved, resulting in low insertion loss filters. The Q -factor of LC resonators at very high frequencies (VHF) are typically of the order of 150 - 500 due to the losses resulting from using inductors. The Q -factors of distributed resonators, such as helical and coaxial resonators, are usually limited by magnetic losses. The losses can be reduced by increasing the physical size of a resonator. The maximum size of a resonator is, however, limited by the appearance of higher order modes. Microwave filters using resonators with Q -factors of the order of a thousand can be realised with practical structures as shown in Chapter 5. The quality factor will be examined in more detail in section 3.4, but the focus for now is to obtain a generalised bandpass prototype circuit using coupled resonators.

To obtain a generalised bandpass prototype, admittance or impedance inverters are used to convert the lowpass prototype circuit into an equivalent lowpass form using only one type of reactive element. The equivalent lowpass prototype is then transformed into a bandpass equivalent. This process will be explained by using a lowpass prototype designed with shunt resonators and admittance inverters as an example [3, 5].

An admittance inverter also known as a J -inverter, displays an input admittance

Y_1 of

$$Y_1 = \frac{J^2}{Y_2} \quad (2.10)$$

when terminated at the output point with admittance Y_2 . In ideal inverters, J is a frequency independent constant. Various circuit topologies can be used as admittance inverters, as discussed in Matthaei, Young and Jones [3].

The inverting property of an inverter makes a series inductance with an inverter on each side look like a shunt capacitance from its exterior terminals. In a similar fashion a shunt capacitance with an inverter on both sides appears as a series inductance from its exterior terminals [5]. As seen in Figure 2.2, using admittance inverters, the circuit is the dual circuit of Figure 2.1(a). The admittance seen from capacitor C_{a1} is the same as that seen from capacitor C'_1 , except for a possible admittance scaling factor. Similarly, the admittances seen from C_{a2} are identical to that of C'_2 , except for a possible admittance scale change.

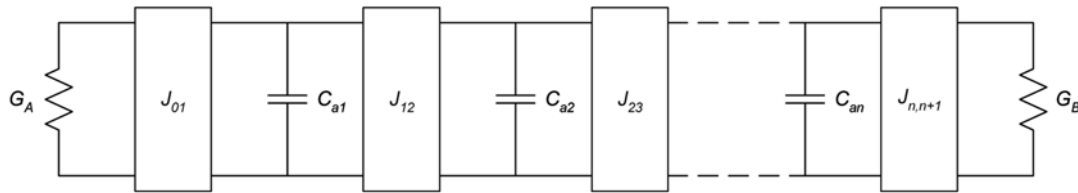


Figure 2.2: Lowpass prototype filter using admittance inverters [3].

A brief discussion will follow to derive the equations for a lowpass prototype circuit using admittance inverters [5].

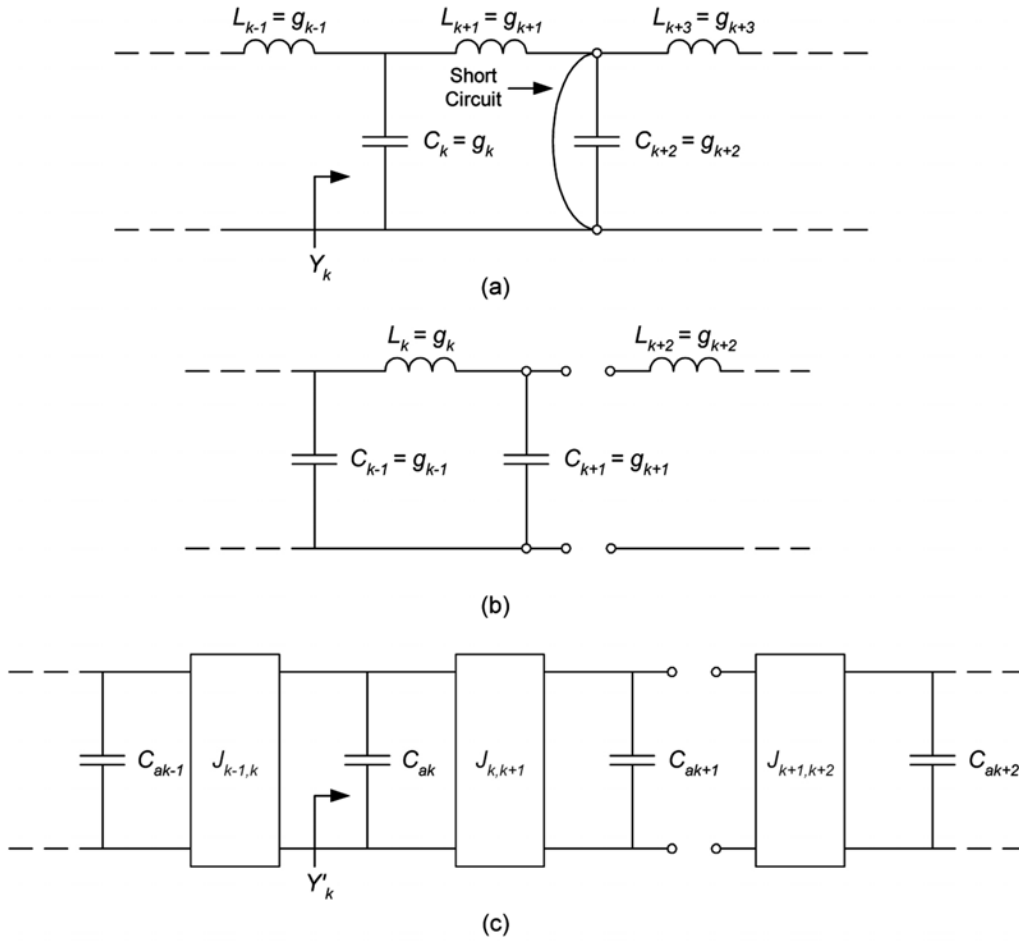


Figure 2.3: A section of the lowpass prototype shown in (a), and its dual in (b). The analogous J -inverter form of these two circuits are shown in (c).

A lowpass prototype circuit that has the node after the inductor L_{k+1} short-circuited to ground, as illustrated in Figure 2.3(a). The duality of the circuit is shown in Figure 2.3(b), where the short-circuit becomes an open-circuit. The series inductors transform to shunt capacitors and shunt capacitors transform to series inductors. Figure 2.3(c) is derived by replacing each series inductor in (b) with a shunt capacitor and an admittance inverter on either side [5].

Figure 2.3(a) and (c) are equivalent, so therefore the admittance can be compared at any two equivalent points. The admittance Y_k is equal to

$$Y_k = j\omega C_k + \frac{1}{j\omega L_{k+1}} \quad (2.11)$$

and by using Equation 2.10, Y'_k in Figure 2.3(c) is equal to

$$Y'_k = j\omega C_{ak} + \frac{J_{k,k+1}^2}{j\omega C_{ak+1}}. \quad (2.12)$$

Except for an admittance scaling factor of C_{ak}/C_k , the admittance Y_k must be identical to Y'_k . Therefore,

$$Y_k = \frac{C_{ak}}{C_k} Y'_k = j\omega C_{ak} + \frac{C_{ak}}{C_k} \frac{1}{j\omega L_{k+1}}. \quad (2.13)$$

Equating the second terms in Equation 2.12 and 2.13 leads to [5],

$$J_{k,k+1} = \sqrt{\frac{C_{ak}C_{ak+1}}{C_k L_{k+1}}} = \sqrt{\frac{C_{ak}C_{ak+1}}{g_k g_{k+1}}}. \quad (2.14)$$

This applies only for inverter parameters where $k = 1, 2, 3, \dots, n-1$ and not for the inverter parameter at the loaded end.

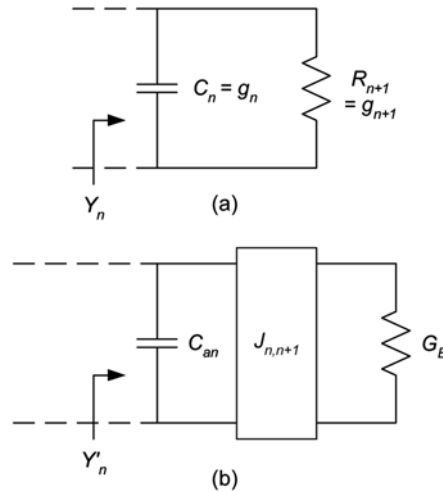


Figure 2.4: End section of the lowpass prototype circuit (a) and the corresponding end portion of Figure 2.2 is shown in (b).

Figure 2.4(a) and (b) will be used to calculate $J_{n,n+1}$. In Figure 2.4(a) the end section of the lowpass prototype circuit is shown, and (b) shows a corresponding form with a J-inverter. The admittance Y_n is equal to

$$Y_n = j\omega C_n + \frac{1}{R_{n+1}} \quad (2.15)$$

and

$$Y'_n = j\omega C_{an} + \frac{J_{n,n+1}^2}{G_B}. \quad (2.16)$$

Y'_n must be equal to Y_n within a scale factor of C_{an}/C_n and therefore Equation 2.15 becomes,

$$Y'_n = \frac{C_{an}}{C_n} Y_n = j\omega C_{an} + \frac{C_{an}}{C_n} \frac{1}{R_{n+1}}. \quad (2.17)$$

Equating the second terms in Equation 2.16 and Equation 2.17 leads to

$$J_{n,n+1} = \sqrt{\frac{C_{an}G_B}{C_n R_{n+1}}} = \sqrt{\frac{C_{an}G_B}{g_n g_{n+1}}}. \quad (2.18)$$

Similarly, it can be shown that

$$J_{01} = \sqrt{\frac{G_A C_{a1}}{g_0 g_1}}. \quad (2.19)$$

Now that the equations for Figure 2.2 have been derived, the lowpass prototype circuit can be transformed into an equivalent bandpass form. The bandpass filter that results from the lowpass prototype filter in Figure 2.1 is shown in Figure 2.5. Ideally, admittance inverters are independent of frequency, and therefore are left unchanged by the frequency transformation. The same applies for the source and load conductances [5, 3].

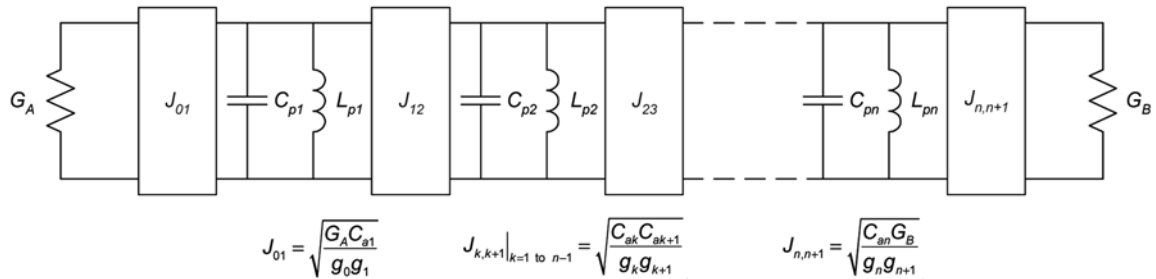


Figure 2.5: Lowpass filter transformed to the bandpass equivalent.

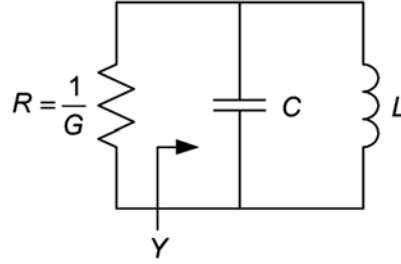


Figure 2.6: Lumped element shunt resonator.

The admittance seen looking into the reactive part of an LC resonator in Figure 2.6 can be defined as a function of frequency $\omega = 2\pi f$, namely

$$Y(j\omega) = jB(\omega) = j\omega C + \frac{1}{j\omega L} = j \left(\omega C - \frac{1}{\omega L} \right) \quad (2.20)$$

where $B(\omega)$ is the susceptance of the resonator. The circuit is resonant at a frequency ω_0 when $\omega_0 C = \frac{1}{\omega_0 L}$, or when $Y(j\omega_0) = 0$. ω_0 is given by

$$\omega_0 = \frac{1}{\sqrt{LC}}. \quad (2.21)$$

Once the input admittance of the resonator has been calculated, it is easy to determine the overall unloaded quality factor (Q -factor) of the resonator. This is accomplished by determining the susceptance slope parameter, which in turn is used to determine the resonance properties of resonators irrespective of their form. The susceptance slope parameter is calculated by

$$b = \frac{\omega_0}{2} \left. \frac{dB(\omega)}{d\omega} \right|_{\omega=\omega_0} = \frac{\omega_0}{2} \left(C + \frac{1}{\omega_0^2 L} \right) = \frac{\omega_0}{2} (2C) = \omega_0 C. \quad (2.22)$$

Equation 2.22 can be re-arranged as

$$C = \frac{1}{\omega_0} \left. \frac{dB(\omega)}{d\omega} \right|_{\omega=\omega_0}. \quad (2.23)$$

The quality factor of the shunt resonator is equal to

$$Q = \frac{\omega_0 C}{G}. \quad (2.24)$$

and quality factor expressed in terms of the susceptance slope parameter, becomes

$$Q = \frac{\omega_0 C}{G} = \frac{\omega_0 \left(\left. \frac{1}{2} \frac{dB(\omega)}{d\omega} \right|_{\omega=\omega_0} \right)}{G} = \frac{b}{G} \quad (2.25)$$

where

b = slope parameter of the shunt resonator

G = represent the losses of the shunt resonator

The circuit in Figure 2.5 can be generalised to accommodate any type of resonator. This is especially useful at microwave frequencies where it becomes very difficult to realise lumped elements.

Using Equation 2.22,

$$b_k = \omega_0 C_{pk} \quad (2.26)$$

where $k = 1, 2, 3, \dots, n - 1$.

The lowpass-to-bandpass transformation for a capacitor, C_p is

$$C_{pk} = \frac{\omega'_1 C}{B\omega_0}. \quad (2.27)$$

Submitting Equation 2.27 into Equation 2.26 it becomes,

$$b_k = \omega_0 C_{pk} = \omega_0 \left(\frac{\omega'_1 C_{ak}}{B\omega_0} \right) = \frac{\omega'_1 C_{ak}}{B}. \quad (2.28)$$

Thus,

$$C_{ak} = \frac{b_k B}{\omega'_1}. \quad (2.29)$$

The same holds for C_{ak+1} ,

$$b_{k+1} = \omega_0 C_{pk+1} = \omega_0 \left(\frac{\omega'_1 C_{ak+1}}{B\omega_0} \right) = \frac{\omega'_1 C_{ak+1}}{B}. \quad (2.30)$$

Thus,

$$C_{ak+1} = \frac{b_{k+1} B}{\omega'_1}. \quad (2.31)$$

Substituting Equation 2.29 and Equation 2.31 into Equation 2.32, yields

$$J_{k,k+1}|_{k=1 \text{ to } n-1} = \sqrt{\frac{C_{ak} C_{ak+1}}{g_k g_{k+1}}} = \sqrt{\frac{\left(\frac{b_k B}{\omega'_1} \right) \left(\frac{b_{k+1} B}{\omega'_1} \right)}{g_k g_{k+1}}} = \frac{B}{\omega'_1} \sqrt{\frac{b_k b_{k+1}}{g_k g_{k+1}}}. \quad (2.32)$$

Repeating the same process for J_{01} and $J_{n,n+1}$, yields

$$J_{01} = \sqrt{\frac{G_A C_{a1}}{g_0 g_1}} = \sqrt{\frac{G_A b_1 B}{\omega'_1 g_0 g_1}} \quad (2.33)$$

and

$$J_{n,n+1} = \sqrt{\frac{C_{an} G_B}{g_n g_{n+1}}} = \sqrt{\frac{b_n B G_B}{\omega'_1 g_n g_{n+1}}}. \quad (2.34)$$

The coupling coefficient can be viewed in more depth in section 3.3, but now using the general definition of the coupling coefficient [3],

$$k_{k,k+1}|_{k=1 \text{ to } k=n-1} = \frac{J_{k,k+1}}{\sqrt{b_k b_{k+1}}}. \quad (2.35)$$

Substituting Equation 2.32 into Equation 2.35 yields

$$k_{k,k+1}|_{k=1 \text{ to } k=n-1} = \frac{\frac{B}{\omega'_1} \sqrt{\frac{b_k b_{k+1}}{g_k g_{k+1}}}}{\sqrt{b_k b_{k+1}}} = \frac{B}{\omega'_1 \sqrt{g_k g_{k+1}}}. \quad (2.36)$$

The external quality factor at the source side, is determined by the susceptance of the first resonator $B_1(\omega)$ and the inverter coupled impedance G_A . Using Equation 2.10, 2.25, 2.33 and 2.34 the external quality factor at the source can be calculated by

$$Q_A = \frac{b_1}{(J_{01}^2/G_A)} = \frac{g_0 g_1 \omega'_1}{B} \quad (2.37)$$

and the external quality factor at the load side is equal to

$$Q_B = \frac{b_n}{(J_{n,n+1}^2/G_B)} = \frac{g_n g_{n+1} \omega'_1}{B}. \quad (2.38)$$

The generalised bandpass filter is shown in Figure 2.7 and the Equations for the external quality factors and coupling coefficients are valid for any type of resonator [3, 5].

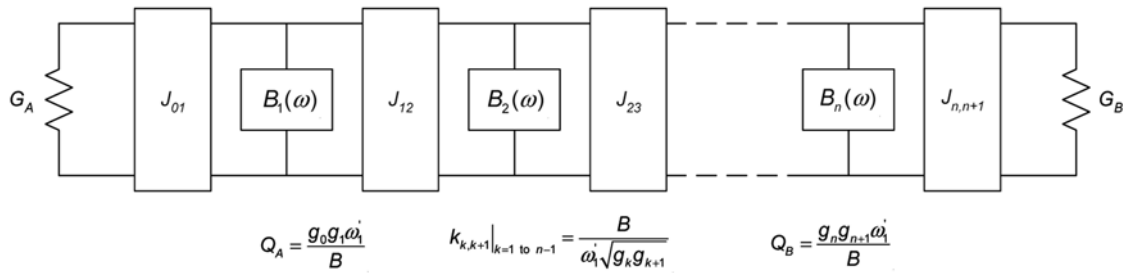


Figure 2.7: Generalised bandpass filter circuit, using admittance inverters and shunt resonators.

2.4 Parallel Coupled Transmission Lines

Every electrical connection that connects a signal to a load is a transmission line. Very few problems are encountered with the behaviour of transmission lines at DC levels and very low frequencies. However, at higher frequencies, short lengths of transmission lines can be used as impedance transformers, resonant circuits and even as capacitors or inductors.

Unshielded transmission lines in close proximity to each other are referred to as coupled transmission lines as shown in Figure 2.8(a). For two uniform parallel lines between ground planes, note that the C_{11} and C_{22} are the self capacitance, i.e. the capacitance per unit length between strip a and ground, and between strip b and ground. C_{12} is the mutual capacitance, i.e. the capacitance per unit length between the strips.

The representation in Figure 2.8 is valid for uniform TEM lines. These two lines in Figure 2.8 support two orthogonal field modes, namely: the even mode, where the currents of the lines are equal in amplitude and in the same direction, and the odd mode, where the currents of the lines are also equal in amplitude but in opposite directions [6].

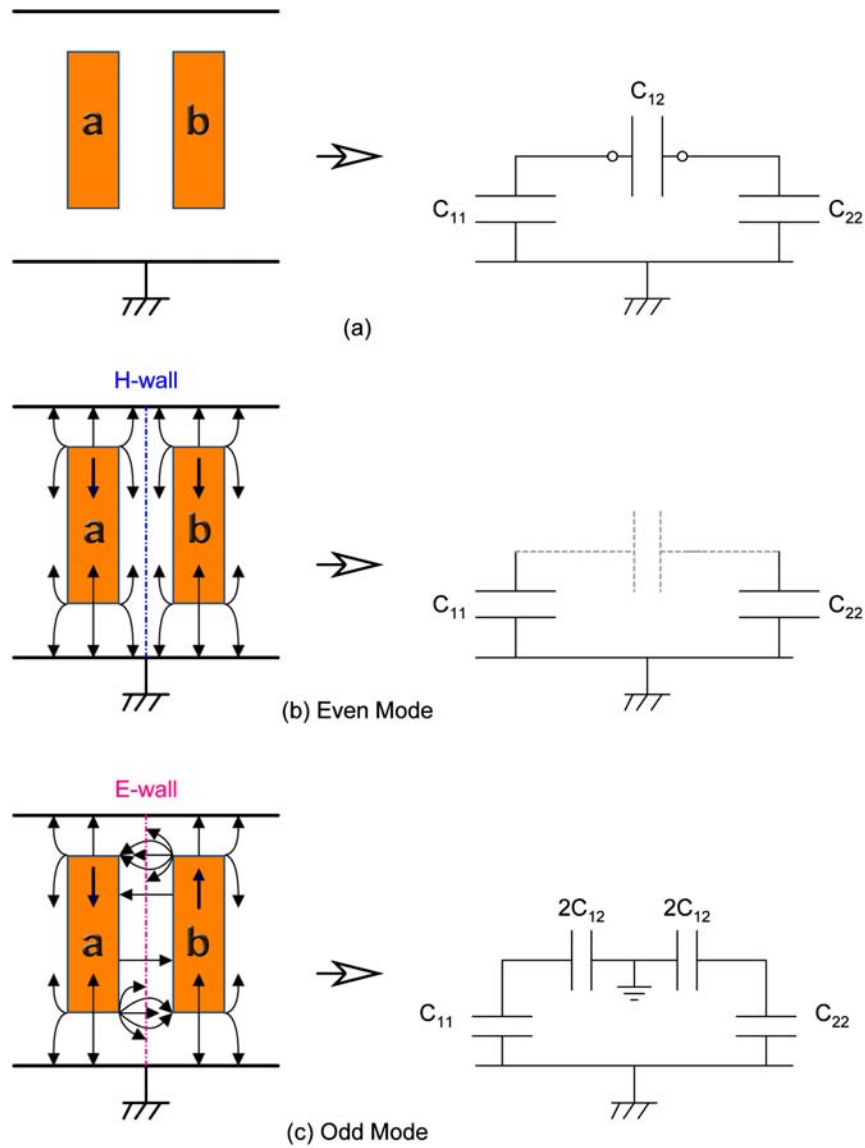


Figure 2.8: A three-wire coupled transmission line and its static capacitance network.

For the even mode, the electric field has even symmetry around the centre line. The voltage differential between the lines, found by integration of the electric field, is therefore zero. From this it is evident that there will be no current flow between the two transmission lines as shown in Figure 2.8(b). The resulting capacitance is

$$C_e = C_{11} = C_{22}. \quad (2.39)$$

Following this, the even mode characteristic impedance can then be calculated by

$$Z_{0e} = \sqrt{\frac{L}{C_e}} = \frac{\sqrt{LC_e}}{C_e} = \frac{1}{v_p C_e} \quad (2.40)$$

$$Y_{0e} = v_p C_e \quad (2.41)$$

where v_p is the phase velocity of propagation along the line, namely

$$v_p = \frac{1}{\sqrt{\mu\epsilon}}. \quad (2.42)$$

For the odd mode, the electric field was odd symmetry around the centre line and there will be a potential between the conductors, as shown in Figure 2.8(c). This can be thought of as a vertical equipotential line, $V = 0$, with respect to ground. For the purposes of admittance calculations, it can be substituted by a ground plane. The effected capacitance between either transmission line and ground is

$$C_0 = C_{11} + 2C_{12} = C_{22} + 2C_{12} \quad (2.43)$$

and the characteristic impedance for the odd mode is

$$Z_{0o} = \frac{1}{v_p C_o} \quad (2.44)$$

$$Y_{0o} = v_p C_o. \quad (2.45)$$

For a lossless uniform transmission line operating in the TEM mode, the characteristic admittance is related to its shunt capacitance by

$$Y_0 = vC = \frac{\sqrt{\epsilon_r}C}{\eta_0\epsilon} = \frac{\sqrt{\epsilon_r}C'}{\eta_0\epsilon} \quad (2.46)$$

where

v = the speed of propagation along the line

ϵ_r = relative dielectric constant of the medium

ϵ = permittivity of the medium

η_0 = impedance of free space

The dimensionless ratio $C' = \frac{C}{\epsilon}$ is used to calculate each of the capacitive components.

From this, one can derive ten coupling arrangements by either placing open- or

short-circuits on various terminal pairs, or by connecting the line ends together. Only two applicable arrangements were found for this thesis:

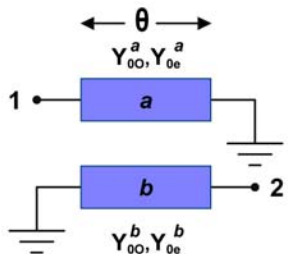
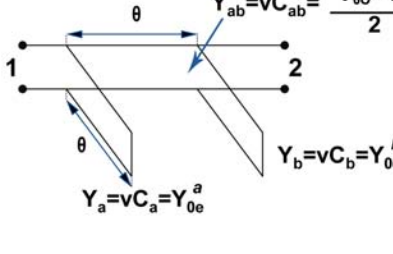
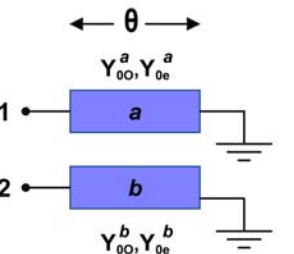
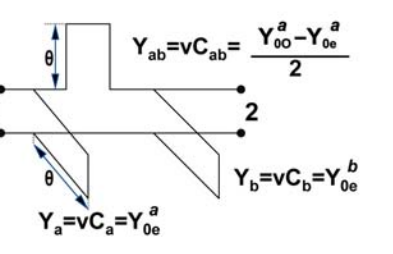
<i>TEM Circuit</i>	<i>Equivalent Open-Wire Line Circuit</i>
<p>1</p> 	
<p>2</p> 	

Table 2.1: Equivalent open-wire line circuits for two TEM networks [3].

The first arrangement in Table 2.1(1) is most commonly used as the building block for Interdigital filters. The circuit includes a -1:1 transformer, which is not shown due to the fact that it will not influence the filter amplitude or group delay.

The second arrangement in Table 2.1(2) is the building block for Compline filters.

2.5 Narrowband Coaxial Resonator Filters

A Compline or Interdigital filter design will be ideal when the response for these filters are similar to the generalised bandpass filter illustrated in Figure 2.7. To achieve this, the external quality factors and coupling coefficients of the Compline or Interdigital filter should be equal to that of the prototype circuit. Recall the two arrangements in section 2.4. Their transformations will be used as a basis to quantify an equivalent electrical circuit model for a Compline and Interdigital filter in this section.

2.5.1 Comblines Filter

A Comblines bandpass filter as shown in Figure 2.9 consists of transverse electromagnetic (TEM) line elements which are shorted at one end and have a lumped capacitance C_j between the opposite end and ground. Lines 1 to n , together with their related lumped capacitance C_1 to C_n form the resonators. Due to the presence of capacitance, the lines will be less than $\lambda_0/4$ long, where λ_0 is the propagation wavelength at midband in the specific medium. The Comblines filter has a transmission zero at the frequency where the line and coupling elements are a quarter wavelength long.

As seen in Figure 2.9 Comblines filters can use a termination line (a), probe coupling (b) or loop coupling (c) on both sides of the filter. In Figure 2.9(a) lines 0 and $n + 1$ are impedance-transforming sections of the filter. Coupling methods (b) and (c) will be discussed in section 3.2.

Coupling between the resonators are achieved by the fringing fields that surround them and the coupling is predominantly magnetic [3].

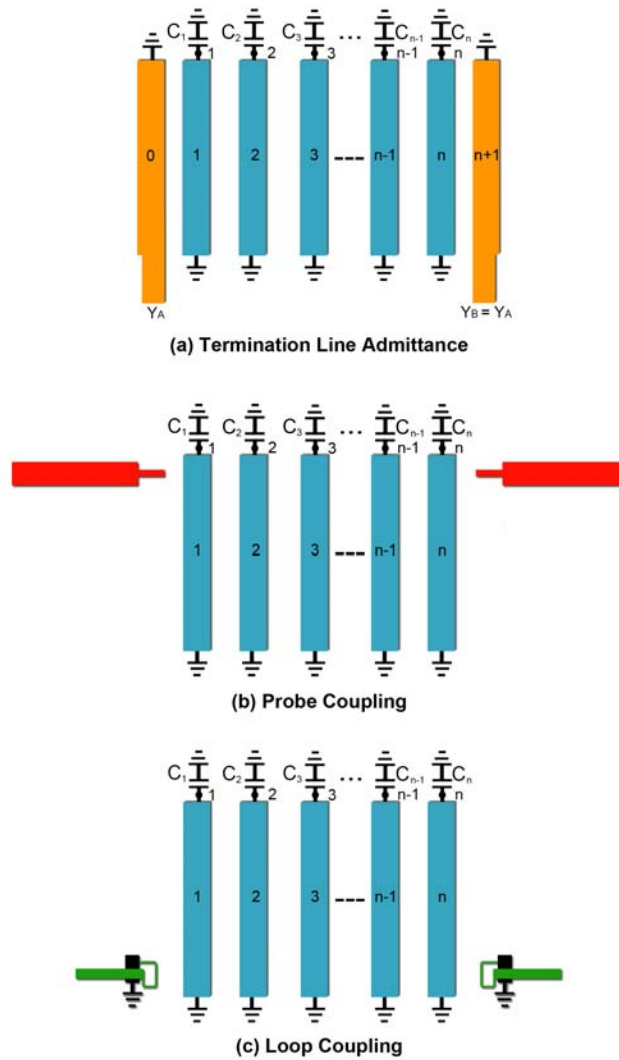


Figure 2.9: Compline Bandpass filter in strip-line form.

The physical size of a compline filter can be reduced by increasing the end capacitance, so that the resonator lines become $\lambda_0/8$ (or less) in length at resonance. A second pass band occurs when the resonator lines become longer than $\lambda_0/2$. If the resonator length is $\lambda_0/8$ at the primary pass band, then the second band will be centred at more than four times the primary passband center frequency [3].

The resonator line admittances Y_{aj} alter the level of admittance within the filter, which will in turn influence the unloaded Q 's that the resonators will have. The admittance Y_{aj} of approximately $0.0143 \text{ } \Omega$ (about $70 \text{ } \Omega$) is an acceptable choice for low loss in the resonator and with a high unloaded Q . It should also be noted that

77Ω gives the lowest loss in a coaxial line with air dielectric. The earth plane spacing should not exceed $\lambda/10$, otherwise additional modes can develop.

The transformation in Table 2.1(2) is used in Figure 2.10(a) to transform the Compline filter into an equivalent electrical circuit.

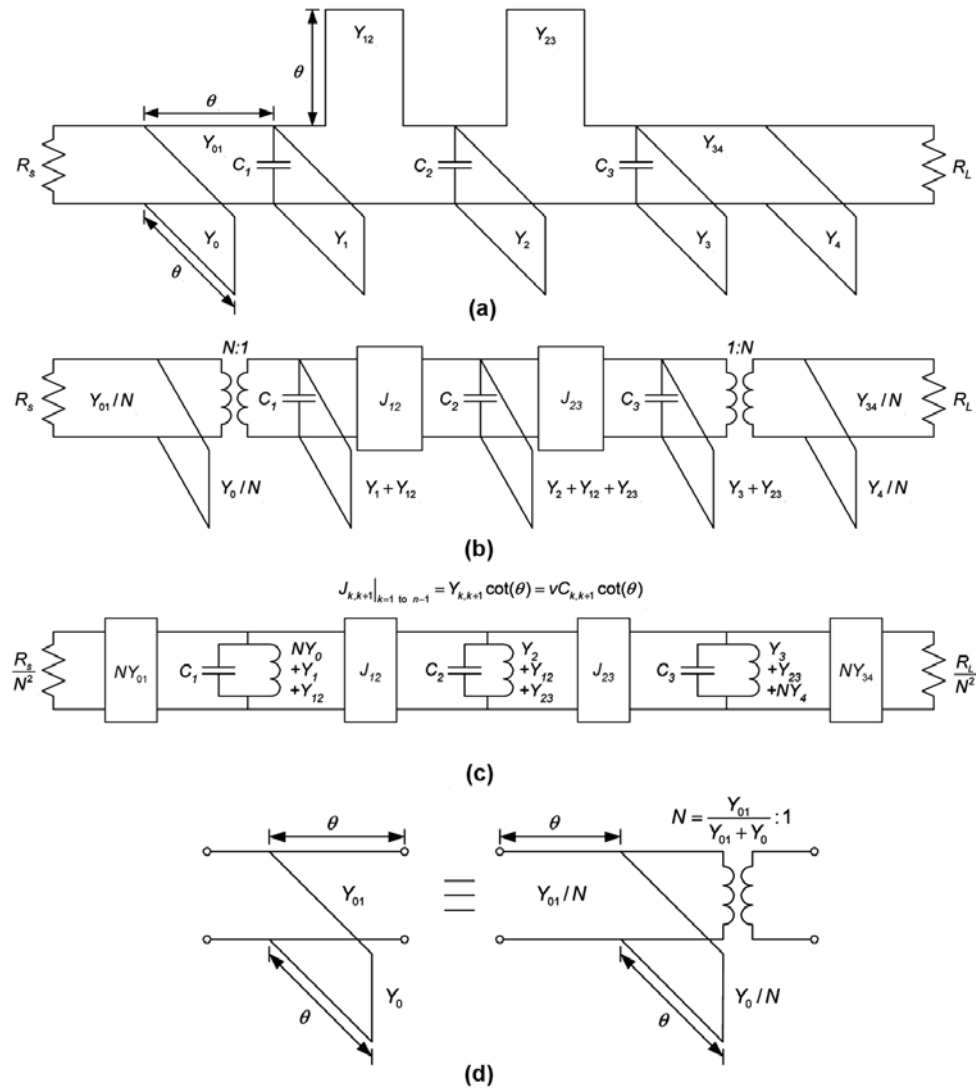


Figure 2.10: Electrical circuit of the Compline filter, together with one of Kuroda's identities.

The circuit in Figure 2.10(b) is obtained by a two step process. The Kuroda identity in Figure 2.10(d) is first applied to the source and load side of the circuit. In the second step, admittance inverters are obtained. This is done by adding additional lines of equal but opposite admittance in parallel with the resonator lines.

Figure 2.10(c) is obtained by replacing the short-circuited transmission lines in (b) with the S (Richards' variable)-plane inductors. This is possible because a short-circuited transmission line, in terms of Richards' variable, will behave like a lumped inductor of the value $L = Z_0$. All the circuitry connected to the exterior terminals of the transformers in (b) are transformed to the other side in (c). The circuit in Figure 2.10(c) has similar form compared to the generalised bandpass filter in Figure 2.7, i.e. it consists of shunt resonators and admittance inverters only.

The external quality factor at the source side can be calculated by considering the first section in Figure 2.10(c), as shown in Figure 2.11.

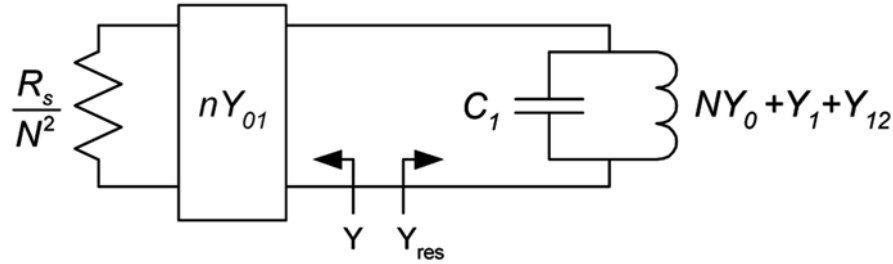


Figure 2.11: First section of a Combline filter circuit up to the first resonator.

The input impedance Z_{in} seen looking into a line with characteristic impedance Z_0 and length l , is given by

$$Z_{in} = Z_0 \frac{Z_L + jZ_0 \tan(\beta l)}{Z_0 + jZ_L \tan(\beta l)} \quad (2.47)$$

where Z_L is the load connected at the end of the transmission line. By using Equation 2.47, the admittance, Y , in Figure 2.11 becomes

$$Y = \frac{NY_{01} \left[\frac{N^2}{R_S} + jNY_{01} \tan(\theta) \right]}{NY_{01} + j\frac{N^2}{R_S} \tan(\theta)} = NY_{01} \frac{\frac{N}{R_S} + jY_{01} \tan(\theta)}{Y_{01} + j\frac{N}{R_S} \tan(\theta)} = g_S + jb_S. \quad (2.48)$$

It will be ideal when b_S is equal to zero and can only happen when

$$R_S = \frac{1}{Y_{01} + Y_0}. \quad (2.49)$$

By adjusting C_1 small values of b_S can be accommodated.

From Equation 2.25 and Equation 2.48, the external quality factor at the source can be written as

$$Q_S = \frac{b_1}{G} = \frac{b_1}{g_S} = \frac{\left. \frac{\omega_0}{2} \frac{dB(\omega)}{d\omega} \right|_{\omega=\omega_0}}{g_S}. \quad (2.50)$$

For the resonator under investigation

$$Y_{res} = j\omega C_1 - j(NY_0 + Y_1 + Y_{12}) \cot(\theta) = jB_1(\omega) \quad (2.51)$$

and at the resonant frequency, $B_1(\omega_0) = 0$, thus

$$\omega_0 C_1 = (NY_0 + Y_1 + Y_{12}) \cot(\theta) \quad (2.52)$$

where $\theta_0 = \frac{\omega_0 l}{v}$ is the electrical length of the lines at the centre frequency.

The susceptance slope parameter can be found by using Equation 2.51 and Equation 2.52,

$$b_1 = \frac{\omega_0 C_1}{2} - \frac{(NY_0 + Y_1 + Y_{12})\omega_0 l}{2 \sin^2\left(\frac{\omega_0 l}{v}\right) v} = (NY_0 + Y_1 + Y_{12}) \left[\frac{\cot(\theta_0)}{2} + \frac{\theta_0}{2 \sin^2(\theta_0)} \right]. \quad (2.53)$$

Substituting Equation 2.53 into Equation 2.50, yields the external quality factor at the source

$$Q_S = \frac{\left. \frac{\omega_0}{2} \frac{dB(\omega)}{d\omega} \right|_{\omega=\omega_0}}{g_S} = \frac{(NY_0 + Y_1 + Y_{12})}{g_S} \left[\frac{\cot(\theta_0)}{2} + \frac{\theta_0}{2 \sin^2(\theta_0)} \right]. \quad (2.54)$$

By using Equation 2.46 the external quality factor can be expressed in terms of the self and mutual static capacitance, by

$$Q_S = \frac{\sqrt{\epsilon_r}(NC'_0 + C'_1 + C'_{12})}{\eta_0 g_S} \left[\frac{\cot(\theta_0)}{2} + \frac{\theta_0}{2 \sin^2(\theta_0)} \right]. \quad (2.55)$$

The external quality factor at the load side can be written similarly as

$$Q_L = \frac{\left. \frac{\omega_0}{2} \frac{dB(\omega)}{d\omega} \right|_{\omega=\omega_0}}{g_L} = \frac{\sqrt{\epsilon_r}(NC'_4 + C'_3 + C'_{23})}{\eta_0 g_L} \left[\frac{\cot(\theta_0)}{2} + \frac{\theta_0}{2 \sin^2(\theta_0)} \right] \quad (2.56)$$

where

$$g_L = Re \left[NY_{34} \frac{\frac{N}{R_s} + jY_{34} \tan(\theta)}{Y_{34} + j\frac{N}{R_s} \tan(\theta)} \right]. \quad (2.57)$$

By using Equation 2.35, the coupling coefficients can be expressed as

$$k_{12} = \frac{J_{12}}{\sqrt{b_1 b_2}} = \frac{Y_{12} \cot(\theta_0)}{\sqrt{(NY_0 + Y_1 + Y_{12})(Y_{12} + Y_2 + Y_{23}) \left[\frac{\cot(\theta_0)}{2} + \frac{\theta_0}{2 \sin^2(\theta_0)} \right]}} \quad (2.58)$$

$$k_{12} = \frac{C'_{12} \cot(\theta_0)}{\sqrt{(NC'_0 + C'_1 + C'_{12})(C'_{12} + C'_2 + C'_{23}) \left[\frac{\cot(\theta_0)}{2} + \frac{\theta_0}{2 \sin^2(\theta_0)} \right]}} \quad (2.59)$$

and

$$k_{23} = \frac{J_{23}}{\sqrt{b_1 b_2}} = \frac{Y_{23} \cot(\theta_0)}{\sqrt{(Y_{12} + Y_2 + Y_{23})(NY_4 + Y_3 + Y_{23}) \left[\frac{\cot(\theta_0)}{2} + \frac{\theta_0}{2 \sin^2(\theta_0)} \right]}} \quad (2.60)$$

$$k_{23} = \frac{C'_{12} \cot(\theta_0)}{\sqrt{(C'_{12} + C'_2 + C'_{23})(NC'_4 + C'_3 + C'_{23}) \left[\frac{\cot(\theta_0)}{2} + \frac{\theta_0}{2 \sin^2(\theta_0)} \right]}}. \quad (2.61)$$

The inner resonator coupling coefficients of an n^{th} -order filter, can be written as

$$k_{n,n+1} = \frac{J_{n,n+1}}{\sqrt{b_1 b_2}} = \frac{C'_{n,n+1} \cot(\theta_0)}{\sqrt{(C'_{n-1,n} + C'_n + C'_{n,n+1})(C'_{n,n+1} + C'_{n+1} + C'_{n+1,n+2}) \left[\frac{\cot(\theta_0)}{2} + \frac{\theta_0}{2 \sin^2(\theta_0)} \right]}}. \quad (2.62)$$

This concludes the derivation of the external quality and coupling factors of the combline filter [3, 5]. The coupling coefficient can be viewed in more depth in section 3.3.

2.5.2 Interdigital Filter

An Interdigital bandpass filter, as shown in Figure 2.12, consists of TEM-mode stripline resonators between parallel ground planes. Each resonator element is $\lambda_0/4$ long, and a short-circuit is applied to alternate ends of each element with the other end left open-circuit. Lines 1 to n in Figure 2.12 serve as resonators. As seen in Figure 2.12, Interdigital filters can use a termination line (a), probe coupling (b) or loop coupling (c) on both sides of the filter. In Figure 2.12(a), lines 0 and $n + 1$ are

impedance-transforming sections of the filter. Coupling methods (b) and (c) will be discussed in section 3.2 [3].

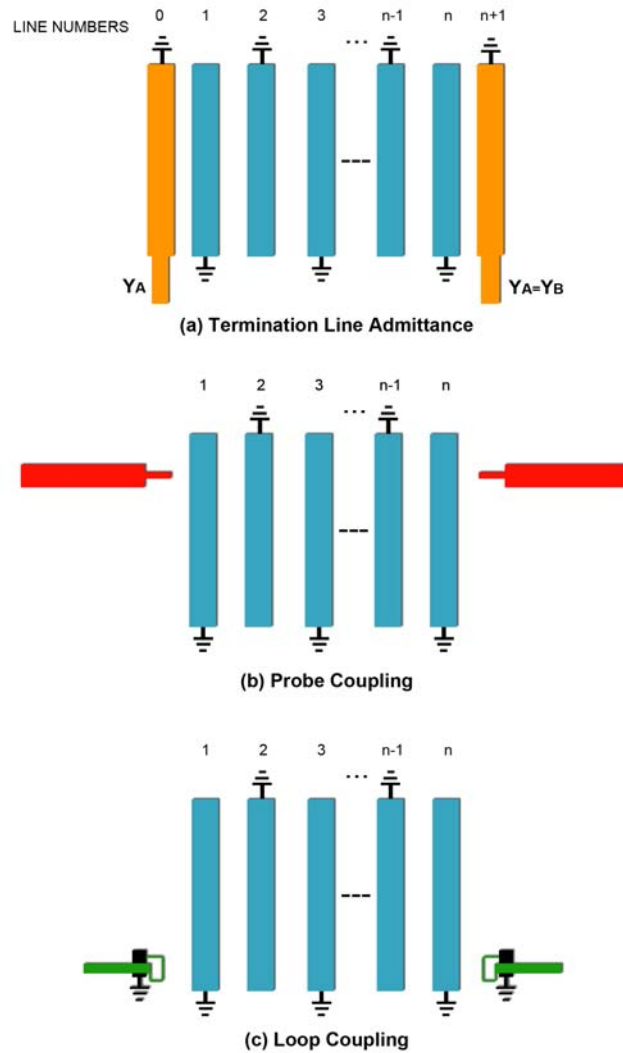


Figure 2.12: Interdigital Bandpass filter.

The transformation in Table 2.1(1) is used to construct an equivalent electrical circuit of the Interdigital filter in Figure 2.13(a) [3, 5]. The Kuroda identity in Figure 2.10(d) is applied to the source and load side of the circuit in Figure 2.13(b). Each quarter wavelength transmission line functions as an admittance inverter, with $J = Y_0$. The short-circuited transmission lines that appear as S -plane inductors in Figure 2.13(c), function as the resonators.

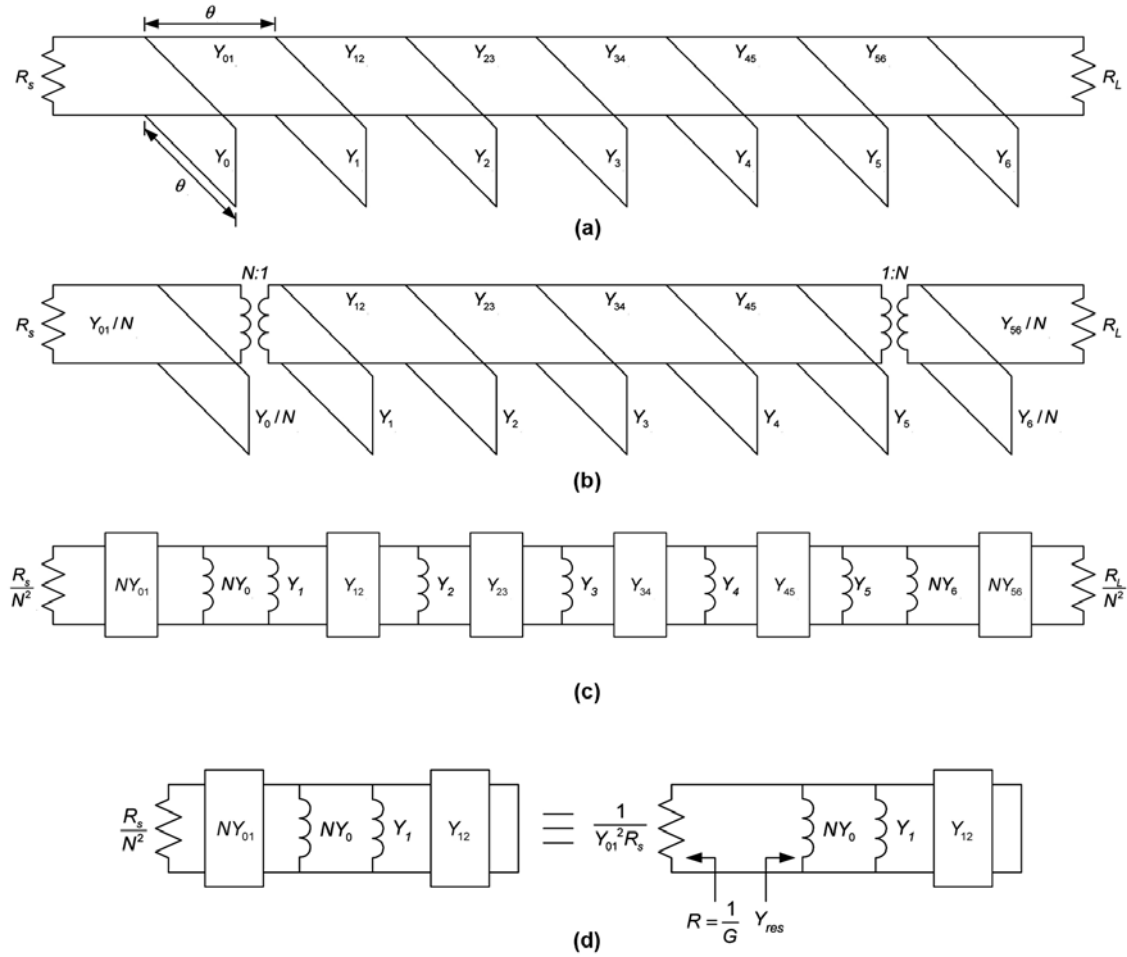


Figure 2.13: Equivalent electrical circuit of a fifth-order Interdigital filter.

Figure 2.13(d) shows a section of the circuit in Figure 2.13(c). By evaluating this section, the external quality factor can be obtained [3, 5].

The admittance Y_{res} in Figure 2.13(d), is equal to

$$Y_{res} = -j(NY_0 + Y_1 + Y_{12}) \cot(\theta) = -j(NY_0 + Y_1 + Y_{12}) \cot\left(\frac{\omega l}{v}\right) = jB_1(\omega). \quad (2.63)$$

The derivative of $B_1(\omega)$ with respect to frequency, is equal to

$$\frac{dB_1(\omega)}{d\omega} = \frac{(NY_0 + Y_1 + Y_{12})l}{v \sin^2\left(\frac{\omega l}{v}\right)}. \quad (2.64)$$

The external quality factor at the source side is equal to

$$Q_S = \frac{b_1}{G} = \frac{\frac{\omega_0}{2} \frac{dB_1(\omega)}{d\omega} \Big|_{\omega=\omega_0}}{Y_{01}^2 R_S} = \frac{(NY_0 + Y_1 + Y_{12})\theta_0}{2Y_{01}^2 R_S \sin^2(\theta_0)}. \quad (2.65)$$

For an Interdigital filter $\theta_0 = \frac{\pi}{2}$, Equation 2.65 becomes

$$Q_S = \frac{(NY_0 + Y_1 + Y_{12}) \left(\frac{\pi}{2}\right)}{2Y_{01}^2 R_S \sin^2\left(\frac{\pi}{2}\right)} = \frac{\pi(NY_0 + Y_1 + Y_{12})}{4Y_{01}^2 R_S}. \quad (2.66)$$

Equation 2.66 can be written in terms of itself and mutual capacitances,

$$Q_S = \frac{\pi\eta_0(NC'_0 + C'_1 + C'_{12})}{4\sqrt{\epsilon_r}C'_{01}{}^2 R_S}. \quad (2.67)$$

The external quality factor at the load can be derived in a similar fashion

$$Q_L = \frac{\pi\eta_0(NC'_6 + C'_5 + C'_{45})}{4\sqrt{\epsilon_r}C'_{56}{}^2 R_L}. \quad (2.68)$$

By using Equation 2.35, the coupling coefficients between the first and second resonators can be expressed as [5, 3]

$$k_{12} = \frac{J_{12}}{\sqrt{b_1 b_2}} = \frac{Y_{12}}{\sqrt{\left(\frac{(NY_0 + Y_1 + Y_{12})\theta_0}{2\sin^2(\theta)}\right) \left(\frac{(Y_{12} + Y_2 + Y_{23})\theta_0}{2\sin^2(\theta)}\right)}} \quad (2.69)$$

$$k_{12} = \frac{4C'_{12}}{\pi\sqrt{(NC'_0 + C'_1 + C'_{12})(C'_{12} + C'_2 + C'_{23})}}. \quad (2.70)$$

Similarly, the coupling coefficients between the fourth and fifth resonators can be expressed as

$$k_{45} = \frac{J_{45}}{\sqrt{b_4 b_5}} = \frac{4C'_{45}}{\pi\sqrt{(NC'_6 + C'_5 + C'_{45})(C'_{45} + C'_4 + C'_{34})}}. \quad (2.71)$$

The inner resonator coupling coefficients of an n^{th} -order filter, can be written as

$$k_{n,n+1} = \frac{J_{n,n+1}}{\sqrt{b_n b_{n+1}}} = \frac{4C'_{n,n+1}}{\pi\sqrt{(C'_{n-1,n} + C'_n + C'_{n,n+1})(C'_{n,n+1} + C'_{n+1} + C'_{n+1,n+2})}}. \quad (2.72)$$

2.6 Conclusion

The two narrowband coaxial resonator filters, which use some of the parallel coupled transmission line arrangements, are the Compline and Interdigital filters. The Compline filter use short-circuited transmission lines as coupling elements, whereas the Interdigital filter utilize transmission line inverters. The Interdigital filter is resonant at a quarter of a wavelength while the Compline filter's passband is around a frequency where the lines are much shorter. The Compline filter has a transmission zero at the frequency where the line and coupling elements are a quarter of a wavelength long. The Compline filter is physically much smaller compared to an Interdigital filter. It was also found that by calculating the external quality factors and coupling coefficients of Compline and Interdigital filters, the mathematical model can be reduced to the qualification of the self and mutual capacitances.

Chapter 3

Filter Implementation Parameters

3.1 Introduction

Three basic implementation parameters which play a vital role in the realisation and improvement of a microwave filter design will be considered, namely input coupling, inter-resonator coupling and resonator Q -factor.

3.2 Input Coupling

Input and output coupling are crucial, because the filter or resonator must be interchangeably connected to either test instruments or RF systems. There are two main coupling techniques that can be used for adjusting the amount of coupling to a resonator, namely magnetic or electrical coupling. In both techniques, different methods can be employed to determine the exact location where the field strength is at its maximum and then attempt to couple at that precise nodal point.

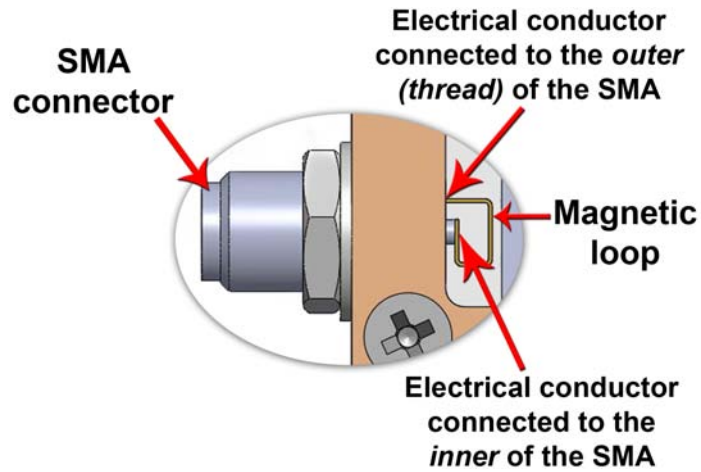


Figure 3.1: Magnetic coupling loop.

As seen in Figure 3.1 and 3.2, a loop consisting of an electrical conductor which connects the ground and the centre of input (or output) port can be used for magnetic coupling. As shown in Figure 3.2 the magnetic flux lines encircling the resonator intersect the loop and induce an electrical current. The magnetic field strength has a maximum magnitude at the lower end of the resonator, therefore the magnetic coupling loop is placed at the bottom.

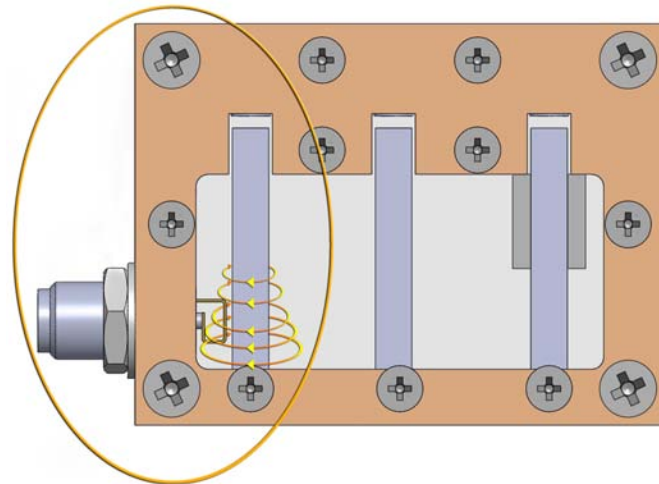


Figure 3.2: Coupling to the Magnetic Field.

Electrical coupling is achieved by extending the inner conductor of a coaxial SMA connector straight into the electric field of the resonator. The electrical field strength increases towards the open end of the resonator, therefore the SMA connector is placed near the top, as seen in Figure 3.3.

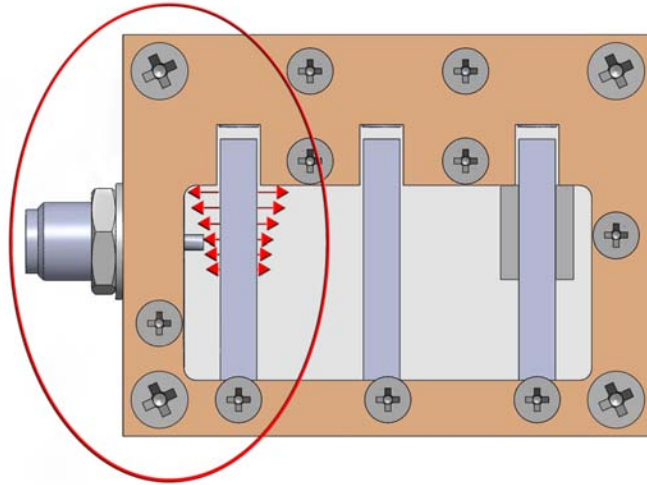


Figure 3.3: Coupling to the Electric Field.

3.3 Inter-resonator Coupling

To transfer energy from one resonator to another, some form of coupling must be used.

In Figure 3.4, two lossless LC resonators with the same resonant frequency, $\omega_0 = \frac{1}{\sqrt{LC}}$, are magnetically coupled to each other. The circuit represents a magnetic circuit with mutual inductance (M) defined as the ratio of induced voltage in one circuit, relative to the rate of change in current in the other.

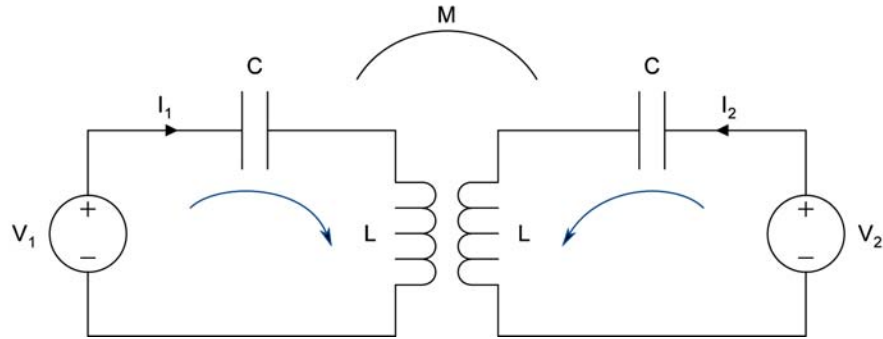


Figure 3.4: Magnetic Coupled LC Resonators.

The degree of coupling is measured by the coupling coefficient, k and for the circuit in Figure 3.4, it is define as

$$k = \frac{M}{\sqrt{L \times L}} = \frac{M}{L} \quad (3.1)$$

and the mutual inductance becomes,

$$M = kL. \quad (3.2)$$

In the Figure 3.5(a) the equivalent circuit is shown.

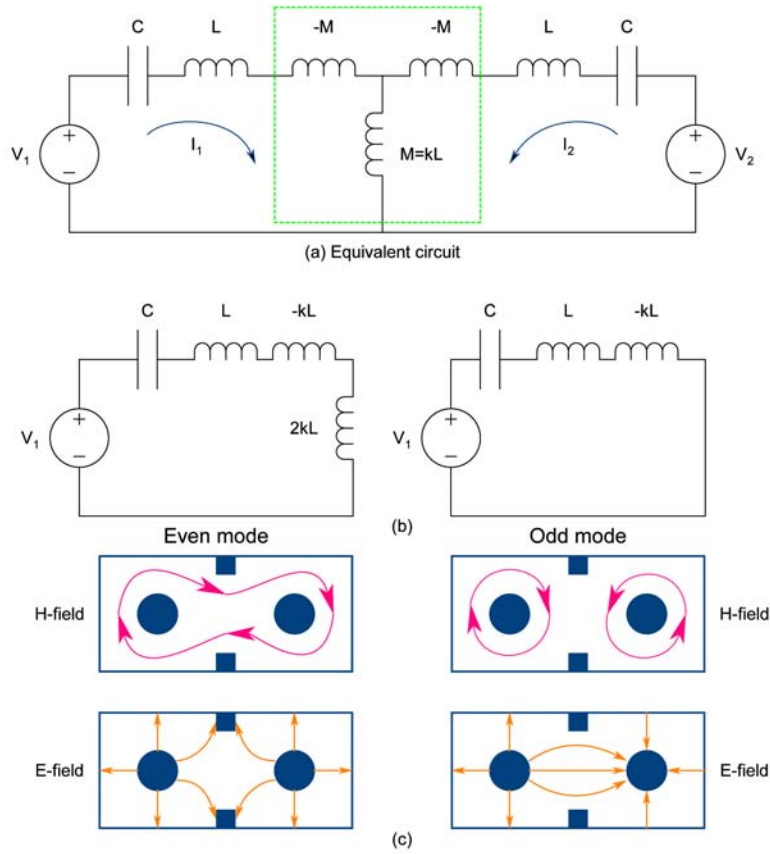


Figure 3.5: Equivalent circuit with Even and Odd modes.

The z-parameters from the coupled resonators are

$$\begin{bmatrix} V_1 \\ V_2 \end{bmatrix} = \begin{bmatrix} sL + \frac{1}{sC} & skL \\ skL & sL + \frac{1}{sC} \end{bmatrix} \begin{bmatrix} I_1 \\ I_2 \end{bmatrix} = [Z][I]. \quad (3.3)$$

From the characteristics of passive and loss-less circuits, it is known that when determining Z_{in} from Equation 3.3, the circuit has two frequencies where the impedance is zero, at series resonance. As seen in Figure 3.5(b) for a pair of coupled transmission line resonators, these two frequencies are in agreement with two modes of oscillation, namely even and odd modes. The Even mode occurs when $I_1 = I_2$ and a magnetic wall is formed at the symmetry plane as seen in Figure 3.5(c). The Odd mode will occur when $I_1 = -I_2$, as seen in Figure 3.5(b) and an electrical wall is formed at the symmetry plane as seen in Figure 3.5(c).

The resonant frequency for the even mode is

$$\omega_{0e} = \frac{\omega_0}{\sqrt{1+k}} \quad (3.4)$$

and the resonant frequency for the odd mode is

$$\omega_{0o} = \frac{\omega_0}{\sqrt{1-k}}. \quad (3.5)$$

As the distance between the 2 resonators decrease, the coupling will increase, forming a second resonant frequency. These two resonant frequencies appear on either side of the original resonant frequency. As the coupling increases, the two resonant frequencies separate further from each other. This occurrence provided the method to measure the coupling factor accurately. From the last Equation

$$\omega_{0o}^2 - \omega_{0e}^2 = \frac{2k}{1-k^2} \quad (3.6)$$

and

$$\omega_{0o}^2 + \omega_{0e}^2 = \frac{2}{1-k^2} \quad (3.7)$$

from which

$$k = \frac{\omega_{0o}^2 - \omega_{0e}^2}{\omega_{0o}^2 + \omega_{0e}^2}. \quad (3.8)$$

The coupling factor is positive when $\omega_{0e} < \omega_{0o}$ and negative if $\omega_{0o} < \omega_{0e}$.

The mutual inductance in Figure 3.5(a), represents a coupled T-network between two series resonators and can be used as an impedance inverter with z-parameters

$$Z = \begin{bmatrix} 0 & jX_0 \\ jX_0 & 0 \end{bmatrix} \quad (3.9)$$

as shown in Figure 3.6(a).

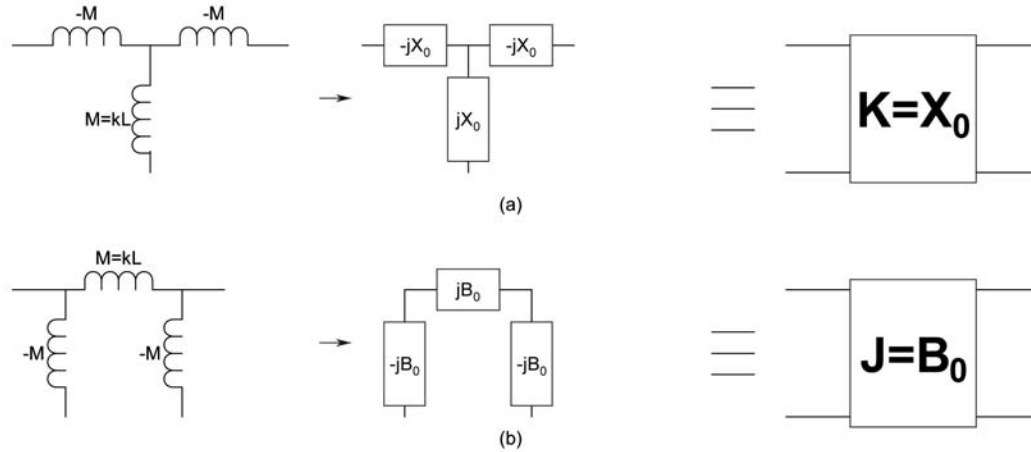


Figure 3.6: Inverters- (a) Impedance, (b) Admittance.

The coupling factor of the T-network is

$$k = \frac{\omega_0 M}{\omega_0 \sqrt{L_1 L_2}} = \frac{X_0}{\sqrt{\omega_0 L_1 \omega_0 L_2}} = \frac{X_0}{\sqrt{x_1 x_2}}. \quad (3.10)$$

The coupling pi-network is used in parallel resonators as an admittance inverter with y-parameters and is shown in Figure 3.6(b)

$$Y = \begin{bmatrix} 0 & -jB_0 \\ -jB_0 & 0 \end{bmatrix}. \quad (3.11)$$

The coupling factor of the pi-network is

$$k = \frac{B_0}{\sqrt{b_1 b_2}}. \quad (3.12)$$

X_0 and B_0 can be either positive or negative, capacitive or inductive.

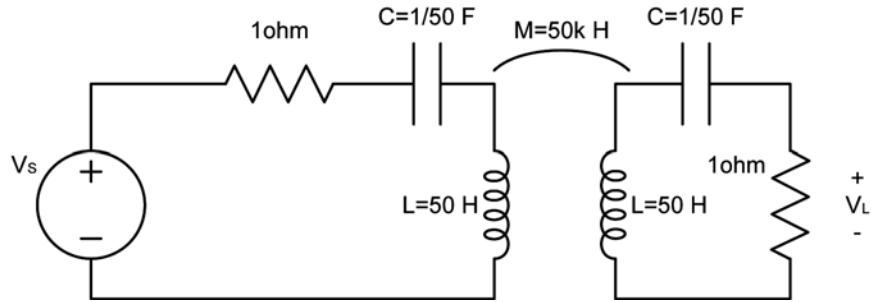


Figure 3.7: Two coupled resonators with external Q -factors of 50 and adjustable coupling factor [7].

As an example in Figure 3.7, when the coupling factor is very small ($k \times Q_e \ll 1$), the maximum magnitude of the transmission coefficient is smaller than one and the relative 3 dB bandwidth is smaller than $\frac{1}{Q}$. We say the resonators are under-coupled. As the product kQ increases, the relative bandwidth will also increase and when $kQ = 1$ the resonators are critical coupled, thus 100% coupling. If the coupling increase, then $|S_{21}|$ decrease at ω_0 and when peaks form on either side of ω_0 , the resonators are said to be overcoupled [8, 7].

3.4 Resonator Q Factor

There are several mechanisms that will produce loss in the capacitors and inductors of the resonating circuit. Dielectric heating and surface resistance on the conducting elements will introduce loss in the capacitors and the inductors show loss from wire resistance. The factor of merit for evaluating these losses and assessing the performance in a resonator is called the quality factor (Q). It is formally defined as [7]

$$Q = 2\pi \frac{\text{maximum energy storage during a cycle}}{\text{average energy dissipated per cycle}}. \quad (3.13)$$

The higher the Q , the bigger the conductance and hence, smaller loss.

The Q -factor consists of three groups. In Figure 3.8(b) and (c), $1/G_u$ represent the internal losses of a resonator and the Q -factor is called the *unloaded* Q -factor (Q_u) of the resonator. $1/G_g$ and $1/G_l$ represents losses outside the resonator (e.g. a generator or load resistance loading the resonator) and the Q -factor is referred to as the *external* Q -factor (Q_e) of the resonator. The combination of the internal and external losses represents the *loaded* Q -factor (Q_L) of the resonator [7].

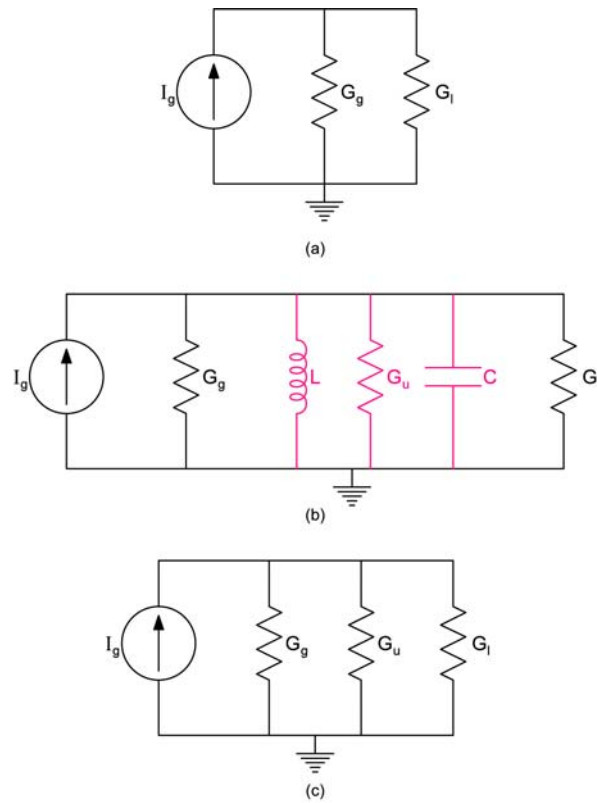


Figure 3.8: LC parallel resonator with equivalent circuit.

Norton's equivalent circuit will be used in deriving the relationship between Q_u and Q_L [9].

Without losing generality, $\omega_0 L$ can be normalised to unity.

In Figure 3.8(a), the available power is

$$P_A = \frac{I^2}{4G_l} \quad (3.14)$$

In Figure 3.8(b), a resonator is inserted in the circuit. The effects of the reactive components disappear at resonance, resulting in the equivalent circuit shown in Figure 3.8(c). The load power at resonance will be

$$P_L = \frac{G_l I^2}{(G_u + G_l + G_g)^2} \quad (3.15)$$

Using Equation 3.14 and 3.15, the insertion loss at resonance is

$$IL = \frac{P_A}{P_L} = \frac{(G_u + G_l + G_g)^2}{4G_l^2} \quad (3.16)$$

The external Q -factor in Figure 3.8(c) is

$$Q_e = \frac{1}{(G_g + G_l)} \quad (3.17)$$

and for the case $G_g = G_l$,

$$G_g = G_l = \frac{1}{(2 * Q_e)}. \quad (3.18)$$

Also in Figure 3.8(c) and for $\omega_0 L = 1$,

$$G_u = \frac{1}{Q_u}. \quad (3.19)$$

The insertion loss in Equation 3.16 can be rewritten in terms of the Q -factors, by using Equations 3.17, 3.18 and 3.19.

$$IL = Q_e^2 \left(\frac{1}{Q_u} + \frac{1}{Q_e} \right)^2 \quad (3.20)$$

The loaded Q -factor is

$$\frac{1}{Q_L} = \frac{1}{Q_u} + \frac{1}{Q_e} \quad (3.21)$$

and can be rewritten in terms of Q_e as

$$Q_e = - \left(\frac{Q_u Q_L}{Q_L - Q_u} \right). \quad (3.22)$$

Substituting Equation 3.22 into Equation 3.20

$$IL = \frac{Q_u^2 Q_L^2 \left(\frac{1}{Q_u} - \frac{Q_L - Q_u}{Q_u Q_L} \right)^2}{(Q_L - Q_u)^2} = \frac{Q_u^2}{Q_L^2 - 2Q_u Q_L + Q_u^2} = \frac{Q_u^2}{(Q_L - Q_u)^2} \quad (3.23)$$

From Equation 3.23, the insertion loss can be rewritten as

$$IL_{dB} = 20 \log 10 \left(\frac{1}{\left(1 - \frac{Q_L}{Q_u}\right)} \right) \quad (3.24)$$

or

$$|S_{21}|_{dB} = 20 \log 10 \left(1 - \frac{Q_L}{Q_u} \right). \quad (3.25)$$

The bandwidth of the single resonator is defined as the frequency where the output power is at the -3 dB point and is related to centre frequency and Q_L by

$$Q_L = \frac{f_0}{-3 \text{ dB BW}} \quad (3.26)$$

where f_0 and BW are both measured in the same units.

When the source and load are lightly coupled to the resonator, the external Q -factor becomes very large, and $Q_u \simeq Q_L$. As the coupling becomes stronger, it can be shown that Q_u can be calculated from the measured Q_L by the use of Equation 3.27 which is derived from Equation 3.25 and Equation 3.26 ,

$$Q_u = - \left[Q_L / \left(10^{\frac{IL}{-20}} - 1 \right) \right] \quad (3.27)$$

where,

Q_L – Measured Quality factor

IL – Insertion Loss.

3.5 Conclusion

The two main coupling methods discussed are electrical- and magnetic coupling. Inter-resonator coupling was also briefly discussed. This chapter concludes by discussing the quality factor. Equation 3.27 will be used to calculate the Q_u of thirteen different resonators in the next chapter.

Chapter 4

Filter Manufacturing

4.1 Introduction

In this chapter the various options and limitations of the critical areas of microwave filter mechanics are discussed.

4.2 Microwave Penetration

At DC, current in a conductor flows with uniform density over the cross section of the conductor. At microwave frequencies, the current only flows in a very thin layer in the conductor surface. The effective conductor cross section decreases and the conductor resistance increases, which is referred to as skin effect and should be taken into account when selecting the proper material.

Skin depth is a measure of how deep electromagnetic current can penetrate into the material. It is defined as the depth at which the current density inside the material falls to $\frac{1}{e}$ (about 37%) of the original value at the surface. The microwave skin depth, δ , of a material can be calculated by [6]

$$\delta = \sqrt{\frac{2}{\omega\mu\sigma}} = \frac{1}{\sqrt{\sigma\pi\mu_0 f}} \quad (4.1)$$

where,

δ = penetration depth (m)

ω = angular frequency (1/s)

f = frequency (Hz)

μ = the permeability of a medium (H/m)

σ = conductivity (S/m).

4.3 Materials used in Microwave filters

Taking microwave penetration into account, the most common base metals used in microwave waveguide and cavity filters are copper, invar, aluminium, brass and silver. Silver will be discussed in section 4.5.1.

4.3.1 Copper

Copper (Cu) is a ductile metal with very high thermal and electrical conductivity. It has a red, orange, or brown colour. Copper has the second highest electrical conductivity of any element, just after silver. Copper, as any other material, should not be in direct physical contact with metals of different electro-potential. In the presence of moisture, the completion of an electrical circuit will cause it to act as an electrochemical cell. It should also be noted that copper has poor mechanical strength and is quite heavy [10].

4.3.2 Invar

Invar is nickel-iron alloy with the lowest thermal expansion coefficient of any nickel-iron alloy. It is mostly used in waveguide filters where dimensional changes, due to temperature variation must be minimized (for example when transmitting high power) and to maximise frequency stability. Invar is a very expensive alloy [10].

4.3.3 Aluminium Alloys

Pure aluminium is soft and has little strength. It is normally used as an alloy. The two most popular alloys used in microwave components are AlMgSil, mostly used in enclosures, and AlMg3, used for sheet metal applications. Aluminium is light weight, resists corrosion, has a high strength to weight ratio, is a good electrical conductor, excellent conductor of heat and non-magnetic. It can be formed into almost any shape. Standard cavity filters are generally designed using aluminium as the base material [10].

4.3.4 Brass

Brass is an alloy of approximately 67% copper and 33% zinc, making it stronger and more durable than copper, although not as strong as metals like steel. Alloys with even less zinc start to turn reddish in colour, and are sometimes called red brass. Sometimes 3% lead is added to make it easier to machine. It conducts heat and electricity very well and offers excellent resistance against industrial, marine and rural atmospheres and various oils. Brass can be gold or silver plated to improve its resistance to corrosion. Brass is usually used in the manufacturing of connector bodies, enclosures, and contact pins of outer conductors. Like copper, brass is very heavy [10].

4.4 Properties of machining techniques

Various technologies and methods exist to manufacture microwave filters. One factor that should not be neglected is that microwave filters usually operate in extremely harsh conditions. For the filter to operate within specifications, various aspects with regards to the environment should be considered. The following are the most important [10]:

- Level of shock and vibration
- Temperature variation
- Humidity
- Dust and moisture
- Chemical liquids or vapours
- Electromagnetic radiation
- Ionizing radiation (nuclear explosions, radiation in space)

In the manufacturing of microwave filters, only the use of modern computer numerically controlled (CNC) machines of high precision are acceptable. There are two main CNC methods for manufacturing of microwave filters, namely CNC Milling and CNC Electrical Discharge Machining (EDM). The advantages and disadvantages of each method will be discussed.

4.4.1 CNC Milling

It is a process by which material is removed by a rotating tool. It is cost effective for short runs, but not as effective as EDM. CNC milling can produce almost any two-dimensional (2D) and three-dimensional (3D) shape provided that the rotating cutting tools can reach the material to remove it. High dimensional tolerances and smooth finishes are advantages that CNC milling has over the other manufacturing processes [10].

4.4.2 CNC Electrical Discharge Machining (EDM)

EDM removes metal by producing a rapid series of repetitive electrical discharges. These electrical discharges are passed between an electrode and the piece of metal being machined. The entire machine process is performed while submerged in a fluid bath. The fluid bath flushes away all the small amounts of material that is removed from the metal and also serves as a coolant. The fluid also acts as a conductor for the current to pass between the electrode and filter. There are two primary EDM methods namely, wire EDM and ram EDM [10].

Wire EDM

In Wire EDM (Wire-cutting) an initial hole must first be drilled in the material and then a very thin wire can be fed through the hole. The wire serves as the electrode and is slowly fed through the material. The path of the wire is computer controlled. The wire itself does not actually touch the metal, but the electrical discharge actually removes small amounts of the material. Special Brass wires are typically used. The wire-cutting process is demonstrated in Figure 4.1 [11]. After the wire cutting process, the brass wire is discarded.

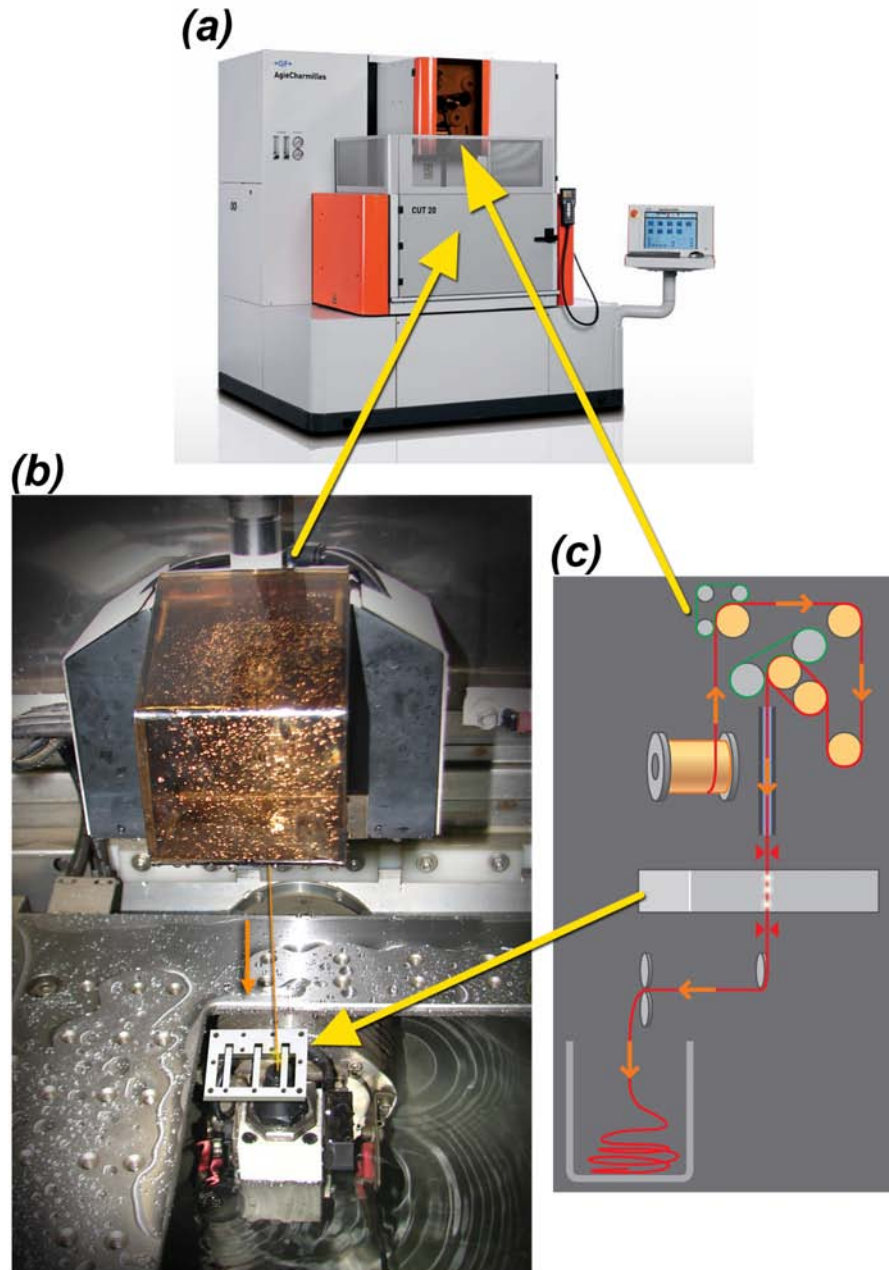


Figure 4.1: Wire-cutting Procedure.

Figure 4.2 below illustrates different Surface Roughnesses (R_a) obtainable with wire-cutting: R_a 0.78 – 1.83 μm seen under a microscope with magnification of 100 times and 250 times. The 0.78 μm finish gives the smoothest surface.

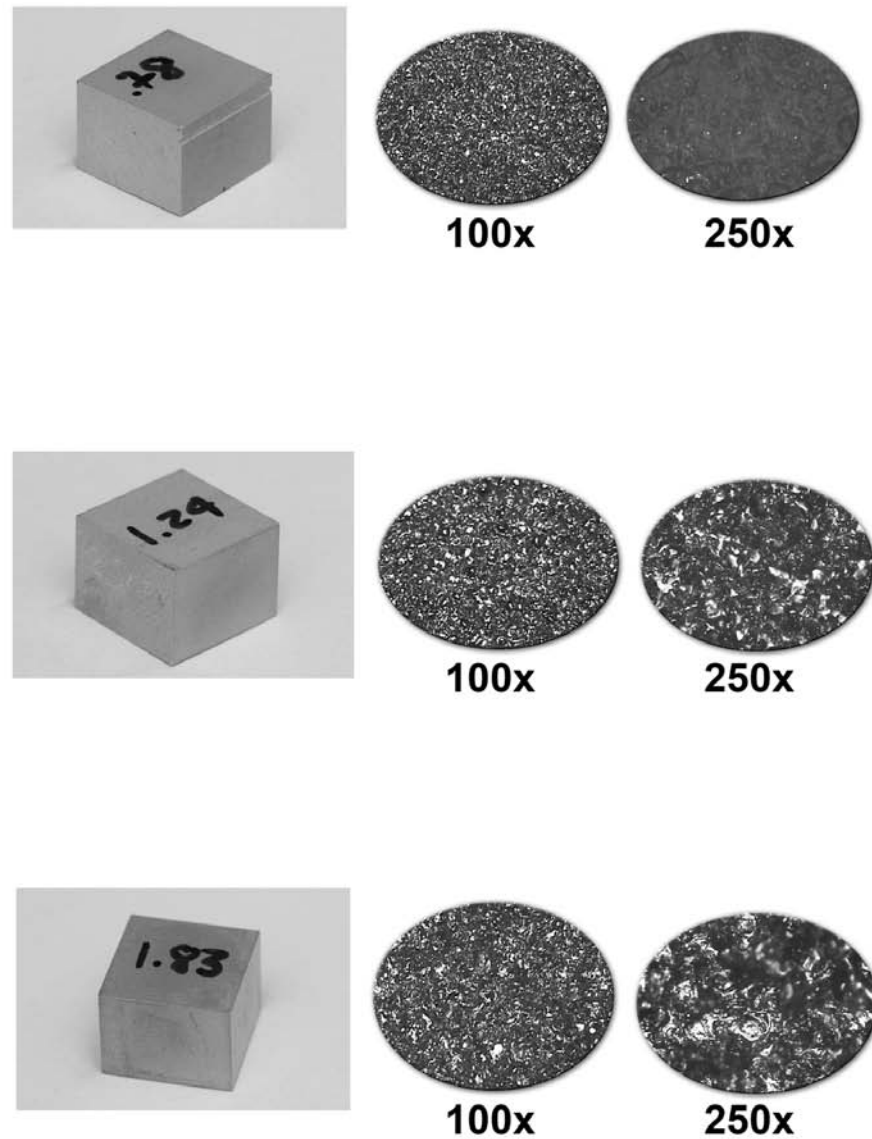


Figure 4.2: Wire-cutting surface finishes.

Ram EDM

Ram EDM (also known as a probe) is generally used for complex geometries where a machined graphite electrode or copper electrode is used to erode the desired shape from the material. EDM is one of the most accurate manufacturing processes used in manufacturing complex or simple parts. It is quite affordable and the turnaround

time can be fast (depending on the complexity of the filter and manufacturer back log).

CNC milling and wire-cutting (EDM) can be combined. The raw material is first milled with a milling machine, while the final stage cutting is done by wire-cutting. In section 4.6 Figure 4.6(C), irregularities (steps) can be seen inside the enclosure due to the filter being wire-cut after the CNC milling process. These irregularities (steps) can negatively impact the coupling as well as the frequency response of the filter and should be minimized as far as possible.

4.4.3 CNC Laser Cutting

Laser cutting can produce almost any two-dimensional (2D) shape cutouts and can cut many types of materials (ferrous- and non-ferrous metals, stone, plastics, rubber and ceramics). Laser cutting works by directing a high power pulsed laser at a specific location on the material. The energy of the laser is converted into heat and melts or vaporizes the material [10].

It has been found that laser cutting is not really desirable for microwave filters due to the following factors [10]:

- Edges may not be as smooth as with milling or EDM
- Certain areas along the edge may be less smooth, for example where the laser cut ends
- The dimensions of the final product is not as accurate as with milling or EDM

4.5 Surface finish

The surface resistivity of a machined surface depends strongly on the surface texture and roughness. The surface texture results from various mechanical flaws that can affect the surface resistance by disrupting current flow on a microscopic scale. These include scratches, cracks, holes, seams, tears, inclusions, surface patterns and waviness of the surface, as illustrated in Figure 4.3.

Each manufacturing technology has its own characteristic features. Smooth surfaces are desirable, but are difficult and expensive to achieve consistently. Manufacturing cost increases exponentially with a decrease in surface roughness. A trade-off

must usually be made between the manufacturing cost and performance of a microwave component.

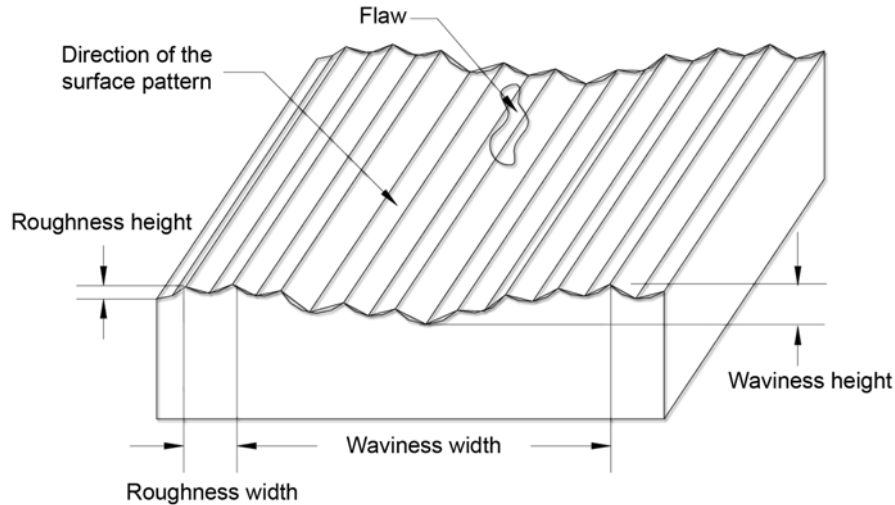


Figure 4.3: Surface Roughness.

The surface resistance of a rough surface can be lowered by plating or chemical polishing.

4.5.1 Silver plating

Silver has the best conductivity of all metals, which means that it can carry a high current load with the least amount of loss at the highest microwave frequencies. Silver plating is performed through electroplating. The surface roughness is improved after silver plating, as seen in section 4.7. Using a base material (for example aluminium) with silver plating is very cost effective. In some applications the base material must first be nickel- and thereafter silver plated. It is important to take the added layer thickness into account when determining dimensions for the final product.

4.5.2 Chemical polishing

Chemical polishing provides an alternative to electroplating, to smooth the metal's surface. It attacks protrusions where the surface to volume ratio is higher and, as a result, a bright finish is achieved. Both alkaline and acid etchants can be used in

chemical polishing. The former are more common as they are less expensive and safer to handle.

Phosbrite is one of the most common chemicals used for polishing aluminium. The solution contains a mixture of concentrated mineral acids. This mixture is highly reactive and will dissolve most metals. An extraction vent should always be used when working with the chemical solution, due to the highly toxic nature of the fumes. The solution operates at temperatures of 95°C to 105°C and immersion of the item is between 0.5 to 3 minutes (depending on the initial condition of the article, the quality of the surface finish required and the age of the Phosbrite solution).

4.6 Connectors and Tuning elements

Coaxial resonator filters usually make use of input and output connectors and tuning screws. SMA connectors and Temex tuning screws are used in the prototype filter design in Chapter 5, and will now be discussed.

SMA Connector

The SMA connector is derived from Sub-Miniature A connector and is used where coaxial connections are required. It is designed for 50 Ω impedance and is specified for frequencies up to 24 GHz. The SMA connector is available in a variety of forms. The spark plug type as shown in Figure 4.4, is popular in coaxial resonator filters for the input and output coupling or termination connections.



Figure 4.4: Spark-plug SMA Connector.

In Figure 4.6(B), Silver Loaded Epoxy Adhesive (a two part electrically conductive thermosetting silver epoxy) is used for bonding the centre conductor of the SMA spark-plug connector to the MW filter. The Teflon must be level with the inside of the enclosure to ensure a 50 Ω connection. The connector must be cleaned with denatured alcohol after the silver epoxy has been cured.

Tuning Element

The tuning elements consist of two parts, a threaded mounting bush and a self locking rotor screw, as seen in Figure 4.5. By adjusting the depth of the tuning screw, the gap size between the resonator and tuning screw is varied, thus varying the capacitance.

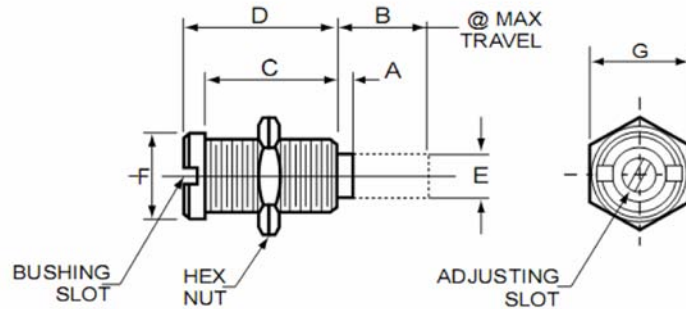


Figure 4.5: Temex Tuning Element.

Figure 4.6(A) shows the assembly of a tuning element. It is very important that the outer threaded section of the tuning element must be level with the inside of the filters' enclosure (which is not the case here). This will influence the tuning range of the filter, i.e. if it still needs to reach the inside of the enclosure, the filter will tune to a lower frequency.

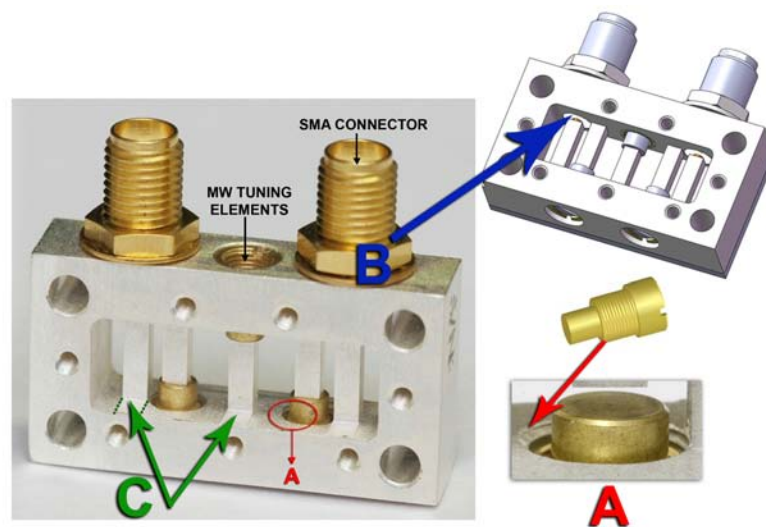


Figure 4.6: Manufacturing and assembly of a MW filter.

4.7 Resonator unloaded Q measurement

An in-depth study was done to determine the best possible unloaded Q value for a resonator with a rectangular cross-section and fixed dimensions. Various metals and their properties, as well as manufacturing methods and their specific limitations were considered. Thirteen different resonators, designed to operate at 2125 MHz were manufactured, eight of which were designed according to the specifications in Figure 4.7 and five designed according to the specifications in Figure 4.8. Each resonator was unique in method of manufacturing, polishing, as well as plating. Various chemical polishing methods were considered, of which Phosbrite and Alu Clean were used on separate resonators. As a final touch, silver or gold plating was added to investigate whether this will further enhance the performance of the resonator.

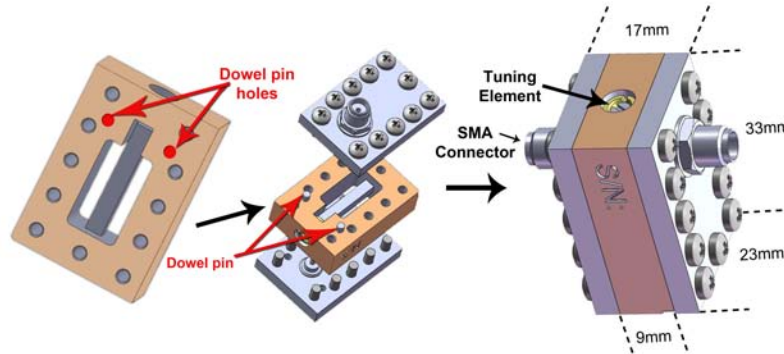


Figure 4.7: Solid Resonator.

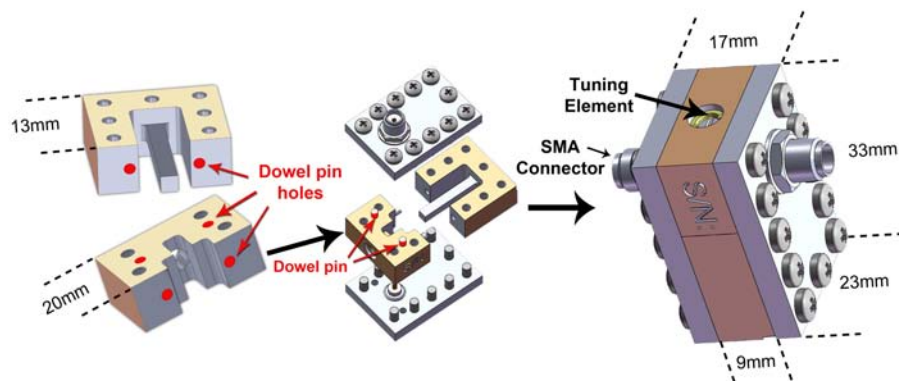


Figure 4.8: Split Resonator.

The unloaded Q values for the different metals used in the resonators were calculated by using CST. CST uses a loss-less metal model to compute the field and surface currents, which are then used to calculate the surface currents. Integrating the current²-surface resistance product yields the loss in the structure, and from this the unloaded Q is calculated. The calculated unloaded Q results for a resonator with dimensions as per Figure 4.7 or 4.8 and with a resonance frequency of 2125 MHz, is shown in Table 4.1.

Metal	Q_u calculated results (CST)
Aluminium	1097
Brass	901
Gold (Au)	1137
Nickel (Eni)	678
Silver (Ag)	1393

Table 4.1: Calculated unloaded Q results.

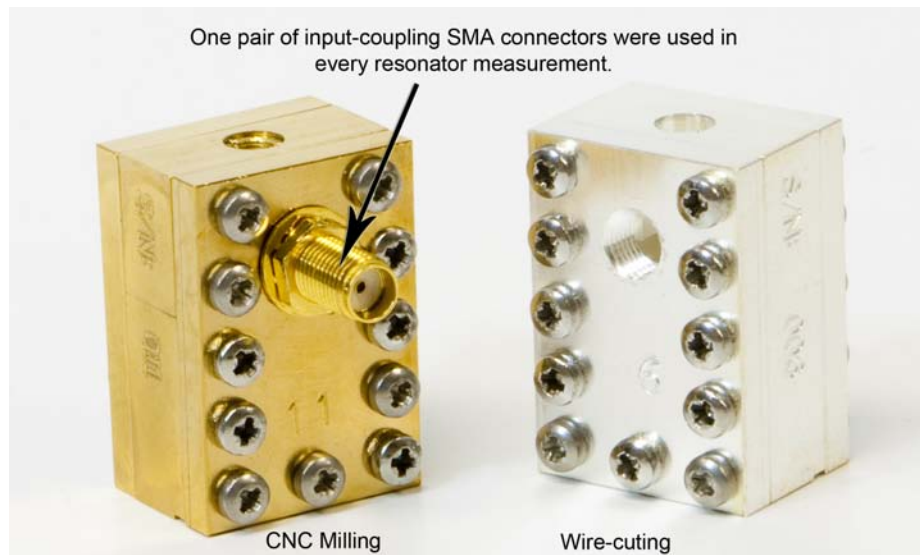
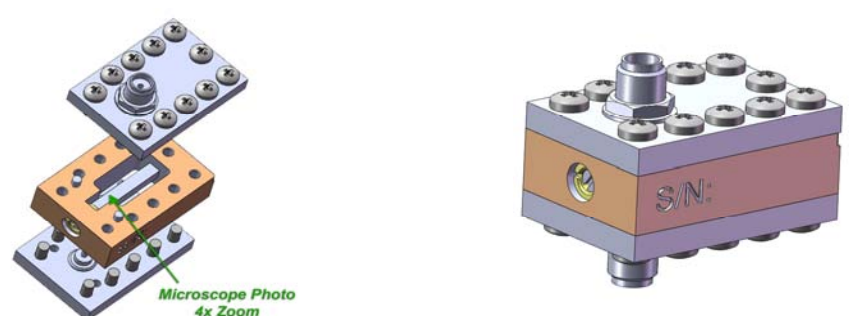
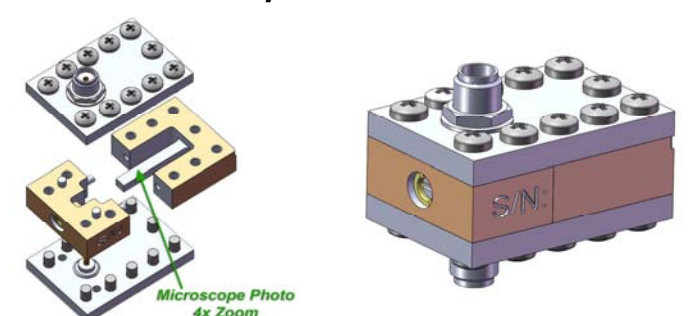


Figure 4.9: 2125 MHz Resonators.

The frequency response of each lightly coupled resonator was measured with a vector network analyser (VNA). The unloaded Q factors shown in Figure 4.10 were calculated with Equations 3.26 and 3.27. The following conclusions are drawn:

Q_u Measurement

S/N:	01	02	03	04	05	06	07	08	09	10	11	12	13
RESONATOR:	 <p>Solid Resonator</p>								 <p>Split Resonator</p>				
MATERIAL:	Aluminium	Aluminium	Aluminium	Aluminium	Aluminium	Aluminium	Aluminium	Aluminium	Aluminium	Aluminium	Brass	Brass	Aluminium
WEIGHT:	0.04kg	0.04kg	0.04kg	0.04kg	0.04kg	0.04kg	0.04kg	0.04kg	0.04kg	0.04kg	0.1kg	0.1kg	0.04kg
MECH. PROCESS:	Wire-cutting (1round)	Wire-cutting (2rounds)	Wire-cutting (3rounds)	Wire-cutting (3rounds)	Wire-cutting (3rounds)	Wire-cutting (3rounds)	Wire-cutting (3rounds)	Wire-cutting (3rounds)	CNC Milling	CNC Milling	CNC Milling	CNC Milling	Wire-cutting (1round)
PHOTO:													
Q _u MEASUREMENT:	566	593	620	628	636	628	610	612	600	579	563	537	496
CHEMICAL POLISH:			Phosbrite - 0.5min				Phosbrite - 1.5min	Phosbrite - 3.0min	Phosbrite - 1.5min			Alu-Clean - 2.0min	Alu-Clean - 2.0min
PHOTO:													
Q _u MEASUREMENT:			704				729	712	423			480	490
PLATING PROCESS:	3µm Eni & 20µm Ag	3µm Eni & 20µm Ag	3µm Eni & 20µm Ag	3µm Eni & 20µm Ag	3µm Eni & 12µm Ag	3µm Eni & 4µm Ag	3µm Eni & 20µm Ag	3µm Eni & 20µm Ag	3µm Eni & 12µm Ag	3µm Eni & 12µm Ag	3µm Eni & 12µm Au	3µm Eni & 12µm Ag	3µm Eni & 12µm Ag
PHOTO:													
Q _u MEASUREMENT:	1141	1070	1105	1186	1124	1198	1155	1174	839	956	297	994	857

- Different wire-cutting roughness's
- Different chemical polishing finishes
- Different silver plating finishes

Figure 4.10: Resonator unloaded Q measurements.

First Stage Eight resonators (1-8) were wire-cut from a solid piece of aluminium, and five (9-13) were made with a split section. From these five (9-12), four went through a milling process (two made from aluminium and two from brass). The last (no. 13) one was made from aluminium which was wire-cut. It is evident that the measured unloaded Q for the split resonators were lower than those of the solid ones. The split causes a disruption in the flow of the surface current, as seen in Figure 4.11.

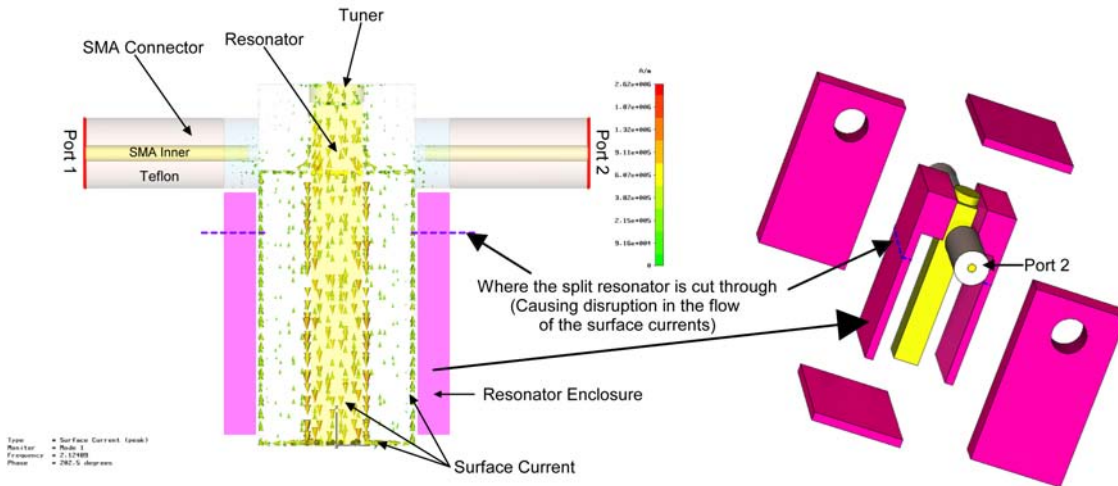


Figure 4.11: Resonator Surface Current.

Resonators 1-3 have different wire-cutting finishes, 1 being roughest cut and 3 the smoothest. It was found that the smoother the surface the higher the measured unloaded Q . The designed unloaded Q for aluminium is 1097 and for Brass 901. The measured unloaded Q is found to be 50% less for aluminium and 40% less for brass, as seen in Figure 4.12.

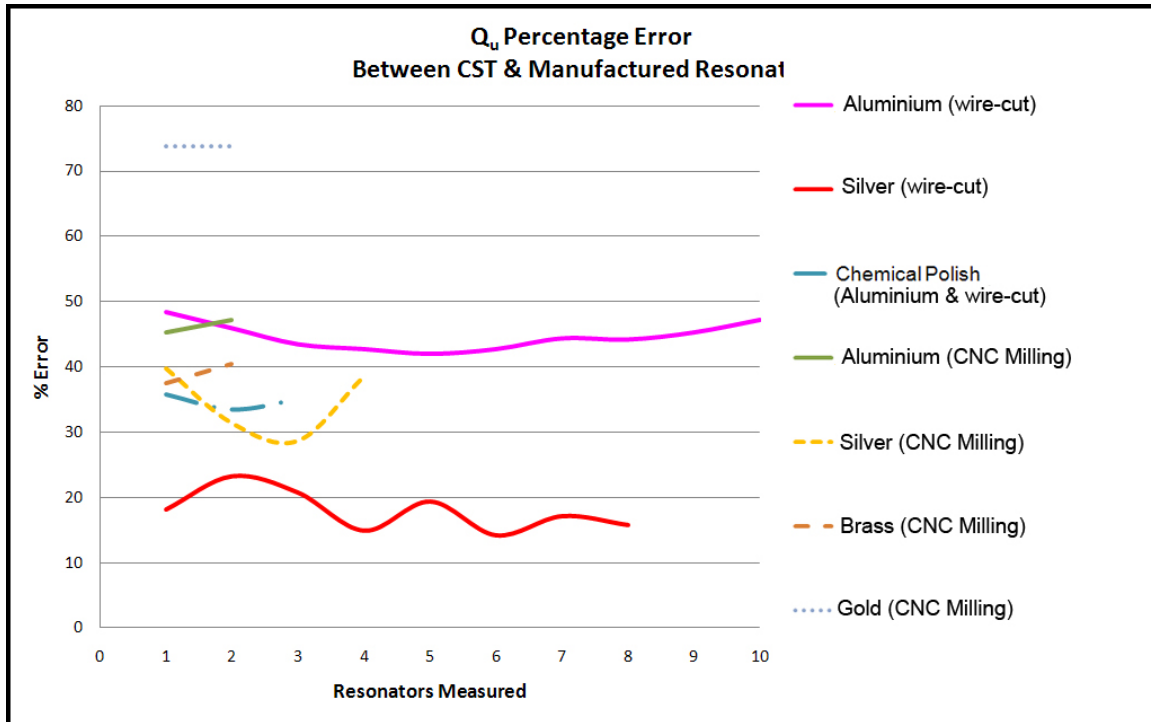


Figure 4.12: Unloaded Q Percentage Error.

Second Stage Selected resonators were either chemically polished or Alu-cleaned. Alu-clean, being a very strong alkaline, is used to clean aluminium surfaces from any excess cutting-fluid and burs.

Resonator 12 and 13 were Alu-cleaned and the results show that the metal is duller and that the measured unloaded Q is a slightly less than measured during the previous stage.

Resonator 12, made from brass, was only placed in the Alu-clean for interest sake.

Resonators 3, 7 and 8 were chemically polished with different time intervals. The results showed a 10% increase compared to the first stage, as seen in Figure 4.12. It was found that for the best result, the resonators must be chemically polished for more or less 1.5 minutes. The chemical polishing can etch holes into the metal if kept longer than 1.5 minutes. In the case of resonator 9, the surface was not very smooth to begin with and the chemical polish etched holes into the uneven areas, causing the measured unloaded Q to be less than the first stage.

Final Stage In the last stage: 12 resonators were silver plated and 1 was gold plated. It was very interesting to see that it did not matter which process were used prior to the silver plating and that the measured unloaded Q results were excellent.

Resonators 4-6 were coated with different silver plating thickness, but no significant improvement could be observed. The designed unloaded Q was 1393 and the measured unloaded Q was at the best 16% less and in worst case, 24 % less than the calculated value, as seen in Figure 4.12.

Resonator 11 was gold plated, but yielded a poor result. The designed unloaded Q was 1137 and the measured unloaded Q was 297. It was first hypothesized that this could be due to skin effect, because every resonator is first plated with nickel and then with silver or gold, but the designed unloaded Q for nickel is 678. The company that did the plating process informed us that a harder type of gold was used (the softer gold was unavailable), which implies that the plating had a higher than expected resistivity. The measured unloaded Q for Gold plating was 80% worse than the designed unloaded Q , as seen in Figure 4.12. It can be concluded that there was a process problem.

4.8 Conclusion

Different aspects concerning the manufacturing of a filter were discussed in this chapter. The pros and cons were considered for each type of metal suitable for microwave filter design. The various methods of machining were also evaluated. Connectors and tuning elements were also briefly discussed. The main focus however was on the unloaded Q factors obtained for thirteen different resonators. The results showed that a resonator, made from aluminium, which was wire-cut and then silver electroplated, yields the best result and is the most cost efficient.

Chapter 5

Prototypes

5.1 Introduction

In this Chapter, three coupled coaxial resonator filters, which are used in a radar system, will be examined. The Tchebyscheff filter response was chosen because of the sharper cut-off rate compared to a Butterworth filter of the same order.



Figure 5.1: Three filters.

5.2 Parallel Coupled Transmission Lines

5.2.1 Filter 1

Specification

Filter 1 is a 2125 MHz filter that should have an S_{21} attenuation flatness of 0,5 dB within a 20 MHz band around the centre frequency. The -15 dB S_{11} bandwidth should be greater than 40 MHz. S_{21} group delay, in the 20 MHz band around the center frequency should be less than 1 ns. Also, Filter 1 should attenuate the local oscillator (LO1) signal at 2 GHz in the radar system by 80 dB and have an attenuation of >80 dB in the band 6.375 GHz - 9.375 GHz for the suppression of LO2.

Two VME PCB cards were used, one for the Receiver chain and one for the Exciter chain. The Receiver uses three of these filters, where the Exciter only uses one. The designer was faced with two difficult problems, namely size and weight. The VME standard has very specific height constraints and due to the size of the PCB and environmental tests, the weight factor added additional stress to the integrity of the VME PCB cards. After considering component height and placement on the VME PCB's, it was determined that the maximum allowable height is 23.0mm and that the filter dimensions must not exceed 35 mm × 60 mm. Also, the filter will be conformal coated, which will add additional overall height.

Filter 1 is expected to operate in very harsh environments, where it will be exposed to shock and vibration, temperature fluctuations, humidity, moisture and dust.

Design

The Compline filter type was chosen instead of the Interdigital filter due to its smaller size. Additionally, it has a broader stopband above the primary passband.

The filter was designed using the technique in Chapter 2. The Microwave Office (MWO) circuit model, including resonator Q -factor of 1670, is shown in Appendix B. The loaded- q value and coupling factors obtained are shown in Table 5.1.

q_L	34.24
k_{12}	0.0247
k_{23}	0.01797
k_{34}	0.01721
k_{45}	0.01797
k_{56}	0.0247

Table 5.1: The External Quality factors and Coupling coefficients.

A sixth order Comblin filter was selected to ensure attenuation greater than 80 dB at 2 GHz.

To reduce the length of the filter, it was folded as shown in Figure 5.2. Where the coupling k_{12} , k_{23} , k_{45} and k_{56} were implemented using standard Comblin constructions. k_{34} was implemented with a square aperture in the plate separating the two halves of the filter.

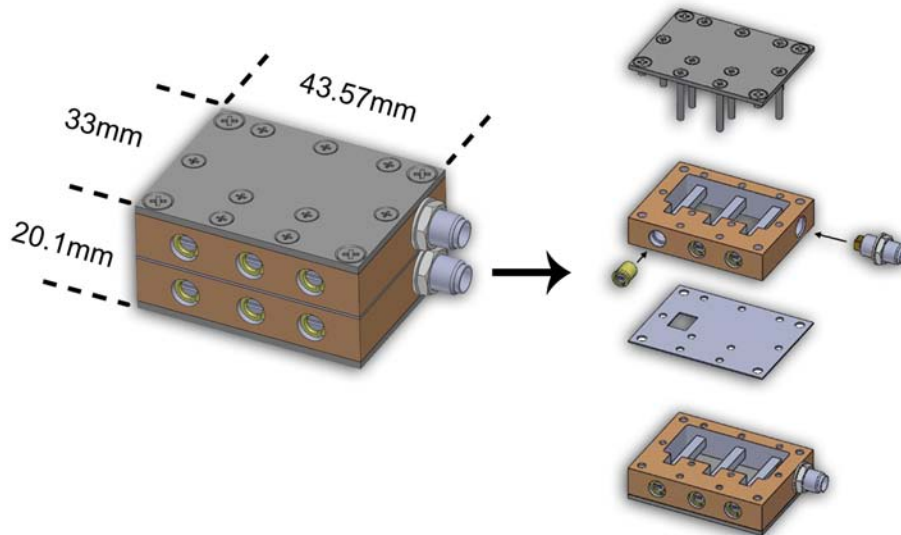


Figure 5.2: Filter 1.

The possibility of placing a transmission zero at 2 GHz, by means of electrical coupling between the first and last resonator, was considered. In practice, this can be achieved by placing either a small piece of wire, surrounded by Teflon, through the inner plate between resonator 1 and 6, or an aperture in the inner plate at the level

of the open end of the resonator. The added complexity caused by this coupling was determined unnecessary, as the specifications were satisfied without it.

In the filter, each resonator consists of a $3\text{ mm} \times 3\text{ mm}$ rectangular bar, with a 9 mm earth plane spacing, as seen in Figure 5.3(b). The diameter of the resonator was restricted to be less than $\lambda_0/10$ to prevent the propagation of unwanted modes. The resonator was modelled in Computer Simulation Technology (CST) where the impedance, Z_0 , was calculated as $74.2\ \Omega$, giving a low loss in the transmission line.

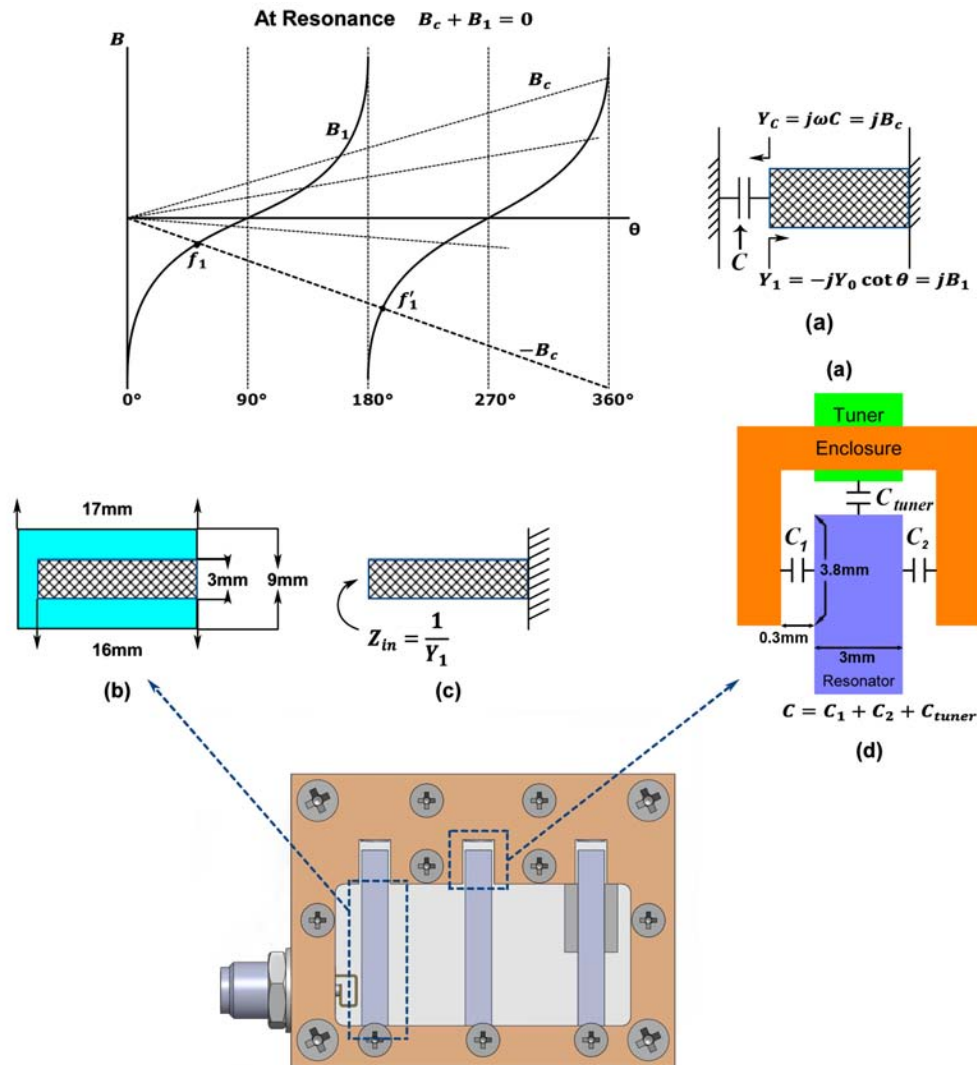


Figure 5.3: Combine Equations.

The combline structure offers the significant advantage of a second passband at a

much higher frequency than to the interdigital type. The position of this passband increases as the length of the resonator is decreased. From Figure 5.3, it can be seen that for resonance to occur, the end-loading susceptance must equal the value of Y_1 . As θ decreases, it can be seen that the value for C increases and the ratio of the second to first passband frequency increases. In Figure 5.3, the response of the Filter 1 is 2125 MHz at f_1 , where the electrical length is 40.8° . The second bandpass response occurs after 180° . The electrical length is direct proportional to the frequency and from this it can be calculated that the f'_1 occurs after

$$2125 \text{ MHz} \times \frac{180^\circ}{40.8^\circ} = 9375 \text{ MHz}, \quad (5.1)$$

which corresponds to a physical length of 16 mm.

The input impedance, Z_{in} , in Figure 5.3(c) can now be approximated by

$$Z_{in} = jZ_0 \tan \theta. \quad (5.2)$$

Thus,

$$Z_{in} = j74.2 \tan 40.8^\circ = j64.06 \Omega \quad (5.3)$$

at f_o .

Because of the short resonator length, the values of the end capacitance are quite high. This can be solved by increasing the length slightly and inserting the resonator's open end into the roof of the enclosure with close spacing between the surface of the resonator and the adjacent walls. This is illustrated in Figure 5.3(d). The parallel plate capacitance can be calculated by

$$C_1 = C_2 \simeq \epsilon_r \epsilon_0 \frac{A}{d} \quad (5.4)$$

where

$C_1 = C_2$ = parallel plate capacitance

ϵ_r = Dielectric permittivity

ϵ_0 = Permittivity of free-space

A = Area of the surface adjoining the sidewalls

d = distance between surfaces

The minimum wire-cutting spacing for manufacturing should normally be greater

than $0,25\text{ mm}$. This also depends on the thickness of the material being cut as well as the wire diameter that is used. The thicker the material, the higher the electrical discharge will have to be, resulting in an increase in wire-cut spacing.

The variable capacitance, C_{tuner} , is obtained by adjusting the tuning screws at the end of each resonator line.

The total end capacitance is equal to

$$C = C_{tuner} + C_1 + C_2 \quad (5.5)$$

which can be simulated in MWO. From this, the total resonator length was calculated to be $19,8\text{ mm}$.

The coupling coefficients between each adjacent resonator pair were determined using the Eigenmode solver of CST and Equation 3.8. The coupling coefficients change inversely proportionally when altering the distance between the two resonators. Figure A.4, in Appendix A, shows the dimensions for the inner plate, which is located between the identical enclosures. The rectangular cut-out (7.7 mm by 6.0 mm) is used for coupling between the two enclosures. By varying the hole diameter of the inner plate slightly the coupling can be altered.

The loaded- q can be implemented by using the group delay of S_{11} as seen from the input point with all the resonators except the first one shorted. The relationship between q and τ is shown in equation 5.6 [7]:

$$\tau_g = \frac{2Q_L}{\pi f_0}. \quad (5.6)$$

A SMA connector with a loop, connecting the centre pin to the outer thread by means of soldering, is used for magnetic coupling into the filter. In CST the Frequency domain solver was used to model the input coupling with the purpose of achieving the desired S_{11} group delay of $\tau_g = 9.88\text{ ns}$. The loop is specifically designed to facilitate group delay adjustments in a 3 mm space inside the filter. As the SMA is screwed into the filter, the coupling increases while the group delay decrease. If the loop is turned perpendicular with regards to the resonator, no coupling between the loop and first resonator occurs, as their respective magnetic field are perpendicular. With the loop in exactly the same plane as the resonator, maximum coupling is achieved. The loop consists of 0.05 mm thick shim stock and was designed to be solder onto the SMA connector prior to assembly, as illustrated in Figure 5.4.

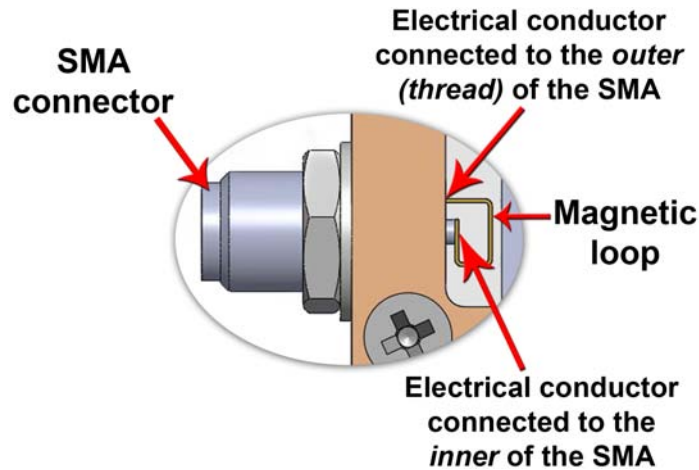


Figure 5.4: SMA connector with Shim Stock loop.

In the final stage of the design, the Frequency domain solver in CST and MWO were used to model the response of Filter 1 and the result was -0.82 dB at 2.125 GHz as shown with the black discontinuous line in Figure 5.6.

Implementation

Aluminium was selected as the preferred metal for manufacturing, due to its light weight, high strength to weight ratio, anti-corrosion properties, as well as being a good electrical conductor.

For manufacturing Wire EDM, also known as wire-cutting, was chosen as the preferred method to minimise costs. With Wire EDM, the filters' enclosure can be manufactured from one piece, which ensures a stronger physical structure and a uniform thermal expansion coefficient throughout the filter.

Six Temex AT6925-8 SL capacitive tuning screws were used for tuning the frequency response.

Measurements

Filter 1 has to be tuned in two stages. Firstly, the two SMA loop connectors must be tuned using a VNA to achieve the desired S_{11} differential group delay of $\tau_g = 9.88$ ns. This is done by first shorting all tuners, except for resonator 1 and 6. Next, tuner 1 is adjusted to 2125 MHz while simultaneously turning the SMA connector into the filter until a S_{11} differential group delay of 9.88 ns is obtained as seen in Figure 5.5. The SMA connector must then be locked and the process repeated for the second

SMA connector and tuner 6. Thereafter, both Dishal- and Ness-methods can be used to tune the filter [12, 13].

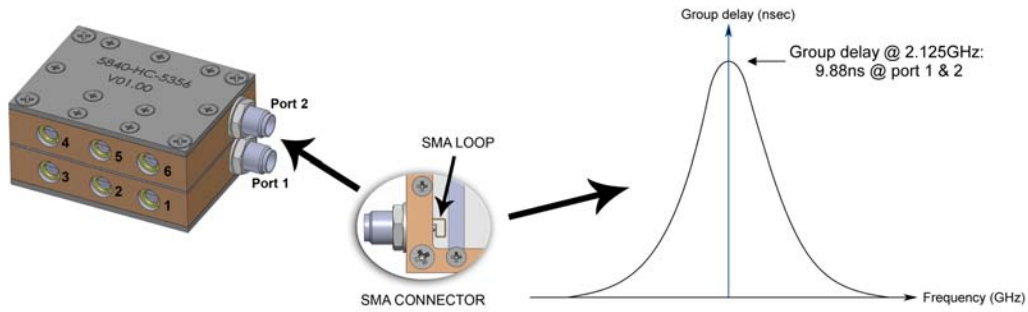


Figure 5.5: Input coupling of Filter 1.

The measured results for Filter 1 is shown in Figure 5.6.

The blue line in Figure 5.6 depicts the results and is referred to as **Version 1**. Filter 1 has an attenuation flatness of 0.5 dB within a 20 MHz band around the centre frequency. The insertion loss at 2.125 GHz is however 2.41 dB, and is too high for the receiver chain.

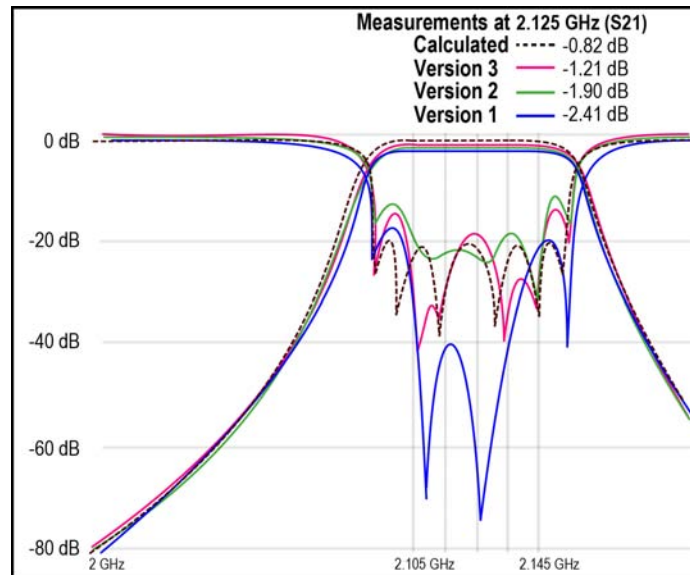


Figure 5.6: Filter 1 Measurements.

Improvements

Two options were considered to improve the insertion loss.

In the first option, referred to as **Version 2**, the filter was chemically polished. The results are shown by the green line in Figure 5.6. S_{21} improved to -1.9 dB at 2.125 GHz. The conclusion is the same as seen with the unloaded Q measurements in section 4.7, namely that loss is reduced when the filter was chemically polished.

In the second option, referred to as **Version 3**, the filter was silver plated by means of electroplating and yielded very good results, as indicated by the pink line in Figure 5.6. S_{21} improved to -1.21 dB at 2.125 GHz.

The conclusion is the same as seen with the unloaded Q measurements in section 4.7, namely that the loss is reduced by 50% when the filter is silver plated.

Group delay plays a very important role in radar systems as mentioned in Chapter 1. It can also be defined as the rate of change of the transmission phase angle with respect to frequency. In other words, if phase versus frequency is non-linear, group delay is not constant. The group delay increases as the order of the filter increases and the frequencies near the band edges takes longer than the rest to pass through the filter. The measured group delay in Figure 5.7 exceeds the design specifications. This is due to material losses rounding the steep amplitude frequency response.

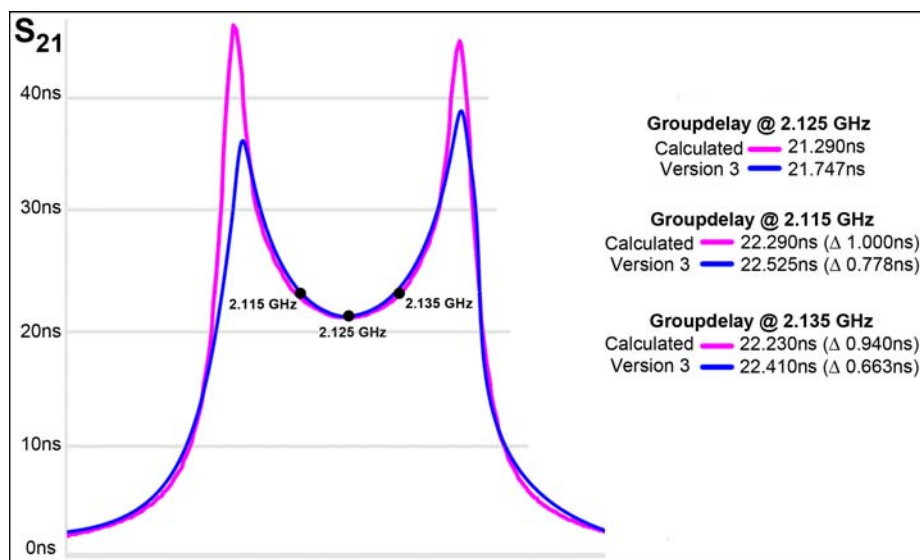


Figure 5.7: Filter 1 - Group delay Response.

Figure 5.8 shows the broad band frequency response of the filter, which was measured on a Rohde & Schwarz VNA. It indicates that the attenuation between 6.375 GHz - 9.375 GHz (LO2) is better than 80 dB.



Figure 5.8: Filter 1, Wider Stopband Response.

All manufacturing details are found in Appendix A.

5.2.2 Filter 2

Specification

Filter 2 is a sixth order Intergidital filter, with a -20 dB S_{11} bandwidth of 8.9 - 9.6 GHz (700 MHz around 9.25 GHz). S_{21} must have an attenuation flatness of 1 dB over the frequency band 8.9 - 9.6 GHz. S_{21} differential group delay for any 20 MHz band within the 700 MHz passband must be less than 1 ns. Filter 2 should attenuate any local oscillator (LO) signals below 7.675 GHz by more than 80 dB.

Filter 2, similarly to Filter 1, is mounted on a VME PCB card and operate in the same harsh environmental conditions. After analysing the component placement on the PCB's, it was found that the filter should not exceed a maximum height of 15 mm and the filter dimensions should also not exceed $50\text{ mm} \times 60\text{ mm}$. The filter will be mounted on the PCB by means of screws and will also be conformal coated, which will increase the height further.

Design

Because of the higher frequency, the resonator length of the interdigital filter is no longer a drawback as it was for Filter 1. The wide bandwidth requirement is also satisfied more easily by the higher inter-resonator coupling of the interdigital filter as compared to the combline approach.

Filter 2 was designed in Matlab using the design code for interdigital filters which can be found in Appendix C. The equations in the Matlab code are given to calculate each of the line capacitive components. The value of the line capacitance depend on the physical dimensions of the bars, the separation between them, as well as the ground plane spacing.

The design bandwidth was chosen to be 30 MHz wider than the specification to compensate for the reduction in S_{21} bandwidth due to losses.

Due to the tight dimensional constrains, a lower limit of 2 mm was placed on the thickness and widths of the bars to reduce the risk of mechanical failure during the wire-cutting process. The end bar spacing was chosen to be located 2.5 mm from the side wall, preventing the SMA's thread from cutting into the side wall. During the Matlab simulating process, the space between the first (or last) resonator and its adjacent end bar was designed to prevent the turner hole from cutting into the end bar.

Table 5.2, show all the parameter values for Filter 2.

Parameter	Value
Filter order	6
Maximum passband reflection coefficient	-20 dB
Centre frequency	9250 MHz
Ripple bandwidth	700 MHz
Earth plane spacing	5 mm
Bar thickness	2 mm
Inner resonator bar width	2 mm
Input line bar width	2 mm
End bar spacing from side wall	2.5 mm
Cavity length	8.11 mm

Table 5.2: Required input parameters for the Interdigital Filter 2 design.

The input and output coupling in this filter is significantly higher than Filter 1. A coupled transmission line coupling which offers much higher coupling values than probe or loop feeds is therefore needed, as shown in the circuit in Figure 2.12(a). This requires two extra lines connected to SMA connectors, as shown in Figure 5.9.

Table 5.3, shows the theoretical and manufactureable spacing parameter values between the resonators. The values were rounded to aid the process tolerance during manufacturing.

Parameter	Theoretical Value	Rounded CST Value
S1	1.2799 mm	1.28 mm
S2	3.64 mm	3.64 mm
S3	4.1642 mm	4.16 mm
S4	4.24 mm	4.24 mm
S5	4.1642 mm	4.16 mm
S6	3.64 mm	3.64 mm
S7	1.2799 mm	1.28 mm

Table 5.3: Interdigital Filter 2 bar spacings.

For tuning purposes, each resonator is shortened by 2.8 mm to accommodate a Temex AT6925-8 SL tuning screw at the open end.

The ideal response of the filter as predicted by CST is indicated by a black discontinuous line in Figure 5.10.

Implementation

Aluminium was selected as the preferred metal for manufacturing. Wire EDM was chosen as the preferred manufacturing method to minimise costs.

Six Temex AT6925-8 SL capacitive tuning screws were used for tuning the frequency response.

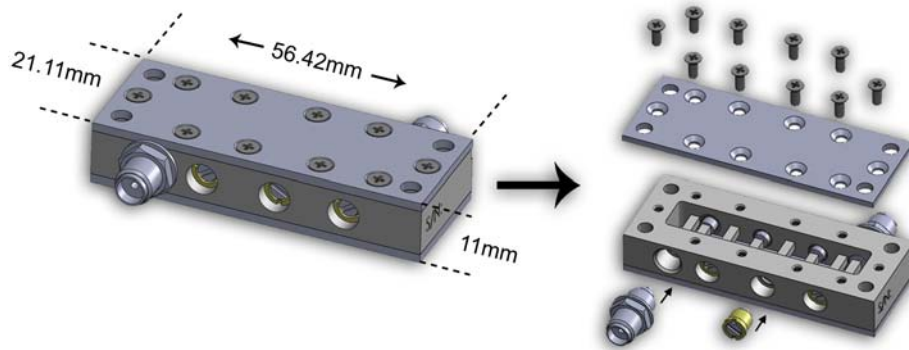


Figure 5.9: Sixth Order Interdigital Filter.

Measurements

Filter 2 was tuned by using the Dishal method [12].

The blue line in Figure 5.10 depicts the results and is referred to as **Version 1**. S_{21} barely meets an attenuation flatness of 1 dB over the frequency band 8.9 - 9.6 GHz. S_{21} differential group delay was found to be greater than 1 ns. S_{21} has a loss of -0.83 dB at 9.25 GHz and the results of S_{11} was poor.

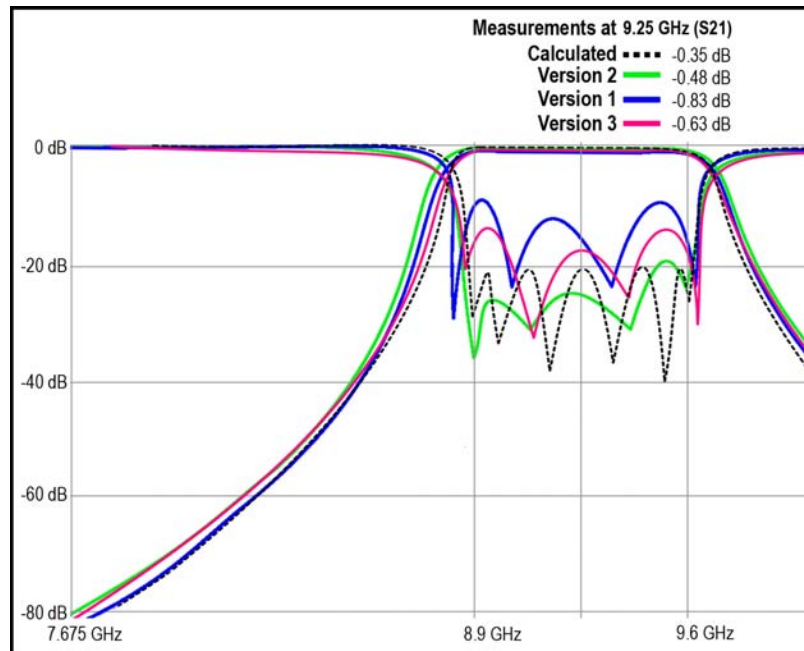


Figure 5.10: Filter 2 Measurements.

Improvements

Two options were considered to improve Version 1.

In the first option, referred to as **Version 2**, the filter was silver plated by means of electroplating to improve the insertion loss.

The green line in Figure 5.10 shows how S_{21} improved to -0.48 dB at 9.25 GHz. The theoretical Matlab model assumes coupling over the whole $\theta = 90^\circ$ length, where in practice the reduced length alters the predicted model. From this, it is clear that by placing shim stock between the resonators 1 and 2, and resonators 5 and 6, coupling can be increased, resulting in a better response. The increase in coupling between resonators, also leads to an improvement in the bandwidth. The shim stock was attached to the filter by means of silver epoxy as illustrated in Figure 5.11.

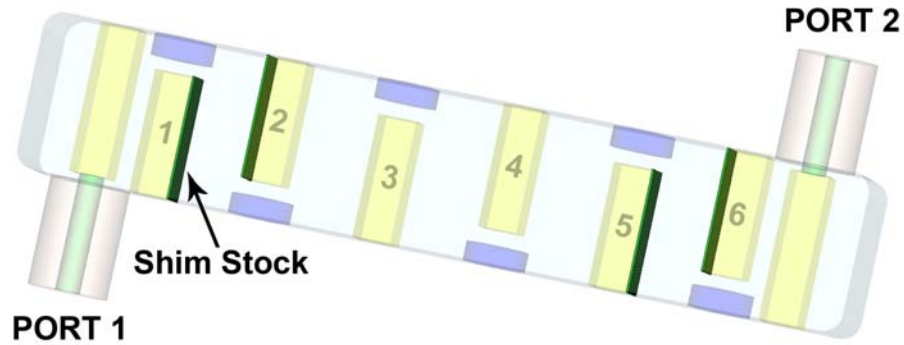


Figure 5.11: Filter 2 - Added shim stock.

In the second option, referred to as **Version 3**, the dimensions were modified for the designed filter, to compensate for the added shim stock in Version 2, but the thickness of the silver epoxy was omitted from the calculation. The filter was also silver plated. The results show that the filter's performance was slightly reduced, compared to Version 2, although the results showed an improvement when compared that of Version 1. The pink line in Figure 5.10 illustrates the results found. S_{21} is -0.63 dB at 9.25 GHz.

Figure 5.12 shows the S_{21} differential group delay of Version 2 and 3. The differential group delay for any 20 MHz band within the 700 MHz passband is less than 1 ns.

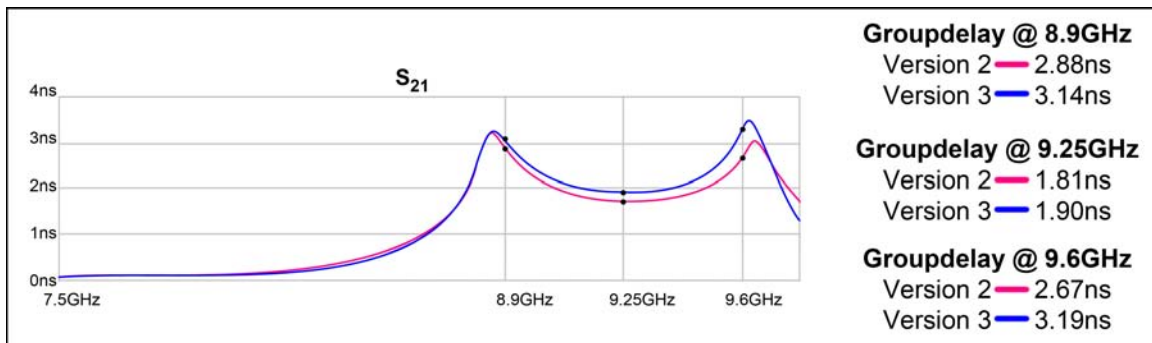


Figure 5.12: Filter 2 - Group delay.

In both Version 2 and 3, the conclusions drawn are the same, i.e. that insertion loss is halved when the filter is silver plated.

All manufacturing data is found in Appendix D.

5.2.3 Filter 3

Specification

Filter 3 is a third order Intergidital filter, with a -20 dB S_{11} bandwidth of 8.9 - 9.6 GHz (700 MHz around 9.25 GHz). S_{21} has an attenuation flatness of 1 dB over the frequency band 8.9 - 9.6 GHz. S_{21} differential group delay for any 20 MHz band within the 700 MHz passband must be less than 1 *ns*.

Filters 3, similarly to Filter 2, is mounted on a VME PCB card and operate in the same harsh environmental conditions. After analysing the component placement of the PCB's, it was found that the filter should not exceed a maximum height of 15 *mm* and the filter dimensions should also not exceed 30 *mm* × 35 *mm*. The filter will be mounted on the PCB by means of screws and also be conformal coated, which will increase the height further.

Design

Filter 3 also faced tight dimensional constrains and a lower limit of 2 *mm* was also placed on the thickness and widths of the bars to reduce the risk of mechanical failure during the wire-cutting process.

Table 5.4, show all the parameter values for Filter 3.

Parameter	Value
Filter order	3
Maximum passband reflection coefficient	-20 dB
Centre frequency	9250 MHz
Ripple bandwidth	730 MHz
Earth plane spacing	5 <i>mm</i>
Bar thickness	2 <i>mm</i>
Inner resonator bar width	2 <i>mm</i>
Input line bar width	2 <i>mm</i>
End bar spacing from side wall	2 <i>mm</i>

Table 5.4: Required input parameters for the Interdigital Filter 3 design.

Table 5.5, shows the theoretical and manufacture-able spacing parameter values between the resonators. The values were adjusted to aid the process tolerance during

manufacturing.

Parameter	Theoretical Value	Rounded CST Value
S1	1.1994 mm	1.2 mm
S2	3.3136 mm	3.32 mm
S3	3.3136 mm	3.32 mm
S4	1.1994 mm	1.2 mm

Table 5.5: Interdigital Filter 3 bar spacings.

In the final stage of the design, the Frequency domain solver in CST was used to model the response of Filter 3. It was found to be -0.22 dB at 9.25 GHz as shown with the black discontinuous line in Figure 5.14.

Implementation

Aluminium was selected as the preferred metal for manufacturing. Wire EDM was chosen as the preferred manufacturing method to minimise costs.

Three Temex AT6925-8 SL capacitive tuning screws were used for tuning the frequency response.

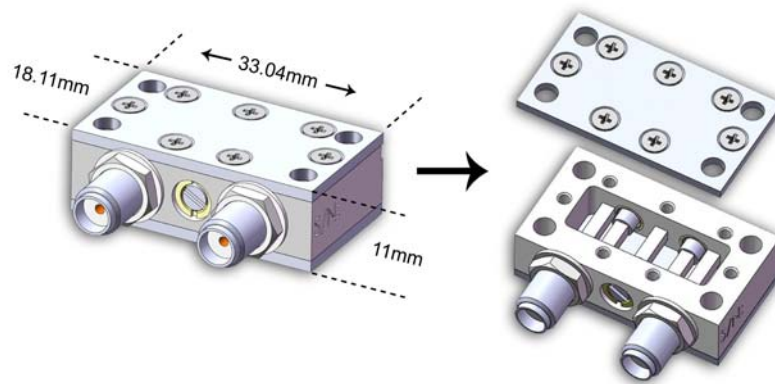


Figure 5.13: Third Order Interdigital Filter.

Measurements

Filter 3 was tuned by using the Dishal method [12].

The blue line in Figure 5.14 shows the results and is referred to as **Version 1**. S_{21} barely meets an attenuation flatness of 1 dB over the frequency band 8.9 - 9.6 GHz. S_{21} differential was found to be greater than 1 ns. S_{21} has a loss of -0.63 dB at 9.25 GHz and S_{11} did not yield good results.

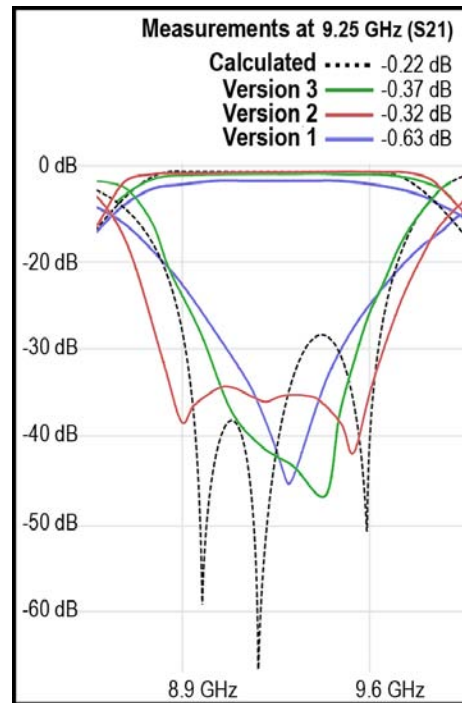


Figure 5.14: Filter 3 Measurements.

Improvements

Two options were considered to improve Version 1.

In the first option, referred to as **Version 2**, was silver plated by means of electroplating to improve the insertion loss.

As with Filter 2, shim stock was also attached to the filter by means of silver epoxy as illustrated in Figure 5.15.

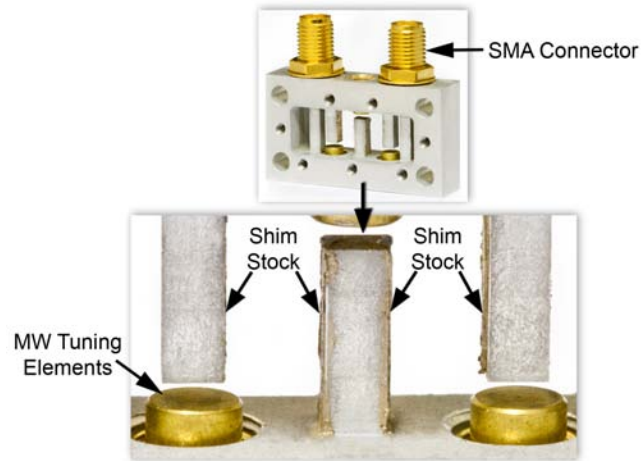


Figure 5.15: Filter 3, Added shim stock.

The red line in Figure 5.14 shows how S_{21} improved to -0.32 dB at 9.25 GHz. By placing shim stock between the resonators 1 and 2, and resonators 2 and 3, coupling can be increased, resulting in a better response. The increase in coupling between resonators, also lead to an increase in the bandwidth.

In the second option, referred to as **Version 3**, the dimensions were modified for the designed filter, to compensate for the added shim stock in Version 2, but the thickness of the silver epoxy was omitted from the calculation. The filter was also silver plated. The results show that the filter's performance was slightly reduced, compared to Version 2, although the results showed an improvement when compared to that of Version 1. The green line in Figure 5.14 illustrates the results found. S_{21} is -0.37 dB at 9.25 GHz.

Figure 5.16 shows the S_{21} differential group delay of Version 2 and 3. The differential group delay for any 20 MHz band within the 700 MHz passband is less than 1 ns.



Figure 5.16: Filter 3 - Group delay.

In both Versions 2 and 3, the conclusions drawn are the same, i.e. that insertion loss is halved when the filter is silver plated.

All manufacturing data is found in Appendix E.

5.3 Conclusion

This chapter discussed the design, modelling, optimisation and measured response of three parallel coupled coaxial resonator filters used in a radar system. Filter 1 consists of a 2125 MHz, sixth order Compline filter. To improve the performance of Filter 1, three versions were considered. Silver electroplating closely matched the simulation results.

Filter 2, which is a sixth order and Filter 3, being a third order, both having a bandwidth of 700 MHz, with a centre frequency of 9250 MHz. Three options were considered to improve the performance of each of these filters. The same pattern were seen in both the filters' results, namely that the simulated results did not closely match the measured results. By silver electroplating and placing shim stock in the right allocated places inside the filters, which increased the coupling between certain resonators, the performance could be improved.

Chapter 6

Conclusion

The main objective of this thesis was to describe the design of various coaxial resonator filters for radar applications.

In Chapter 1, an Introduction to filtering radar signals was discussed. A broad-band Pulse-Doppler Radar system was used as an illustration to define the different building blocks and filters needed to restrict unwanted signals entering the radar system.

Chapter 2 used a well-known LC-Ladder prototype filter to derive a generalised bandpass filter. From this, a generalised Compline- and Interdigital filter could be derived.

In Chapter 3, three basic implementation parameters which plays a vital role in the realisation and improvement of a microwave filter design was discussed, namely Input Coupling, Inter-resonator Coupling and the Resonator Q -factor.

In Chapter 4, different aspects concerning the manufacturing of a filter were discussed. Thereafter, an in-depth study was done to determining the unloaded quality factor for thirteen different resonators. The results conclusively showed that a resonator, made from aluminium, which was wire-cut and then silver electroplated, yields the best result and was the most cost efficient.

Chapter 5 followed an in-depth discussion pertaining to the design, modeling, optimisation and measuring the response of three parallel coupled transmission line filters used in a radar system. The design of Filter 1, a 2125 MHz, sixth order Compline filter, was a success. It was also noted that in the results for Filter 1, that the insertion loss could be reduced by 50% just by silver electroplating alone. Filter 2, which is a sixth order and Filter 3, being a third order, both having a bandwidth of 700 MHz, with a centre frequency of 9250 MHz. Their simulated and measured results did not closely matched the measured results. By silver electroplating the insertion loss

could be reduced by 50%. Placing shim stock in the correct allocated place inside the filters, the performance could also be improved due to the increased coupling between certain resonators. The increase in coupling between resonators, also leads to an improvement in the bandwidth.

Bibliography

- [1] P. W. van der Walt, "Private communication," November 2010. 1-9
- [2] P. W. van der Walt, *RSR210 IF and RF Filter Design Considerations for the Receive and Transmit Chains*. Reutech Radar Systems (PTY) LTD, 2009. 10, 13
- [3] G. L. Matthaei, L. Young, and E. M. T. Jones, *Microwave Filters, Impedance-Matching Networks, and Coupling Structures*. Artech House, Inc., 1980. viii, xi, 16, 18, 19, 22, 25, 29, 30, 31, 35, 36, 37, 38
- [4] P. Vizmuller, *RF Design Guide (Systems, Circuits, and Equations)*. Artech House, INC., 1995. 17, 18
- [5] H. J. Moes, "A low noise pll-based frequency synthesiser for x-band radar," Master's thesis, Stellenbosch University, March 2008. 18, 19, 20, 21, 22, 25, 35, 36, 37, 38
- [6] D. M. Pozar, *Microwave Engineering*. John Wiley and Sons, Inc., third ed., 2005. 26, 51
- [7] P. W. van der Walt, "Gekoppelde resoneerder filters," 2008. ix, 47, 72
- [8] C. Waits, *Electronic Communications (TEL221)*. Cape University of Technology. 47
- [9] P. W. van der Walt, "Unloaded quality factor," 2010. 48
- [10] H. Eskelinen and P. Eskelinen, *Microwave Component Mechanics*. Artech House, INC., 2003. 52, 53, 54, 57
- [11] AgieCharmilles, *Cut 20 (Wire EDM Machine) Brochure*, 2008. 54
- [12] M. Dishal, "Alignment and adjustment of synchronously tuned multiple-resonant-circuit filters," *Proc. IRE*, vol. 39, pp. 1448 - 1455, November 1951. 74, 79, 84

- [13] J. B. Ness, "A unified approach to the design, measurement, and tuning of coupled-resonator filters," *IEEE Transactions on Microwave Theory and Techniques*, vol. 46, pp. 343 - 351, April 1998. 74

Appendix A

Filter 1 Dimensions

Figures A.1 to A.5 shows the manufacturing measurements of filter 1. Figure A.1 and A.2 shows the first process step where the filter is CNC milled (pre wire-cut). The mounting holes for the SMA connector and tuning elements are also machined during this stage.

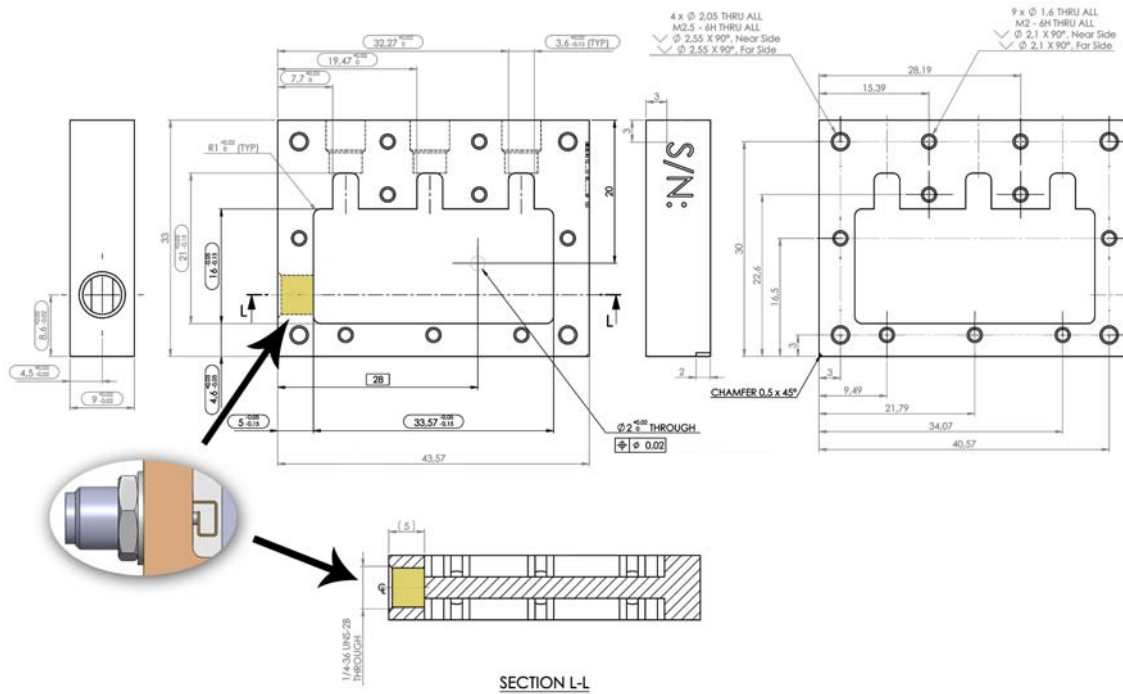


Figure A.1: Filter 1, Dimensions (a).

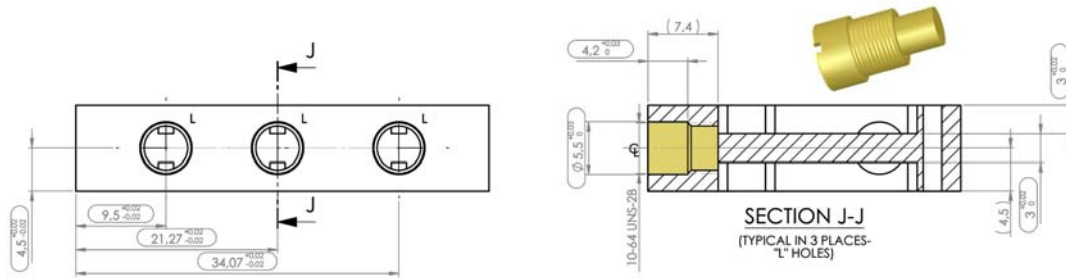


Figure A.2: Filter 1, Dimensions (b).

Figure A.3 shows the wire-cutting (EDM) measurements of the enclosure. It is cut with a surface roughness of $0.8 \mu\text{m}$.

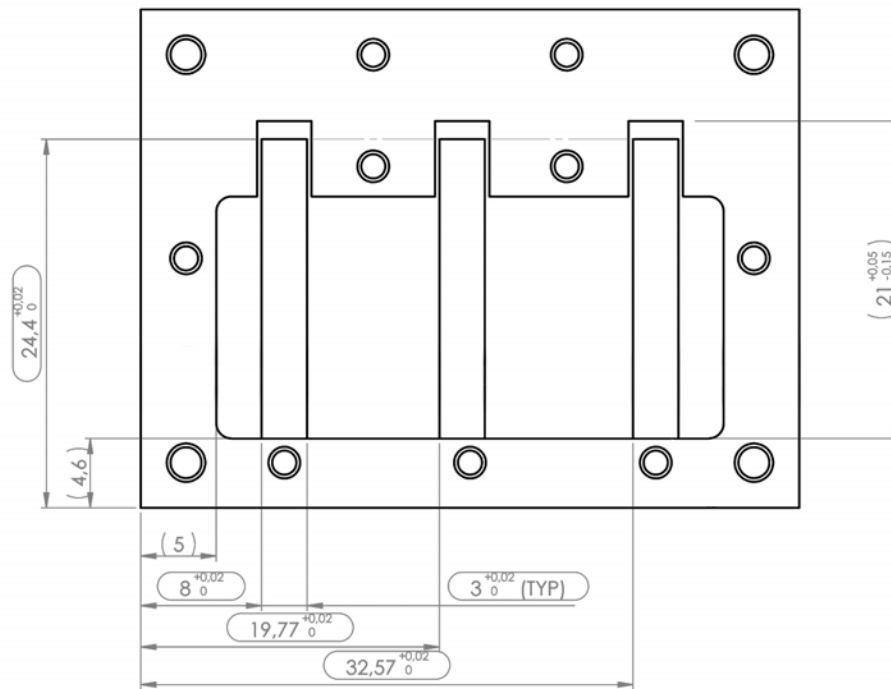


Figure A.3: Filter 1, Dimensions (c).

Figure A.4 shows the measurements for the inner plate, which is situated between the identical enclosures. The rectangular cut out (7.7 mm by 6.0 mm) is used for the coupling between the two enclosures.

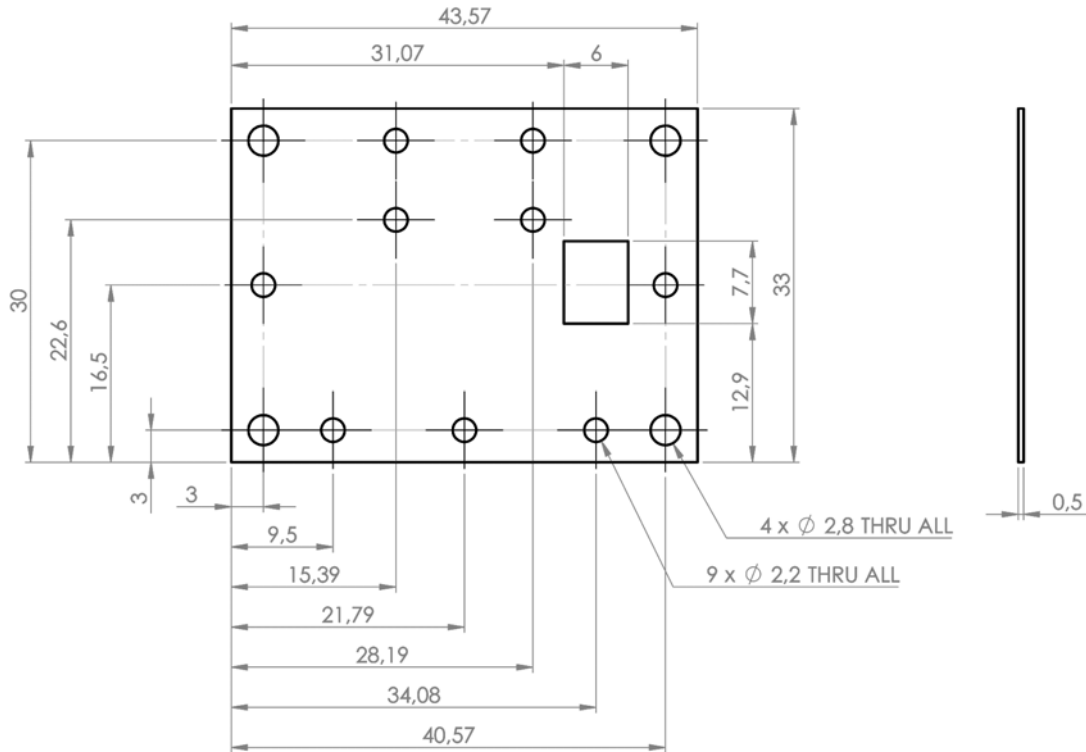


Figure A.4: Filter 1, Dimensions (d).

Figure A.5 shows the measurements for the lids. The mounting holes must preferably be in line (or as close as possible), to improve the electrical flow performance in the filter.

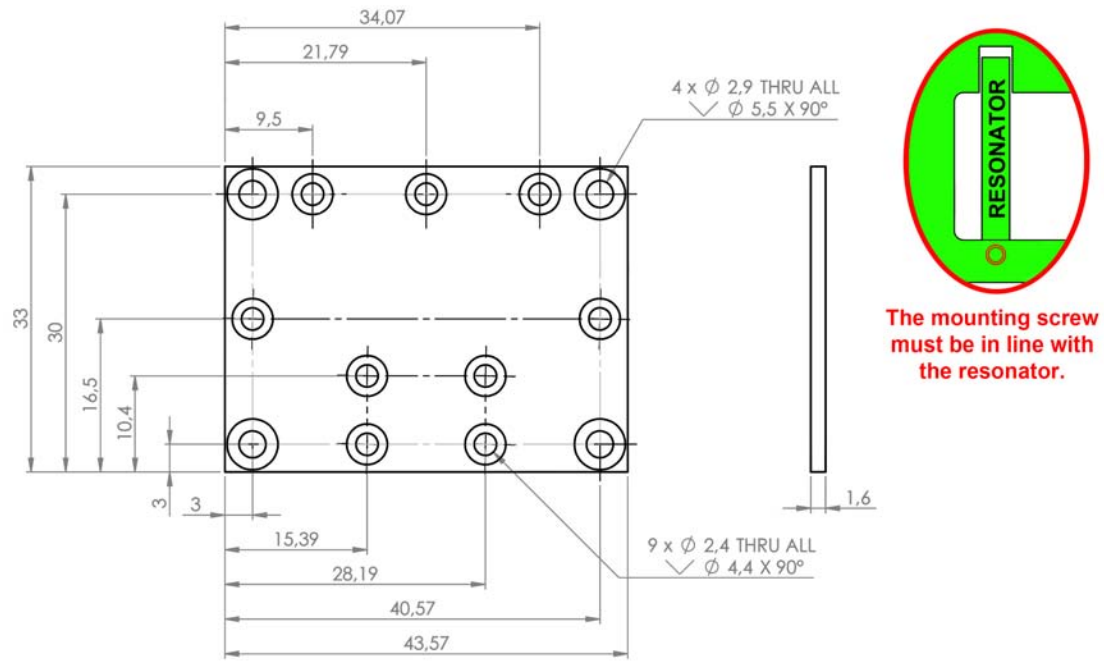


Figure A.5: Filter 1, Dimensions (e).

Appendix B

Comblin Filter - MWO Simulation

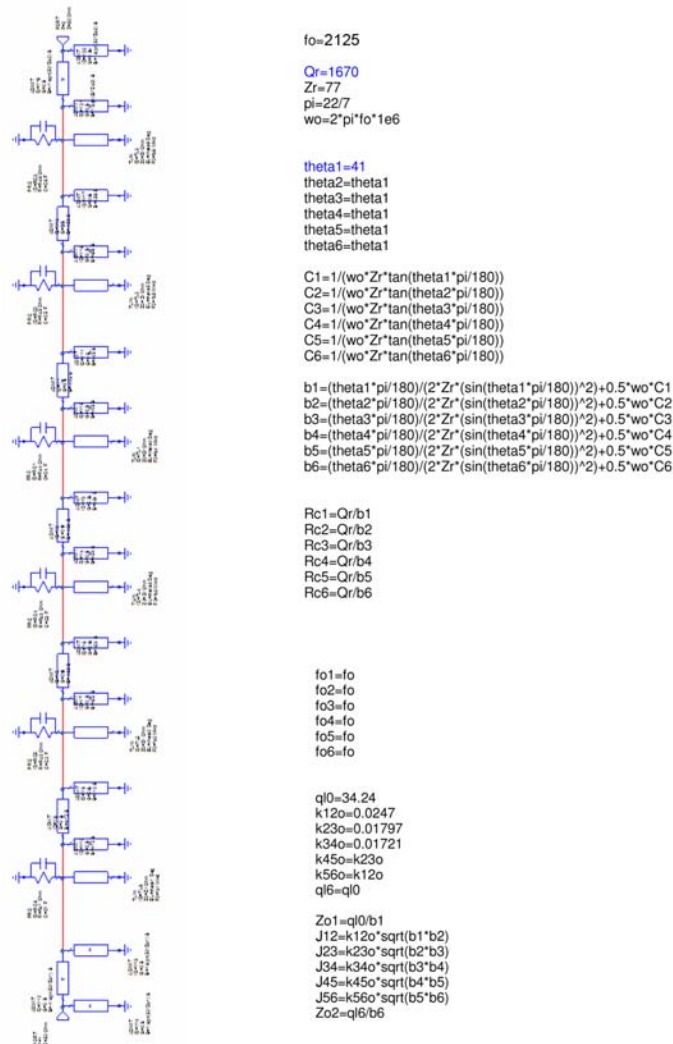


Figure B.1: Filter 1 - MWO Simulation.

Appendix C

Interdigital Filter - Matlab Code

The Matlab code was provided by Prof. PW van der Walt and used to design the Interdigital filters in Chapter 5. Copy the following files in one folder and run IDF.m:

- CalcC.m
- CalcKQ.m
- cBar.m
- chebkq.m
- K12.m
- Kmn.m
- Qext.m

IDF.m

```
% Interdigital filter with coupled bars and input transformers design
```

```
% Tchebyscheff response
```

```
close all
```

```
clear all
```

```
clc
```

```
n = input('Low pass prototype order: ');
```

```
s11 = input('Max passband reflection coefficient (dB): ');
```

```
if s11 >= 0
```

```
s11 = -s11;
```

```

end
f0 = input('Centre frequency of bandpass filter (MHz): ');
bandwidth = input('Ripple bandwidth of bandpass filter (MHz): ');
ep_spacing = input('Earth plane spacing (mm): ');
t = input('Bar thickness (mm): ');
w = input('Inner resonator bar widths (mm): ');
Widths = ones(1,n+2)*w;
w = input('Input line bar widths (mm): ');
Widths(1) = w; Widths(n+2) = w;
x_end = input('End bar (input line) spacing from sidewall (mm): ');
% Calculate k and q values
% Low pass Prototype
QKQ = chebkq(n,s11);
% Scale for band pass filter
QKQ(1) = QKQ(1)*f0/bandwidth;
QKQ(n+1) = QKQ(1);
for i = 2:n
QKQ(i) = QKQ(i)*bandwidth/f0;
end
S = Widths(2)*linspace(1,1,n+1);
S(1) = S(1)/3;
S(n+1) = S(n+1)/3;
QKQFil = CalcKQ(n,S,t,Widths,ep_spacing,x_end);
inv_grad = (1.05*S - .95*S)./...
(CalcKQ(n,1.05*S,t,Widths,ep_spacing,x_end)-CalcKQ(n,.95*S,t,Widths,ep_spacing,x_end));
DeltaS = inv_grad.*(QKQ-QKQFil);
NormStep = sqrt(DeltaS*DeltaS');
S = S + 0.3*DeltaS;
count=0;
while NormStep > ep_spacing/10000
count = count + 1;
QKQFil = CalcKQ(n,S,t,Widths,ep_spacing,x_end);
inv_grad = (1.05*S - .95*S)./...
(CalcKQ(n,1.05*S,t,Widths,ep_spacing,x_end)-CalcKQ(n,.95*S,t,Widths,ep_spacing,x_end));
DeltaS = inv_grad.*(QKQ-QKQFil);
NormStep = sqrt(DeltaS*DeltaS');

```



```

S = S + DeltaS;
end
disp('_____*****_____')
disp(['Dimensions determined after ',num2str(count),' refinements'])
disp('Spacing between bars ')
S
S1 = S;
ok = input('Do you want to round the spacings? y to round, n to finish ','s');
while ok == 'y'
for i = 1:n+1
disp(['S(',num2str(i),') = ',num2str(S(i))])
S1(i) = input('Input rounded value: ')
end
QKQrounded = CalcKQ(n,S1,t,Widths,ep_spacing,x_end);
Error = 100*(QKQrounded-QKQ)./QKQ;
disp('Percentage errors after rounding, Q1, K12, K23...Qn')
Error
ok = input('Not satisfied? y to round again, n to end ','s');
end
FilterInnerWidth = sum(Widths) + 2*x_end + sum(S1)
CavityLength = 75000/f0
C = CalcC(n,S1,t,Widths,ep_spacing,x_end);
% C(1,2)=C(1,2)+2*C(1,1);
% C(1,1) = 0;
% C(n+2,2) = C(n+2,2) + 2*C(n+2,3);
% C(n+2,3) = 0;
disp('Bar capacitances')
C
disp('Bar transmission line characteristic impedances')
Z = 376.7*(C.^-1)
filename = input('Input name (between quotes) of file in which to save
results: ')
save(filename, 'n', 'f0', 'bandwidth', 's11', 'ep_spacing', 'CavityLength',...
'Widths', 'x_end', 't', 'S1', 'FilterInnerWidth', 'C', 'Z', 'QKQ')

```

CalcC.m

% Calculate the bar capacitances of n+2 parallel bars

```
function C = CalcC(n,S,t,W,b,x_end)
C=[];
C = cBar(W(1),t,b,2*x_end,S(1));
for i = 2:n+1
C = [C;cBar(W(i),t,b,S(i-1),S(i))];
end
C = [C;cBar(W(n+2),t,b,S(n+1),2*x_end)];
C(1,2) = C(1,2)+2*C(1,1);
C(1,1) = 0;
C(n+2,2) = C(n+2,2)+2*C(n+2,3);
C(n+2,3) = 0;
end
```

CalcKQ.m

% Function to calculate capacitances from physical data

% S contains the n+1 spacings between the n+2 bars

```
function QKQ = CalcKQ(n,S,t,W,b,x_end);
```

% C contains n+2 rows of data, cl, cg, cr for each bar.

```
C=[];
C = cBar(W(1),t,b,2*x_end,S(1));
for i = 2:n+1
C = [C;cBar(W(i),t,b,S(i-1),S(i))];
end
C = [C;cBar(W(n+2),t,b,S(n+1),2*x_end)];
QKQ = [1:n+1];
QKQ(1) = Qext(50,2*C(1,1)+C(1,2),C(1,3),C(2,2),C(2,3));
QKQ(n+1) = QKQ(1);
QKQ(2) = K12(n,2*C(1,1)+C(1,2),C(1,3),C(2,2),C(2,3),C(3,2),C(3,3));
QKQ(n) = QKQ(2);
for i = 3:n-1 QKQ(i) = Kmn(C(i,1),C(i,2),C(i,3),C(i+1,2),C(i+1,3));
end
end
```

cBar.m

% Function cBar calculates the capacitances (C/Eps values)

```

% for parallel coupled bars.
% Reference SM Perlow, "Analysis of edge-coupled shielded
% strip and Coupled Rod structures",
% Trans IEEE MTT-35 No 5, May 1987, pp 522 - 529.
function C = cBar(w,t,b,sl,sr)
if ((nargin < 5) || (nargin > 5))
error ('usage: cBar(w, t, b, sl, sr)');
end
cpar = Cp(w,t,b);
cfel = Cfe(sl,t,b);
cfer = Cfe(sr,t,b);
C = [];
C(1) = Cc(sl,t,b);
C(2) = 2*(cpar+cfel+cfer);
C(3) = Cc(sr,t,b);
end
function a = A(s,t,b)
if (s/b) < 0.30
a = 1.0+2.13507*(t/b)*exp(-0.57518*log(s/b));
else
a = 1.0+3.89531*(t/b)*exp(-0.11467*log(s/b));
end
end
function b = B(s,t,b)
if ((t/b) <= 0.5636)
if ((s/b) < 0.08) b = -(0.2933+3.333*s/b)*t/b;
else
b = -(0.56)*t/b;
end
else
if ((s/b) < 0.08)
b = -0.1653-5.6814*(s/b)+6.7475*(s/b)*(t/b);
else
b = -0.62+0.54*(t/b);
end
end
end

```

```

end
function c = Cp(w,t,b)
wc0 = 2*log(2)/pi+(w/b)-1/((2/pi)*log(abs(2*coth(pi*w/(4*b)))));
if ~(((w*t)/(b*b))>0.015)|(w/b>0.4)
weff = w-b*(wc0*(1.0-Sqrt(w*t/(b*b)/0.015))^2)
else
weff = w;
end
c = 2*weff/(b-t);
end
function c = Cc(s,t,b) c = 2*A(s,t,b)*log(coth(pi*s/(2*b)))/(pi);
end
function c = Cfe(s,t,b)
cfeo = A(s,t,b)*(s/b-2*log(cosh(pi*s/(2*b)))/pi)+B(s,t,b);
if s/b > 1
cfeo = (Cf(t,b)-cfeo)*(1-exp(-4*(s/b-1)))+cfeo;
end
c = cfeo;
end
function c = Cf(t,b) tb = 1/(1-t/b);
c = (2*tb*log(tb+1)-(tb-1)*log((tb)^2-1))/pi;
end

```

Chebq.m

```

%Tchebyscheff filter k and q values
%Ripple cut-off frequency =1 r/a
%Give order, max passband reflection coefficient

```

```

function kq = chebkq(N,MaxRefl)
sm_sq = 10^(MaxRefl/10);
e_sq = sm_sq/(1-sm_sq);
e = sqrt(e_sq);
a = asinh(1/e)/N;
x = sinh(a);
kq=[];
kq(1) = 2*sin(pi/2/N)/x;
for r = 1:N-1;

```

```

kq(r+1) = sqrt((x^2+sin(r*pi/N)^2)/(4*sin((2*r-1)*pi/2/N)*sin((2*r+1)*pi/2/N)));
end
kq(N+1)=kq(1);
end

```

K12.m

```

% Function K12

```

```

% Evaluates the coupling between first and second resonators in filter
% with input line ("=resonator 0") and transformer for load matching

```

```

function k = K12(n,c0,c01,c1,c12,c2,c23)
n1 = c01/(c0+c01);
if n>2
k = (4/pi)*c12/sqrt((n1*c0+c1+c12)*(c12+c2+c23));
else
k = (4/pi)*c12/(n1*c0+c1+c12);
end
end

```

Kmn.m

```

% Function _Kmn

```

```

% Calculates the coupling coefficient between inner lines of an interdigital
filter

```

```

function k = Kmn(cml,cm,cmn,cn,cnr)
k = (4/pi)*cmn/sqrt((cml+cm+cmn)*(cmn+cn+cnr));
end

```

Qext.m

```

% Calculated first resonator external Q with transformer-input

```

```

% Input quantities C_ refer to C/eps values

```

```

% C_0 input line; C_01 unit element coupling input line and first resonator

```

```

% C_1 First resonator; C_12 unit element coupling first and second
resonators

```

```

function Q = Qext(Rg,C_0,C_01,C_1,C_12)
n = C_01/(C_01+C_0);
Q = (pi*376.7*(n*C_0+C_1+C_12))/(4*Rg*C_01^2);
end

```

Appendix D

Filter 2 Dimensions

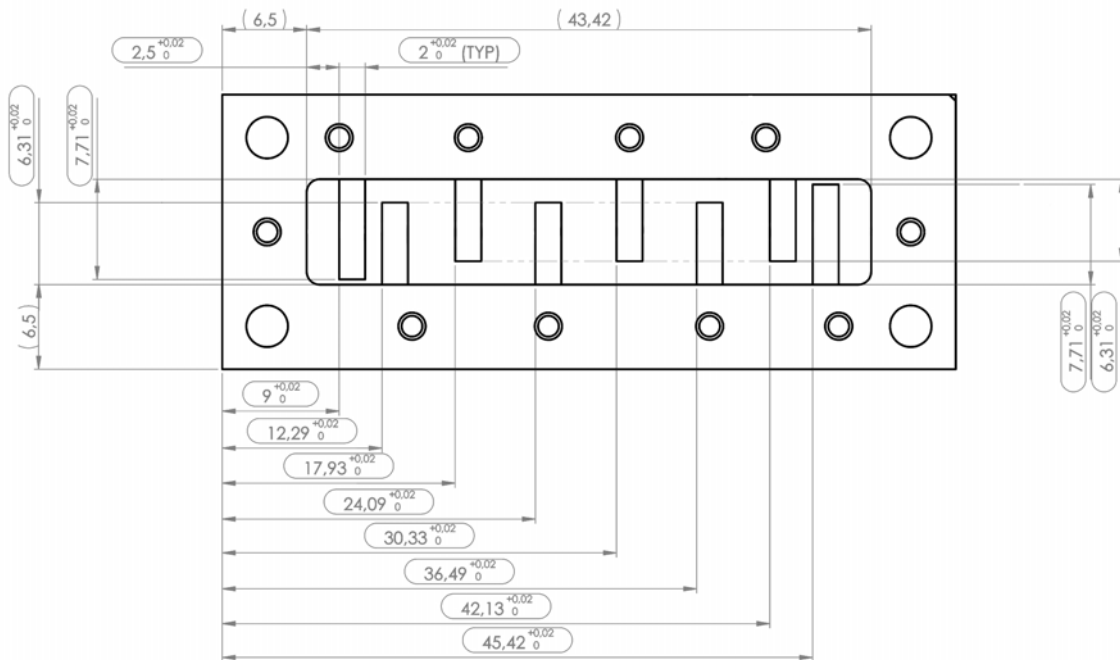


Figure D.1: Filter 2 (Version1), Dimensions (a).

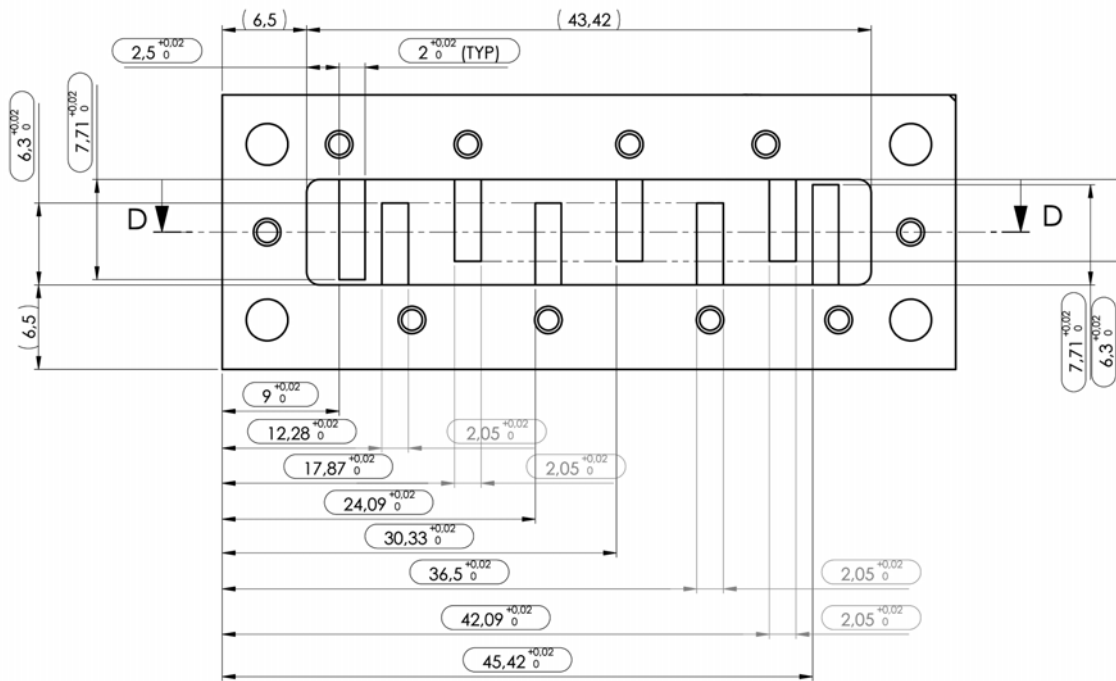


Figure D.2: Filter 2 (Version 3), Dimensions (a).

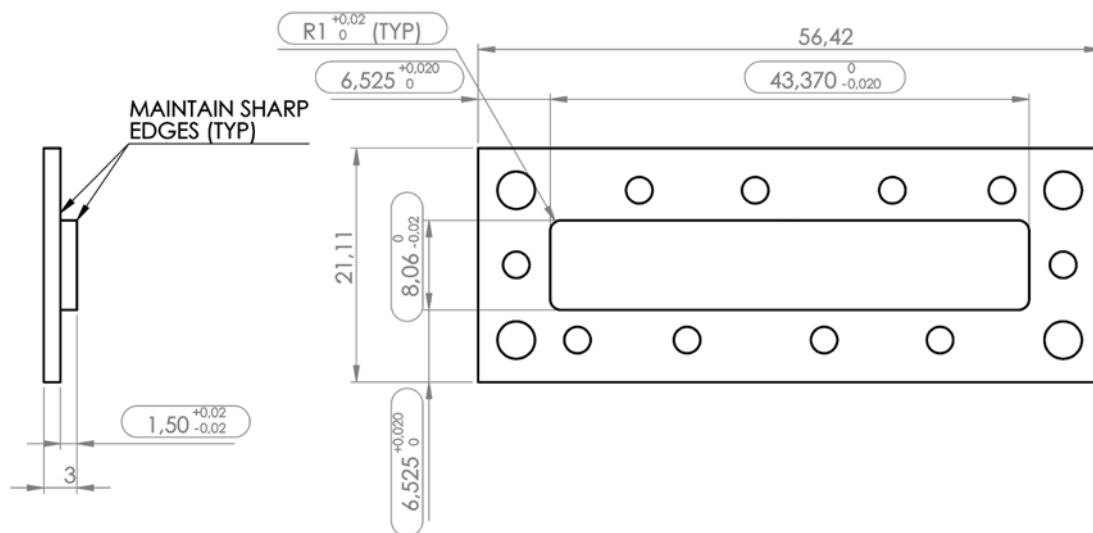


Figure D.3: Filter 2 (Version 3), Dimensions (b).

APPENDIX D. FILTER 2 DIMENSIONS

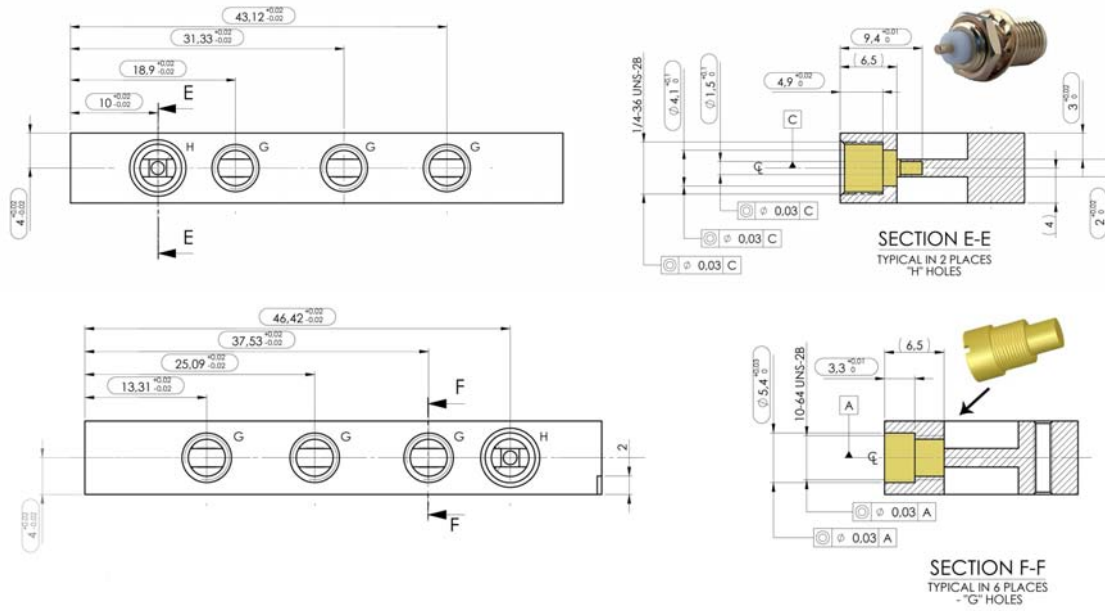


Figure D.4: Filter 2 (Version 3), Dimensions (c).

Appendix E

Filter 3 Dimensions

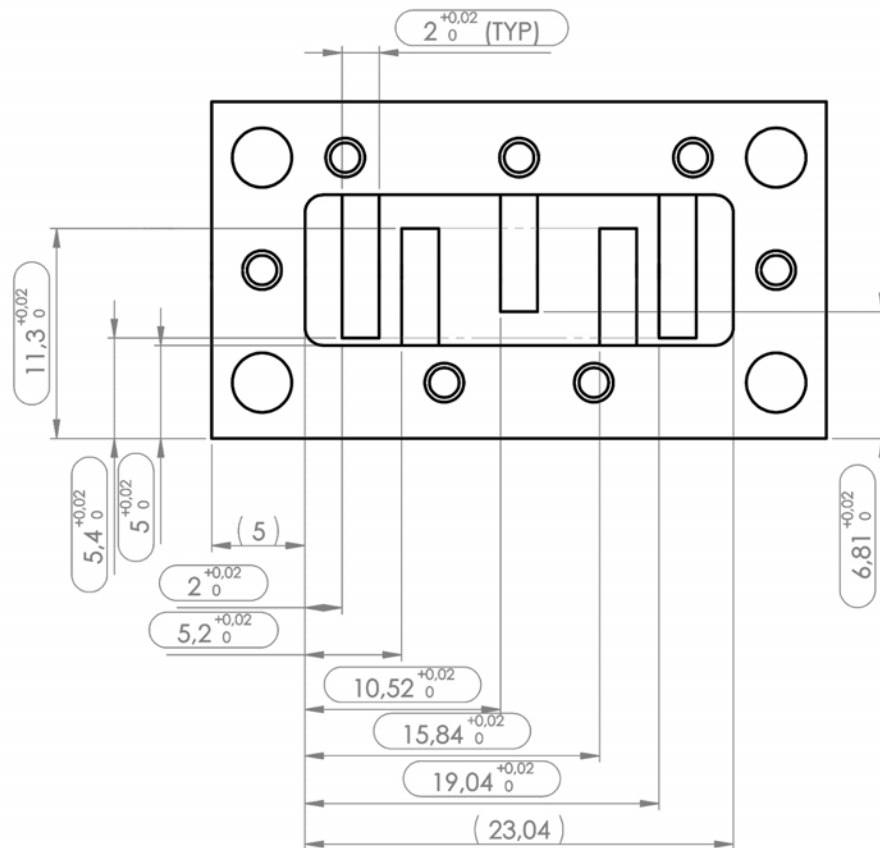


Figure E.1: Filter 3 (Version1), Dimensions (a).

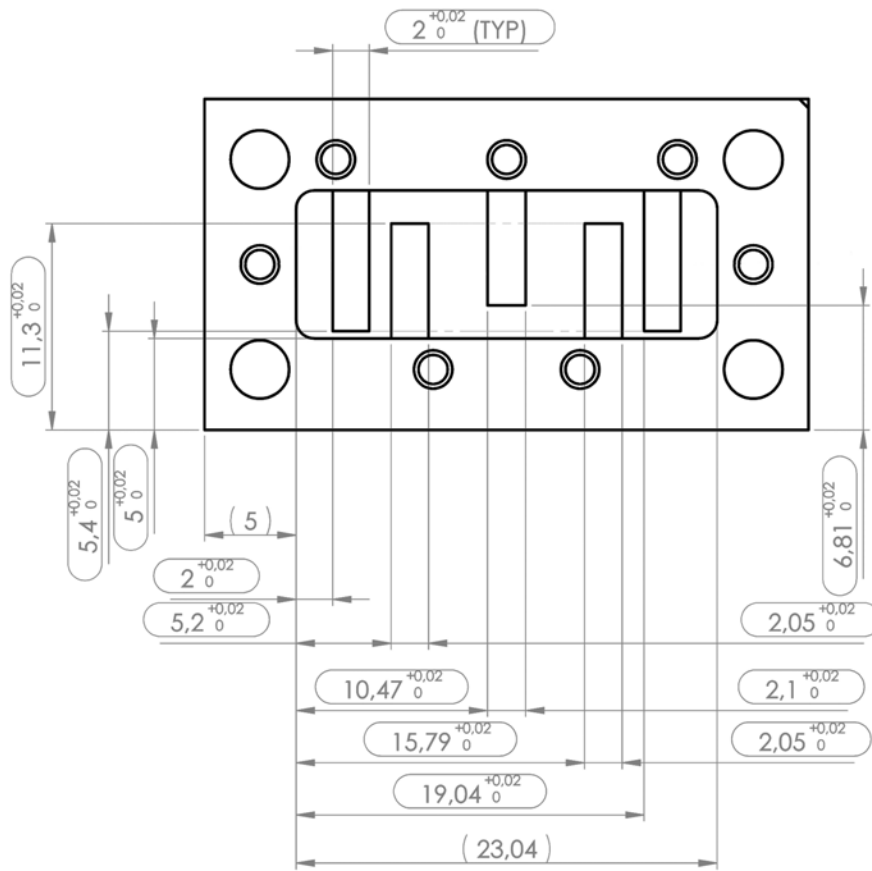


Figure E.2: Filter 3 (Version 3), Dimensions (a).

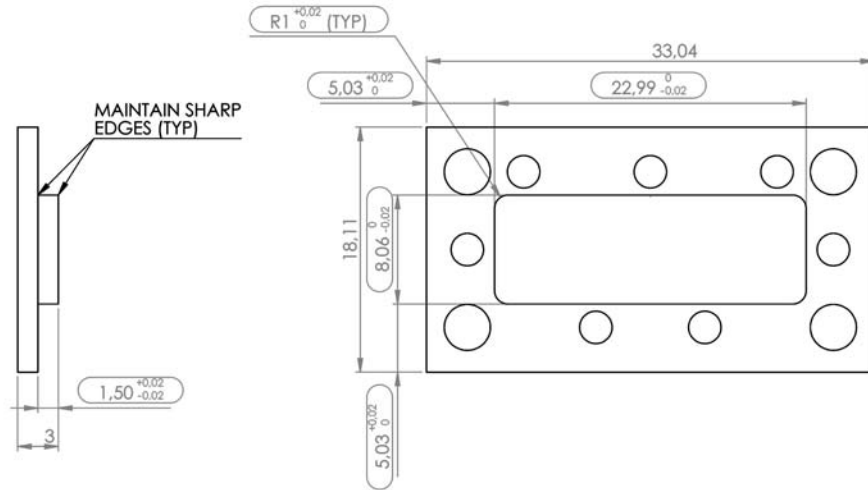


Figure E.3: Filter 3 (Version 3), Dimensions (b).

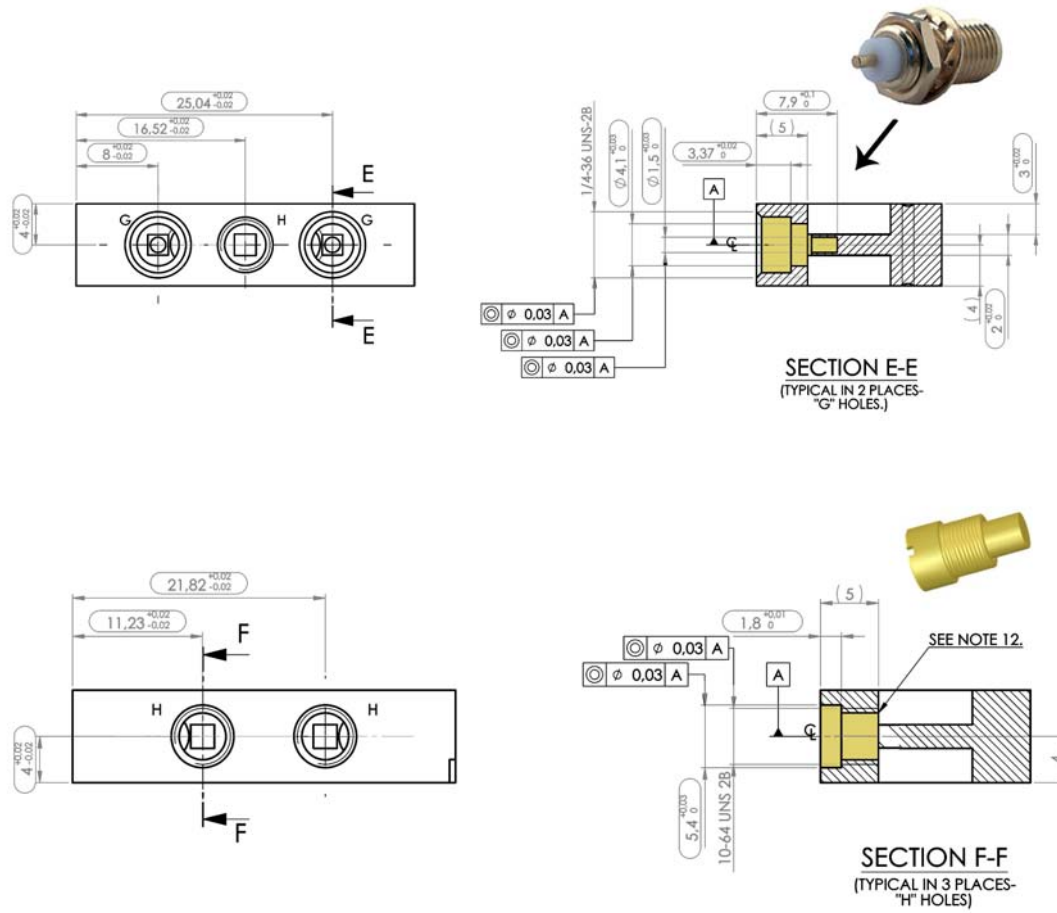


Figure E.4: Filter 3 (Version 3), Dimensions (c).